From the Institute of Pharmacology and Clinical Pharmacology
at Heinrich Heine University Düsseldorf

Novel effects of the Helix-Loop-Helix Factor Id3 on Hyaluronan-mediated Adipose Tissue Inflammation

Dissertation

To obtain the academic title of Doctor of Philosophy (PhD)
from the Faculty of Medicine at Heinrich Heine University Düsseldorf

submitted by

Angelina Misiou

2021

As an inaugural dissertation printed by permission of the Faculty of Medicine at Heinrich Heine University Düsseldorf

signed:

Dean:

Examiner A: Prof. Dr. med. Maria Grandoch

Examiner B: Prof. Dr. Martina Krüger

To my family

Στην Οικογένειά μου

Publications

Parts of this work have been published:

1. **Misiou A,** Garmey JC, Hensien JM, et al. Helix-Loop-Helix Factor Id3 (Inhibitor of Differentiation 3). Arterioscler Thromb Vasc Biol. December 2020. doi:10.1161/atvbaha.120.315588

Zusammenfassung

Fettleibigkeit ist eines der führenden Gesundheitsprobleme weltweit und betrifft Millionen von Menschen. Eines der Hauptmerkmale von Fettleibigkeit ist die chronische, niedriggradige Entzündung des Fettgewebes, die durch die Infiltration verschiedener Immunzellen gekennzeichnet ist. Der Transkriptionsfaktor Inhibitor der Differenzierung 3 (Id3) ist ein Schlüsselregulator für viszerale Fettleibigkeit und spielt vermutlich auch eine schützende Rolle bei Gefäßerkrankungen. Es ist seit einigen Jahren bekannt, dass Hyaluronsäure (*hyaluronic acid*, HA), die von den drei Isoenzymen HA synthase (HAS) 1, -2 und -3 synthetisiert wird, an metabolischen Erkrankungen wie der Fettleibigkeit und dem Typ-2-Diabetes mellitus (T2DM) und beispielsweise Entzündungen des Fettgewebes (*adipose tissue*, AT), beteiligt ist. Ob Id3 auch die HA-Matrix reguliert, ist derzeit nicht bekannt. Ziel der vorliegenden Studie war es daher zu untersuchen, ob ein Zusammenhang zwischen *Id3* und HA bei AT-Entzündungen und Fettleibigkeit besteht. Zu diesem Zweck wurden 8 Wochen alte männliche *Id3*$^{-/-}$ Mäuse und die jeweiligen Wildtyp (Wt) Kontrollen 4 Wochen lang einer fettreichen Diät (*high fat diet*, HFD) unterzogen. Nach 4 Wochen Behandlung mit HFD zeigte das Körpergewicht der Mäuse keine Unterschiede, jedoch war das epididymale AT-Gewicht in *Id3*$^{-/-}$ Mäusen im Vergleich zu den Wt Kontrolltieren signifikant reduziert war. Interessanterweise wurde die Glukosetoleranz dieser Mäuse nicht wie erwartet verbessert, trotz des schlankeren Phänotyps, und so wurde der Entzündungsstatus der Mäuse untersucht. Die Analyse mittels Durchflusszytometrie ergab mehr entzündliche B2-Zellen im AT von HFD-gefütterten *Id3*$^{-/-}$ Mäusen. Darüber hinaus konnte mit immunhistochemischen Untersuchungen gezeigt werden, dass HA sich im epididymalen AT dieser Mäuse im Vergleich zu Wt Kontrollen akkumulierte. Ein Anstieg der zirkulierenden HA wurde mittels ELISA bestätigt. Die Expression von HA-Synthase 2 (*Has2*) war in den epididymalen AT- und Aortengefäß-Glattmuskelzellen von *Id3*$^{-/-}$ Mäusen hochreguliert. Funktionell förderte HA die B2-Zelladhäsion im Fettgewebe und auf glatteb Muskelzellen von *Id3*$^{-/-}$ Mäusen, ein Effekt, der gegenüber

Hyaluronidase empfindlich war. Zusammenfassend legen unsere Ergebnisse nahe, dass ein *Id3*-Defizit die HFD-induzierte AT-Gewichtszunahme verringert und die *Has2*-Expression in der stromalen Gefäßfraktion aktiviert, was zu einer HA-Akkumulation führt. Ein erhöhter HA-Gehalt führt wiederum zu einer Erhöhung der B2-Zellpopulation im AT, indem die HA-abhängige Bindung von B2-Zellen gefördert wird und somit zur AT-Entzündung beiträgt.

Summary

Obesity is one of the leading health problems worldwide, affecting millions of people. One of the main characteristics of obesity is chronic, low-grade adipose tissue inflammation, characterized by the recruitment of different immune cells in the area. The transcription factor Inhibitor of differentiation 3 (Id3) is involved in visceral obesity and has a protective role against vascular disease. Hyaluronic acid (HA), synthesized by three isoenzymes, HAS1, -2 and -3, was found to be implicated in metabolic dysfunction in obesity, Type 2 diabetes mellitus (T2DM) and adipose tissue (AT) inflammation. Whether Id3 also regulates the HA matrix is currently unknown. The present study aimed to investigate if an interrelationship between Id3 and HA in AT inflammation and obesity exists. For this purpose, male *Id3*$^{-/-}$ mice and respective wild type (Wt) controls were treated with a 60% high fat diet (HFD) for 4 weeks. After treatment, the body weight of the mice was not altered, but the epididymal AT weight was significantly decreased in *Id3*$^{-/-}$ mice compared to Wt littermates. Interestingly, despite the leaner phenotype, glucose tolerance was not improved in *Id3*$^{-/-}$ mice as expected, and so the inflammatory status of the mice was examined. Flow cytometry revealed more inflammatory B2 cells in the AT of HFD-fed *Id3*$^{-/-}$ mice. Furthermore, immunohistochemistry showed that HA accumulated in the epididymal AT of these mice compared to Wt littermate controls, and circulating HA was also increased, as shown by ELISA. HA synthase 2 (*Has2)* was upregulated in the epididymal AT and in aortic vascular smooth muscle cells of *Id3*$^{-/-}$ mice.

Functionally, HA promoted B2 cell adhesion in adipose tissue and on smooth muscle cells from *Id3*$^{-/-}$ mice, an effect sensitive to hyaluronidase. In conclusion, our data suggest that lack of *Id3* reduces HFD-induced AT weight gain and activates *Has2* expression in the stromal vascular fraction, leading to increased HA content in the AT. Accumulation of HA induces an increase in the B2 cell population in the AT by increasing the HA-dependent adherence of B2 cells and thus contributing to AT inflammation

Abbreviations

µl	microliter
µm	micrometre
4-MU	4-methylumbelliferone
AKC	Ammonium-Chloride-Potassium) lysing buffer
ANOVA	Analysis of variance
ApoE	Apolipoprotein E
AT	adipose tissue
BAT	Brown adipose tissue
bHLH	basic helix–loop–helix factor
BSA	Bovine serum albumin
CD	Cluster of differentiation (e.g. CD5)
cDNA	Complementary deoxyribonucleic acid
Da	Dalton
DAB	3,3'-diaminobenzidine
DAPI	4′,6-diamidino-2-phenylindole
DIO	Diet-induced obesity
dl	deciliters
DMEM	Dulbecco's Modified Eagle's Medium
DNA	deoxyribonucleic acid
ECM	extracellular matrix
EDTA	ethylene-diamine-tetraacetic acid
ELISA	Enzyme linked immunosorbent assay
F4/80	EGF-like module-containing mucin-like hormone receptor-like 1
FACS	Fluorescence-activated cell sorting
FBS	fetal bovine serum
g	Gramm
g	gravity
GAG	Glycosaminoglycan
GlcA	D-glucuronic acid
GlcNAc	N-acetyl-D-glucosamine
h	hour
HA	hyaluronic acid
HABP	hyaluronic acid binding protein
HAS	hyaluronan synthase
HDL	high-density lipoprotein
HEPES	4-(2-hydroxyethyl)-1-piperazineethanesulfonic acid
HFD	High fat diet
HLH	helix–loop–helix factor
HMW-HA	High molecular weight HA
HRP	horseradish peroxidase
HYAL	Hyaluronidase
Id3	Inhibitor of differentiation 3
Id3$^{-/-}$	*Id3*-deficient mouse

IFN	Interferon
IgG	immunoglobulin G
IL	Interleukin
IMT	intima-media thickness
IR	insulin resistance
Kb	Kilo Base
kg	Kilogramm
KRH	Krebs-HEPES buffer
LMW-HA	Low molecular weight HA
LPS	lipopolysaccharide
LYVE	Lymphatic vessel endothelial HA receptor
mg	Milligram
ml	Milliliter
mmHg	millimetre of mercury
NaOH	Sodium Hydroxide
Ng	nanogram
PBS	Phosphate buffered saline
PEB	protein extraction buffer
PFA	Paraformaldehyde
qPCR	Quantitative polymerase chain reaction
RNA	Ribonucleic acid
ROI	region of interes
ROS	reactive oxygen species
RT	room temperature
SAA3	adipocyte-derived serum amyloid A3
SAT	subcutaneous adipose tissue
SD	standard deviation
SLRPs	Small leucine rich proteoglycans
SMC	smooth muscle cell
SNP	single nucleotide polymorphism
SVF	stromal vascular fraction
T2DM	Type 2 Diabetes
TG	triglyceride
TGF-β	transforming growth factor beta
TNF	Tumour necrosis factor
U	Unit
UDP	Uridine diphosphate
VAT	visceral adipose tissue
VEGFA	Vascular endothelial growth factor A
VSMC	Vascular smooth muscle cell
WAT	White adipose tissue
Wt	Wild type

Contents

1. Introduction

1.1 Obesity

Obesity is one of the major health problems worldwide and its prevalence has increased alarmingly over the past decades. One of the main characteristics of obesity is excessive accumulation of fat, which begins to expand when energy intake exceeds energy expenditure[2]. Research over the past years has shown that not all fat depots in the body have the same characteristics and function and hence pathogenicity induced by obesity depends strongly on the location as well as the amount of body fat[3].

Overnutrition in combination with a sedentary lifestyle can lead to obesity, which is often paralleled with metabolic syndrome: a cluster of several known cardiovascular risk factors[4,5]. According to the literature, the criteria to identify metabolic syndrome are: waist circumference over 40 inches (men) or 35 inches (women), blood pressure over 130/85 mmHg, fasting triglyceride (TG) level over 150 mg/dl, fasting high-density lipoprotein (HDL) cholesterol level less than 40 mg/dl (men) or 50 mg/dl (women) and fasting blood sugar over 100 mg/dl[6].

Further, the rise in obesity is accompanied with increased prevalence of type 2 Diabetes mellitus (T2DM), which is also becoming one of the most serious diseases worldwide[7]. T2DM and the metabolic syndrome are very closely related, since diabetic patients have an increased risk of cardiovascular diseases[8].

1.1.1 Glucose homeostasis in obesity

T2DM is a complex chronic disease, characterized overall by impaired glucose homeostasis. Glucose homeostasis depends on the balance between insulin secretion and insulin action. Insulin is the main glucoregulatory hormone and is secreted by the β-pancreatic cells in response to increasing plasma levels of glucose, for example following a meal. Its main function is to lower the levels of blood glucose by mediating its uptake and utilization[9]. Insulin can

have a direct action, for example in white adipose tissue, where it suppresses lipolysis and increases glucose transport and lipogenesis, or an indirect action on specific target tissues[10]. The main counter-regulatory molecule of insulin is glucagon, which is secreted by the α-pancreatic cells when there is a fall in blood glucose levels and promotes glucose production by the liver[11,12].

In T2DM, deterioration in insulin secretion by the pancreas occurs, along with peripheral insulin resistance (IR), which together ultimately lead to hyperglycaemia. IR is a pathological state in which cells, such as adipocytes, fail to respond properly to insulin[13]. IR is a common characteristic of many metabolic disorders and strongly correlated with caloric imbalance. IR can be a consequence of obesity and obesity-induced comorbidities, as shown by a study where IR was observed in different mouse models of obesity[14]. In that study, increase of pro-inflammatory cytokines and macrophages was associated with disrupted insulin action and signalling, leading to IR[14]. Many of the events that lead to IR are also observed during obesity-related adipose tissue inflammation, which will be addressed in the next Sections.

1.2 Adipose tissue (AT)

Body fat or adipose tissue (AT) is a loose, connective tissue that consists of a variety of cells, such as white or brown adipocytes, which predominate, fibroblasts, endothelial cells, smooth muscle cells as well as immune cells. All these cells secrete important adipokines, cytokines, and hormones, mediating adipose tissue function[15]. AT is a complex organ and plays a major role in regulating nutritional homeostasis and energy balance, not to mention the mechanical support for important organs[16]. Morphologically, AT can be classified in white, beige, and brown AT, with white being more prevalent and biologically important.

White adipose tissue (WAT) is anatomically distributed in different parts of the body in humans and rodents, with two main compartments: visceral adipose tissue (VAT), which also includes

omental fat and subcutaneous adipose tissue (SAT). In humans, VAT depots can be found around the heart and vessels (perivascular AT) and the intraabdominal organs (mesenteric, perigonadal, perirenal, and retroperitoneal AT). SAT is distributed throughout the human body and can be divided into upper (abdominal) and lower (gluteofemoral) SAT[17]. In rodents, VAT is found in the perigonadal region (epididymal in males and periovarian AT in females) as well as in retroperitoneal fat depots on the kidneys and the mesenteric fat pad alongside the intestinal tract. Epididymal AT is typically the largest depot and the one most commonly used in research[18]. Regarding SAT, rodents only have two main depots, anterior and posterior SAT. An important subtype of VAT is omental fat. In humans, omental fat is a large, peritoneal fat pad that covers the abdominal organs and is connected to the spleen, stomach, colon and pancreas. In mice, omental fat is a thin strip of fat found close to the stomach and connected to the pancreas[19]. This type of VAT presents important differences in its composition compared with epididymal or subcutaneous AT, since it contains the “milky spots”, which are clusters of leukocytes embedded in the omental tissue[20].

Functionally, WAT is the responsible organ for energy storage, as white adipocytes undergo hypertrophy (to increase in size) and hyperplasia (to increase in number) in order for the adipose tissue to expand and store triglycerides, which can be used by the body during exercise or periods of fasting[21]. However, in response to nutrient excess, white adipose tissue and specifically the visceral depots, can expand uncontrollably, altering AT function and leading to a pathological condition called visceral adiposity[22].

Brown AT (BAT) is formed during early foetal development, while formation of beige fat is induced within WAT later in life with a process called browning of WAT[23]. Brown and beige adipocytes have similar properties: they carry a large number of mitochondria, hence the characteristic brown colour, and they utilize mitochondrial UCP1 to uncouple ATP and dissipate chemical energy as heat[21]. In humans, BAT is located in axillary, cervical, perirenal, and periadrenal regions and is found at its largest size at birth. BAT starts

decreasing with age and is considered to be of minor importance in adults, although scientific interest in brown fat is rising considerably[24]. The functions of BAT and beige fat include mainly thermogenesis, in order to maintain body temperature, regulation of energy balance and body weight and control of glucose and lipid metabolism[25].

1.2.1 Obesity-induced AT inflammation

Visceral adiposity is defined as increased adipose tissue surrounding the intraabdominal organs. It is characterized by chronic, low-grade AT inflammation. Almost 2 decades ago it was shown that the pro-inflammatory cytokine tumour necrosis factor α (TNF-α) was overexpressed in the AT of obese mice and humans, while TNF-α neutralization in obese mice improved insulin sensitivity and glucose metabolism[26,27].

A key event that takes place during obesity-induced AT inflammation and has been well established in the literature, is macrophage infiltration[28]. In a study from 2002, it was demonstrated that the population of macrophages in the AT increases during obesity and that this immune cell type is responsible for almost all AT production of pro-inflammatory molecules linked with obesity. Moreover, macrophages recruited in the AT in response to obesity presented pro-inflammatory properties, meaning that there was a phenotypic switch from the protective, anti-inflammatory M2 to the pro-inflammatory M1 macrophages, which contribute to insulin resistance[29,30]. In a subsequent study, it was demonstrated that T cells also increase in number during obesity and that the recruitment of macrophages in the AT is initiated by activated $CD8^+$ T cells, thus involving another immune cell type in the progress of AT inflammation and insulin resistance[31].

Another major lymphocyte population is B cells, whose involvement in AT inflammation has not been studied so thoroughly. B cells are involved in both adaptive and innate immunity and are divided in two major, developmentally distinct classes: B1 and B2 cells, with B1

cells being further divided into $CD5^+$ B1a and $CD5^-$ B1b subtypes[32]. Research has shown that B cells are increased in the AT of mice in the early stages of obesity. In diet-induced-obese (DIO) mice fed an obesity diet for only 3 weeks, B cells, and in particular B2 cells, were increased even at that early time point, an event that preceded the accumulation of T cells and macrophages and was correlated with insulin resistance and glucose intolerance[33,34]. Interestingly, total depletion of B cells attenuated high-fat-diet (HFD) -induced AT inflammation and insulin resistance and decreased the secretion of pro-inflammatory cytokines[35]. In the same way, transfer of B cells from obese mice into B-cell–deficient mice worsened the glucose tolerance of these mice, pointing to the significance of B cells in inducing the inflammatory/insulin-resistant state in the obese AT[34,36].

The events that lead to obesity-induced AT inflammation are described in **Figure 1**. All the above-mentioned immune cells are crucially involved in the AT inflammatory state and elucidating the underlying mechanisms is of paramount importance for the design of future therapies against obesity.

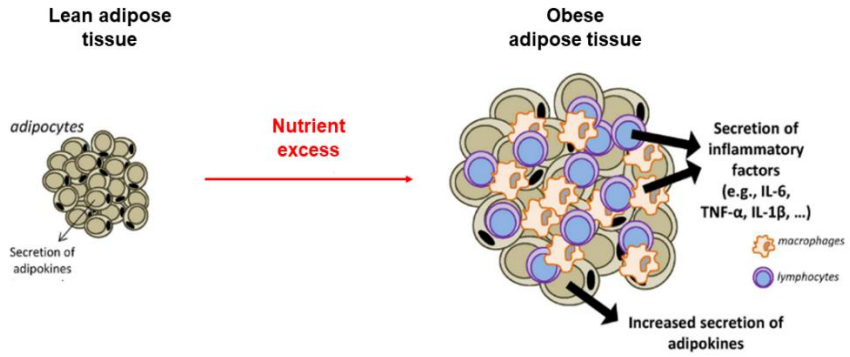

Figure 1: Chronic low-grade adipose tissue inflammation during obesity. Overnutrition leads to alterations in adipose tissue, which expands and increases the secretion of adipokines and inflammatory factors. Recruitment of immune cells, such as macrophages and lymphocytes (B and T cells) in the adipose tissue is also responsible for the secretion of inflammatory cytokines, leading to chronic, low-grade inflammation. Modified from Castanon *et al* [37].

1.3 Extracellular Matrix (ECM)

ECM is an intricate, three-dimensional, non-cellular network present within all tissues and organs. ECM consists of many different molecules such as collagens, proteoglycans, glycosaminoglycans, elastin, fibronectin, laminins, and several other glycoproteins, which are secreted by different cells[38]. The exact composition of the ECM varies among different tissues. Generally, the ECM can be divided in two major categories that differ in composition and structure: the interstitial and pericellular matrix. The interstitial matrix surrounds cells in connective tissues, whereas the pericellular matrix is in close contact with the cells, with one example being the basement membranes[39,40].

Functionally, ECM provides structural support for tissues, while it also facilitates biochemical and mechanical processes of tissue-resident cells, such as cell adhesion, migration, proliferation, repair and survival[39]. For this purpose, the ECM components interact not only with each other, creating a complicated architectural scaffold, but also with the surrounding cells, through specific cell surface receptors, called integrins[41]. There are 24 distinct integrins in mammals, that participate mainly in cell adhesion[42]. Integrins bind to ECM components and can activate intracellular signalling pathways through the plasma membrane, thus playing important roles in development, immune responses, as well as in many human diseases[43,44].

Under pathological conditions, ECM undergoes a dynamic remodelling and integrin expression is altered. For example, during osteoarthritis, cancer and pathological processes like fibrosis, ECM degradation and disorganization take place and pro-inflammatory cytokines are secreted by immune cells, leading to inflammation and creating a loop of further alterations to the ECM structure and function[45–48].

The main components of the ECM as mentioned before, are glycosaminoglycans, like hyaluronan and several proteoglycans, for instance biglycan, decorin, aggrecan and versican. These molecules

will be described in the next Sections, as they are of great importance for the present study.

1.3.1 Hyaluronan (HA)

1.3.1.1 Structure, synthesis, and degradation

Hyaluronan (HA) is an unbranched polysaccharide and an important component of the ECM that can be found in every tissue and body fluid of vertebrates. The chemical structure of HA is simple and consists of repeating disaccharides of β (1,4)-N-acetyl-d-glucosamine (GlcNAc) and β (1,3)-d- glucuronic acid (GlcUA), classifying HA in the group of glycosaminoglycans (GAGs) **(Figure 2A)**. However, HA presents major differences from the other GAGs: it does not bind covalently to any proteoglycan core proteins, is non-sulfated and is not synthesized in the Golgi apparatus, rather than within a complex on the cytoplasmic surface of the plasma membrane[49,50].

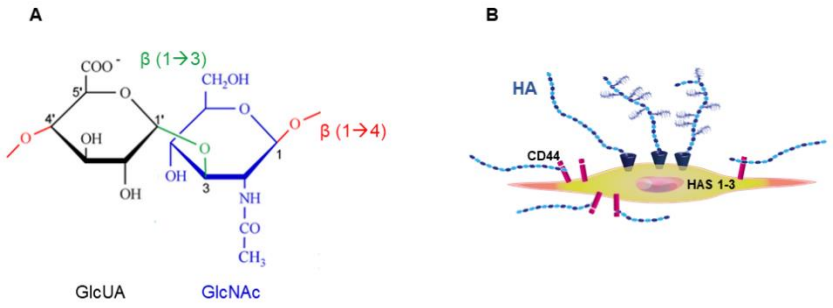

Figure 2: Structure of hyaluronan. **A**. The repeating disaccharide units of N-acetyl-β-D-glucosamine (GlcNAc) and β-D-glucuronic acid (GlcUA) linked via alternating β-1,3 and β-1,4 glycosidic bonds. **B.** HA is synthesized by 3 membrane-bound isoenzymes, namely HAS1-3. Modified from Arantes *et al* [51].

There are three, independently regulated, membrane-bound enzymes that synthesize HA in mammals, namely HAS1, HAS2 and HAS3, which are encoded by the respective genes **(Figure 2B)**. The three HAS isoenzymes use cytoplasmic uridine diphosphate (UDP) - GlcNAc and UDP-GlcUA to polymerize the HA chain, which is released in the extracellular space. The most abundant HAS in

mammalian tissue is HAS2, whereas HAS3 is mostly found under certain conditions. Analysis has shown that HAS isoenzymes may have different functions, for example during development or in terms of the length of the HA chain produced. Genetic deletion of *Has1* and/or *Has3* in mice does not induce any significant phenotype under normal conditions. However, *Has2* deletion leads to impaired cardiac development and ultimately to embryonic lethality[52,53]. Moreover, HAS1 and HAS2 were shown to produce large-sized HA, whereas HAS3 produces lower molecular mass HA[54]. The activity of the HAS isoenzymes also differs and is controlled by several growth factors, cytokines or signalling molecules, such as platelet-derived growth factor (PDGF), epidermal growth factor (EGF), TNF-α, or prostaglandins and other hormone-type molecules[55].

The molecular weight of HA is also of great importance for its function. High-molecular-weight (HMW) HA predominates under normal conditions and it usually has a size of more than 1000 kDa[56]. However, under inflammatory conditions or injury, low-molecular-weight (LMW) HA is preponderant, with different biological functions from HMW HA[57]. Fragmented HA can be a result of altered HA synthesis and degradation, which both increase under pathological conditions[58]. LMW HA can also accumulate through fragmentation by reactive oxygen species (ROS)[59].

Degradation of HA is regulated by enzymes called hyaluronidases (HYAL). Hyaluronidases belong to the class of endoglycosidases and hydrolyse the β-endo- N-acetylglucosamine bonds between GlcNAc and GlcUA, leading to the breakdown of HA. In humans, 6 transcriptionally active genes (*Hyal1, Hyal2, Hyal3, Hyal4,* and *PH-20/Spam1*) along with one pseudogene (*Phyal1*), that encodes for hyaluronidase-like sequences have been identified so far, with *Hyal1* and *Hyal2* being the most prominent ones[60]. In mice, there are also 6 Hyal-like sequences that present great homology with the human ones.

1.3.1.2 Receptors of HA and HA binding proteins

The multiple roles that the HA matrix plays are interdependent with the various hyaladherins and the different HA receptors, such as CD44, receptor for hyaluronan-mediated motility (RHAMM) and lymphatic endothelial receptor 1 (LYVE1). RHAMM is a hyaladherin expressed on the cell surface (designated as CD168) and in the cytoplasm. HA-RHAMM interactions affect cell proliferation and migration[61]. LYVE1 is lymph-specific HA receptor on the lymph vessel wall of humans and mice and is involved in the transport of HA from tissue to lymph[62].

The most important receptor of HA is CD44, which is a glycoprotein expressed broadly in many cell types. CD44 is encoded by one gene but it can be found in many isoforms, due to post-transcriptional modifications[63]. CD44 has multiple receptor functions regarding cell-cell interactions and cell-matrix interactions[64]. The HA binding properties of CD44 are determined by the isoform and the cell type on which it is expressed[65]. HA-CD44 binding affects the aggregation, proliferation, and migration of cells, while it is also important for angiogenesis and in many pathological processes[66].

1.3.1.3 Role of HA in inflammation

A growing body of literature has investigated the relationship between HA and inflammation. For example, elevated HA levels were first detected in synovial fluid of arthritis patients several decades ago, as well as in patients with other respiratory diseases, for instance pulmonary fibrosis and asthma[67–69]. Moreover, LMW HA was shown to contribute to chronic inflammation by inducing the expression of inflammatory genes in certain cell types, such as Interferon γ (IFN-γ) expression in macrophages[70]. HA is also involved in monocyte recruitment after injury, as it creates a complex with adipocyte-derived serum amyloid A3 (SAA3), promoting monocyte adhesion and chemotaxis.

This finding was further confirmed when digestion of HA with hyaluronidase decreased in part the infiltration of monocytes[71].

Furthermore, HA was increased in inflamed intestinal tissue, promoting the recruitment of immune cells into the tissue and their interaction with the matrix[72].

Interactions of the HA receptors such as CD44 are also responsible for promoting inflammation. Research has revealed that CD44 can mediate the rolling of leukocytes on activated endothelial cells, facilitating their migration to the site of inflammation[73]. Moreover, CD44 was found to facilitate the migration of neutrophils to the endothelium, a phenomenon that was dependent on the presence of HA[74]. Inhibition of CD44 function and/or its ability to interact with HA led to decreased recruitment of macrophages to the aorta in *Apoe*$^{-/-}$ mice[75].

1.3.1.4 HA in metabolism

Significant research has been carried out regarding a possible involvement of HA in metabolic function and many studies argue towards a strong correlation with diabetes. In more detail, serum HA was elevated in diabetic patients compared with non-diabetic subjects[76], and it was subsequently associated with impaired vascular function in these patients[77]. Moreover, HA was increased in diabetic rats and in the injured aorta of insulin-resistant rats, along with increased hyaluronidase production and HA degradation[58,78].

Further, a study revealed that HA was increased in the skeletal muscle of HFD-fed C57BL/6J mice, followed by insulin resistance[79]. Specifically, Kang *et al* found that after HFD, HA content in the skeletal muscle was elevated and that administration of hyaluronidase decreased HA levels, in parallel with an improvement in insulin action.

Association of HA with AT function has also been discussed, although not quite extensively. It is known that HA is increased in 3T3-L1 adipocytes during differentiation, with possible implications in the development of adipose tissue[80]. Moreover, HA secreted by hypertrophic adipocytes *in vitro* was increased, while an increase of HA was also observed *in vivo* in the AT of two different mouse

models of obesity[71]. In both of these cases, the effect was attributed to *Has2* upregulation[71]. Moreover, HA was found in the AT of HFD-fed mice, while its content was decreased after hyaluronidase injection -a finding very important for the present study. Together with the reduction in HA, a decrease in the expression of the pro-inflammatory markers IL-12 and IL-1b in the AT was observed[79].

In summary, studies have proven that HA is strongly correlated with insulin resistance and HFD–induced dysmetabolism and that inhibition of HA synthesis could have beneficial outcomes.

1.3.1.5 Pharmacological inhibition of HA synthesis

4-Methylumbelliferone (4-MU) or “hymecromone” is a derivative of coumarin and a drug that is used safely by humans as a prescription-free choleretic drug. 4-MU has been discussed in the literature regarding its abilities to inhibit HA synthesis in a number of different cell types[81–83]. Regarding the mechanism of action, 4-MU antagonizes with endogenous substrates for UDP-glucuronyltransferase, an enzyme involved in HA synthesis. As a result, the available for the HAS isoenzymes UDP-GlcUA decreases and is consumed by 4-MU glucuronidation, thus inhibiting HA synthesis[84]. Furthermore, the precursors of GlcUA and GlcNAc accumulate and probably participate in other catabolic pathways. It has also been suggested that 4-MU reduces the expression of *Has2* and *Has3*, thereby reducing HA synthesis[85].

Inhibition of HA synthesis though 4-MU has been found to play a role in ameliorating inflammation. For example, administration of 4-MU reduced the production of the pro-inflammatory cytokines IL-1 and IL-6 in mice with lipopolysaccharide (LPS) -induced lung inflammation[86]. Moreover, treatment with 4-MU had a beneficial effect in a mouse model of renal ischemia-reperfusion injury, by decreasing plasma HA and preventing kidney inflammation[87]. 4-MU-mediated inhibition of HA synthesis was also associated with decreased proliferation of T cells and reduced levels of certain pro-inflammatory cytokines[81]. However, Nagy *et al* showed that long treatment with 4-MU can have

detrimental effects, since it has been linked with increased atherosclerosis in HFD-fed *Apoe*$^{-/-}$ mice, probably through damage of the glycocalyx[82].

A few studies have also examined the possible impact of HA synthesis inhibition by 4-MU on metabolic function. Research showed that HFD-fed mice treated with 4-MU had improved hyperlipidaemia and hyperglycaemia[88]. More recent research revealed that when HA synthesis was systemically inhibited by 4-MU, the expression of thermogenic markers in brown AT was induced, which in turn led to improved glucose tolerance and insulin resistance[89].

The above-mentioned studies provide evidence that 4-MU could be used as an anti-inflammatory treatment aiming at reducing HA production and thus mitigating the consequences of inflammation. Since 4-MU is established as a safe drug to be used by humans, it could potentially be used as a therapeutic strategy inhibiting HA synthesis for several diseases.

1.3.2 Proteoglycans (PGs)

PGs are a heterogenous group of molecules that consist of a core protein to which one or more GAG chains, such as chondroitin sulfate, dermatan sulfate, keratan sulfate, heparin or heparan sulfate, are covalently attached[90] **(Figure 3).** They can be divided into 4 families based on their localization: intracellular, cell surface, pericellular and extracellular PGs. Within each family, there are different classes of PGs depending on their size, protein core or the GAGs attached[91].

Regarding intracellular PGs, the only molecule of this group that has been identified so far is serglycin, which is covalently attached with heparin and regulates inflammation[91,92]. In the class of cell surface PGs, there are thirteen genes that either encode for transmembrane proteoglycans, such as syndecans and glypicans, or for GPI-anchored proteoglycans[91]. Syndecans can have multiple biological

functions and they are involved in many pathologies, including different cancers, as well as wound healing and inflammation, mostly by binding with different growth factors via their GAGs[93]. Pericellular PGs are associated with the surface of many cell types anchored via integrins or other receptors and include perlecan and agrin[91].

Of note, the largest family of PGs is the extracellular proteoglycans, which is divided into two classes: the hyalectans and the small leucine-rich proteoglycans (SLRPs). Hyalectans are HA-binding PGs with a common structure, such as versican and aggrecan. The SLRPs class contains 18 genes. SLRPs have a relatively small protein core with a central region constituted by leucine-rich repeats: The members of this family are further divided into five classes depending on protein, genomic homology and chromosomal organization[94]. SLRPs can interact with collagen and are involved in the stabilization and organization of collagens and elastic fibers, cell-matrix interactions, ECM structure and tissue function, while they also participate in many signalling pathways[95]. Biglycan and decorin are the two most studied SLRPs and will be addressed separately in the next Sections.

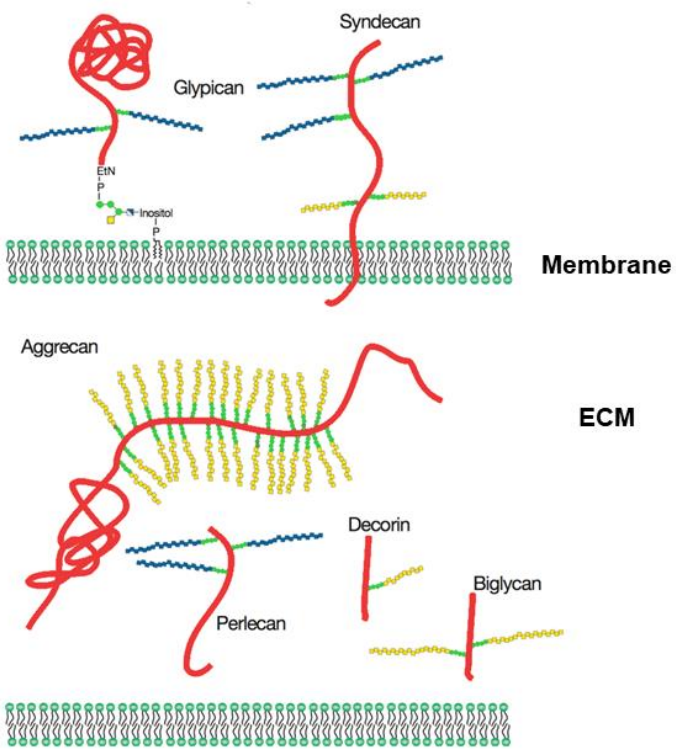

Figure 3: Structure of proteoglycans. Proteoglycans consist of a protein core (red) and one or more covalently attached glycosaminoglycan chains: blue, heparan sulfate; yellow, chondroitin sulfate/dermatan sulfate. Membrane proteoglycans are either associated with the plasma membrane or are linked by a GPI anchor. ECM proteoglycans are usually secreted, but some proteoglycans can be proteolytically cleaved and shed from the cell surface. Modified from Li *et al* [96].

1.3.2.1 Biglycan

Biglycan belongs to the group of SLRPs, and it has two GAG chains attached in its protein core. In humans, it is encoded by one gene (*BGN*) located on the X chromosome, which is translated to a 42 kDa protein core where one or two GAGs are bound[97]. Biglycan is expressed ubiquitously and interacts with many other components of the ECM, such as collagen[97]. Biglycan was first discovered in the developing bone almost 40 years ago, and since then it has been shown to play a vital role in many processes, for example in skeletal growth, innate immunity and in many human pathological conditions[97,98]. Furthermore, biglycan is abundant in the human aorta and studies have demonstrated that biglycan deficiency was associated with increased aortic aneurysm development and promotion of atherosclerosis in a mouse model [99].

Biglycan also has a function in the AT. An interesting study revealed that biglycan mRNA was upregulated in the epididymal AT of HFD-fed Wt mice, and that *bgn*$^{+/0}$ mice expressed and produced more adiponectin[100]. A subsequent study showed increased biglycan gene expression in the AT of mice after 8 weeks of HFD, which was correlated with AT inflammation, especially in the subcutaneous depot[101]. More recent evidence revealed that the majority of biglycan found in the AT of obese mice came from infiltrating macrophages and that macrophage-specific biglycan deletion led to a decrease in AT macrophages and inflammatory gene expression[102].

1.3.2.2 Decorin

Decorin is also a SLRP, very closely associated with biglycan, with analyses showing that their genes are more than 50% homologous at the protein level[103]. The human gene for decorin (*DCN*) is found on chromosome 12 and its protein has a size of 90-140 kDa. Decorin is expressed in many cell types and is involved in collagen fibril formation and the regulation of transforming growth factor beta (TGF-β)[104]. Furthermore, decorin is expressed in the AT, more highly in the visceral rather than in the subcutaneous fat depot[105]. In HFD-fed rats, decorin was markedly increased in the AT and skeletal muscle and was indicated to play a role in obesity-induced inflammation, although without a clear mechanism proposed[105]. In a more recent study, loss of decorin in mice deteriorated glucose tolerance, suggesting a protective role for decorin in the regulation of glucose metabolism[106]. Importantly, decorin was upregulated in the subcuatenous AT of obese humans after bariatric surgery, and particularly in the stromal vascular fraction (SVF) of this fat depot[106].

1.3.2.3 Aggrecan

Aggrecan is chondroitin sulfate and in humans it is encoded by the gene *ACAN* found on chromosome 15[107]. As a hyalectan, aggrecan binds to HA and thus aggregates are formed, contributing greatly to the complex architecture of the ECM[91]. Numerous studies have

identified aggrecan as an important component of the cartilage and more recently, of the brain[91,107]. Furthermore, aggrecan was present in human intimal hyperplasia, pointing to a possible role of this PG in vascular biology[108]. Aggrecan was also found to be expressed in the AT, where it was produced mostly by cells of the SVF[109]. In the same study, it was interestingly shown that aggrecan mRNA expression was decreased in the AT of two mouse models of obesity, while its catabolism was increased[109].

1.3.2.4 Versican

Versican is a chondroitin sulfate PG and the largest hyalectan, with structure highly similar with that of aggrecan[91]. In humans it is encoded by one gene (*VCAN*) found on chromosome 5. Functionally, versican has multiple roles in many processes, such as adhesion, migration, and inflammation. Regarding an implication in metabolism, it was shown that versican was produced mainly by adipocytes in the AT of mice that were fed a HFD and was correlated with IR, which was attenuated after adipocyte-specific deletion of versican[102]. Moreover, versican was increased in hypertrophic 3T3-L1 adipocytes and was found in the subcutaneous and omental fat depot in humans undergoing bariatric surgery[102].

1.4 Inhibitor of differentiation 3 (Id3)

1.4.1 Id proteins

Inhibitor of Differentiation 3 (Id3) is a broadly expressed transcription factor (TF) that belongs to the family of Id proteins. The Id family is part of the Superclass 1 of TFs, which contain basic DNA binding domains[110]. Superclass 1 is divided based on specific motifs, with one example being the basic-helix-loop-helix (bHLH) factors, that have a bHLH motif. bHLH factors are further categorized into classes depending on their biochemical and functional characteristics[111].

Class 1 bHLH factors or E-proteins are expressed in many tissues and can regulate transcription by forming homo- or heterodimers with other proteins of the same family; these dimers bind DNA to specific consensus sequences, termed E-Boxes[112,113]. E-Box elements contain a characteristic motif which consists of a hexanucleotide sequence, CANNTG, with N being any nucleotide. E-box sites have been found in promoters of genes expressed in muscles, neurons, pancreas and immune cells[113].

Id proteins consist a specific Class of bHLH factors that act primarily against E-proteins. Id factors lack the basic DNA binding domain that bHLH proteins have and thus are incapable of binding DNA; therefore, they are named HLH factors. Instead, they form non-functional dimers with E-proteins or other tissue-specific HLH factors and prevent them from binding DNA to the E-Box elements[114,115] **(Figure 4)**. The Id protein group consists of 4 members (Id1-4) in mammals and its members are expressed in many cell types, but their expression pattern varies considerably. Specifically, *Id2* is expressed more abundantly compared to *Id1*, which is only found in specific cell types, for instance cells of the nervous system. Furthermore, *Id1* and *Id3* expression is mostly activated during development and can be affected by certain stimuli[116]. Apart from E-proteins, Id factors can antagonize the function of other proteins that do not contain an HLH motif, such as proteins of the retinoblastoma family (Rb), or ETS-domain transcription factors[117–119].

Id proteins have evolved into negative regulators of transcription and can regulate the expression of multiple genes, for example genes that control the cell cycle or developmental processes[114].

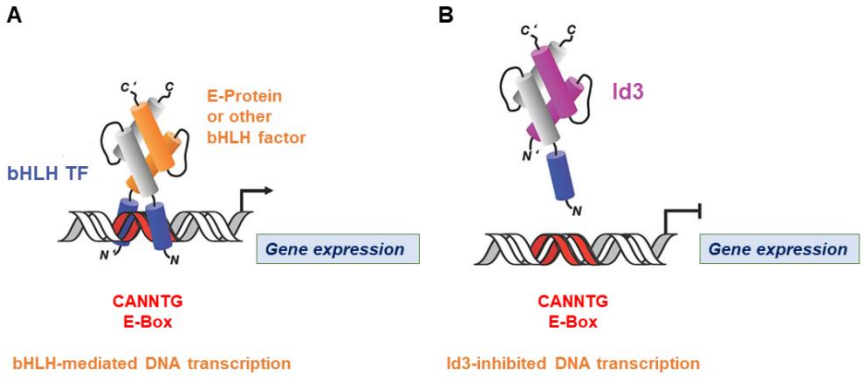

Figure 4: Id3 regulation of DNA transcription. **A.** bHLH transcription factors (TF) can form homo- or heterodimers with E-proteins or other members of the bHLH family and bind DNA at promoter consensus sites called E-boxes, functioning as transcriptional regulators, either activating or repressing genes. **B**. Id3 is an HLH factor that lacks the basic DNA binding domain and inhibits DNA transcription by forming nonfunctional dimers that are incapable of binding to DNA. Modified from Roschger *et al*[120].

1.4.2 Id3 in the vascular system

Id3 is particularly essential in the cell cycle regulation and growth of vascular smooth muscle cells (SMCs)[112,121]. Specifically, McNamara *et al* showed for the first time that *Id3* is expressed in the vessel wall and that it is important for the attenuation of neointimal SMC growth during vascular lesion formation, through post-transcriptional regulation[122]. Moreover, the same group demonstrated that *Id3* expression was increased in VSMCs of the vessel wall in a HFD-fed porcine model and that this effect was induced by hyperlipidaemia and LDL oxidation, leading to increased growth of VSCMs. Respectively, in *Id3*-deficient primary aortic SMCs the effect of oxidized-LDL on SMC proliferation was eliminated[123].

Id3 has also emerged as an atheroprotective factor. Mice deficient for both *Id3* and *apolipoprotein E* (*Id3*$^{-/-}$*Apoe*$^{-/-}$ mice) developed significantly more atherosclerosis than just *Apoe*$^{-/-}$ mice[124]. The atheroprotective function of Id3 was further investigated in a subsequent study, where it was shown that Id3 can regulate the trafficking of aortic B cells and is involved in B cell-mediated atheroprotection[125]. Moreover, experiments in *LDL receptor*-deficient mice (*Ldlr*$^{-/-}$ mice) confirmed that Id3 is important for the homing of aortic B cells and that it may act on Vascular cell adhesion protein 1

(VCAM-1) in the vessel wall, leading to reduced recruitment of monocytes/macrophages and finally atheroprotection[126].

1.4.3 Id3 in human vascular diseases

Consistently with the results from murine studies, Id3 has also been identified as an important atheroprotective factor in humans. A study from 2011 revealed that a single nucleotide polymorphism (SNP) in the human *ID3* gene (at rs11574) was significantly linked with carotid intima-media thickness (IMT), which is used to detect the presence of atherosclerosis in humans[124]. This finding was further corroborated by another study which associated the *ID3* SNP rs11574 directly with human coronary artery pathology in a large diabetic cohort[127]. Together, these studies demonstrated that Id3 could be used as a potential biomarker of atherosclerosis diagnosis in humans.

The human *ID3* gene is a small gene that spans only three exons. Six SNPs have been identified within the gene, but only the rs11574 SNP was significantly correlated with subclinical atherosclerosis in humans, as evaluated by IMT. The rs11574 SNP is located in the second exon of the coding region of the human *ID3* gene. This SNP results in a substitution of alanine with threonine at amino acid 105, that affects the function but not the expression of the gene. Specifically, the protein encoded by the variant *ID3* gene was shown to have attenuated function as an inhibitor of gene activation, affecting the regulation of many genes involved in atherosclerosis-related pathways[124].

1.4.4 Role of Id3 in AT function

There is a considerable amount of literature regarding the role of Id3 in AT function. It has been demonstrated that Id3 is present in 3T3-L1 adipocytes, but its expression is decreased early during adipocyte differentiation, preventing them to convert to adipose cells[128]. Moreover, Id3 was shown to interact with ADD1/SREBP-1c, which are transcription factors expressed mainly in the AT and are involved in lipid homeostasis[129,130]. Later, Doran *et al* reported that Id3 negatively regulates the expression of adiponectin not only *in vitro* in cultured adipocytes, but also *in vivo* in epididymal and mesenteric fat depots[131].

Furthermore, *Id3* mRNA expression was increased in the AT of HFD-fed mice and deficiency of *Id3* limited the expansion of the epididymal AT in response to HFD, pointing to a potential role of Id3 in visceral adiposity[132]. The authors demonstrated that Id3 acted on the AT through regulation of angiogenesis by decreasing the mRNA expression of the Vascular endothelial growth factor A gene (*VEGFA*)[132].

These studies clearly underscore the importance of *Id3* in adiposity. Further research is needed in order to identify how Id3 mechanistically acts on AT and affects its functions in the setting of obesity.

1.4.5 Id3 implication in B cell function

Research has shown that Id3 is involved in lymphocyte development, including B cells, mainly via interactions with E proteins[133–135]. Pan *et al* utilized the *Id3*-KO mouse model and showed that these mice contained a normal number of B cells in the spleen, lymph nodes, thymus, and bone marrow. However, in the same study, Id3 was found to have a highly specific role in B cell proliferation within the B cell receptor (BCR) signalling pathway, as B cells isolated from *Id3*-KO mice showed a proliferative defect[134]. The exact mechanism involved is beyond the scope of the present study.

Regarding other roles of Id3 in B cell biology, Doran and colleagues showed that this transcription factor is also crucial for the trafficking of B cells in the aorta in the context of atherosclerosis, as *Id3* deficiency reduced B cell homing to the aorta, through decreased CCR6 expression[125]. Id3 may also have specific roles when it comes to the different B cell subsets, as it was found to regulate specifically B1a homeostasis[136]. Moreover, mice lacking *Id3* specifically in B cells (*Id3*^{BKO}) had increased B1b cell numbers in several organs, including AT, where these cells showed a protective, anti-inflammatory effect in response to HFD[137,138].

Briefly, B1 cell subsets functions were regulated by *Id3* and were classified as anti-inflammatory. Whether Id3 is also implicated in the regulation of B2 cells, which are mostly known for their pro-inflammatory action especially in the obese AT, is currently unknown.

1.4.6 *Id3*-dependent regulation of HA-rich matrix

Preliminary experiments performed by the McNamara lab at the University of Virginia (UVa, Charlottesville) examined whether an interrelationship between Id3 and HA exists and aimed at identifying the molecular mechanism behind this. The rationale was that, since Id3 is a transcription factor expressed in many tissues and HA is an abundant molecule, a possible role of Id3 in regulating the transcription of the genes that encode for the HAS isoenzymes might exist. Briefly, using the BioMart tool from the Ensebl project (http://www.ensembl.org)[139], the sequence information was retrieved for the first 2000 bases of the promoter regions of the *Has* genes and then the E-box elements that the promoter sequences contained were manually located. The promoter of the *Has2* gene was shown to contain many E-box elements (CANNTG), whilst *Has1* and *Has3* contained fewer ones. Approximate positions of the E-boxes in the first 1000 bases of the promoter region of *Has2* gene are depicted in **Figure 5**.

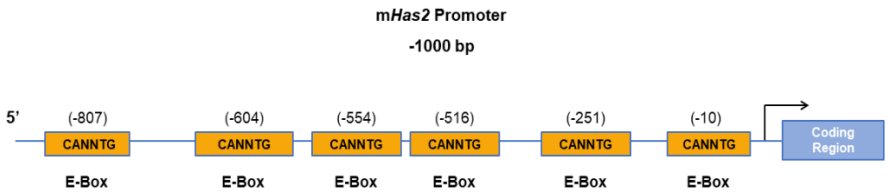

Figure 5: Illustration depicting consensus CANNTG (E-Box) Id3 binding sites located within the first 1000 bases of the mHas2 promoter region

With permission from Wolters Kluwer Health, Inc.: Misiou, A. *et al,* Helix-Loop-Helix Factor Id3 (Inhibitor of Differentiation 3) A Novel Regulator of Hyaluronan-Mediated Adipose Tissue Inflammation, *Arteriosclerosis, Thrombosis, And Vascular Biology*, 41(2), 796-807, doi: 10.1161/atvbaha.120.315588[1].

SMCs isolated from the aorta of C57BL/6J mice were transfected with *Has2* promoter-luciferase reporter construct together with increasing concentrations of h*Id3*. The results of this assay showed that the *Has2* promoter activity was inhibited in a concentration-dependent manner, with increasing amounts of pcDNAId3 **(Figure 6A)**.

Next, Wt and *Id3*$^{-/-}$ aortic SMCs were transfected with the *Has2* promoter-luciferase reporter. The *Has2* promoter activity was significantly increased when *Id3* was absent **(Figure 6B).** These data conclusively demonstrated that when *Id3* was absent, *Has2* promoter activity was stimulated, identifying *Id3* as a novel regulator of *Has2* transcription[1]. These data showed that *Id3* inhibits *Has2* transcription in VSMCs, but it is possible that it may also regulate this isoenzyme in other cell types residing in the AT. This matter will be addressed in future research.

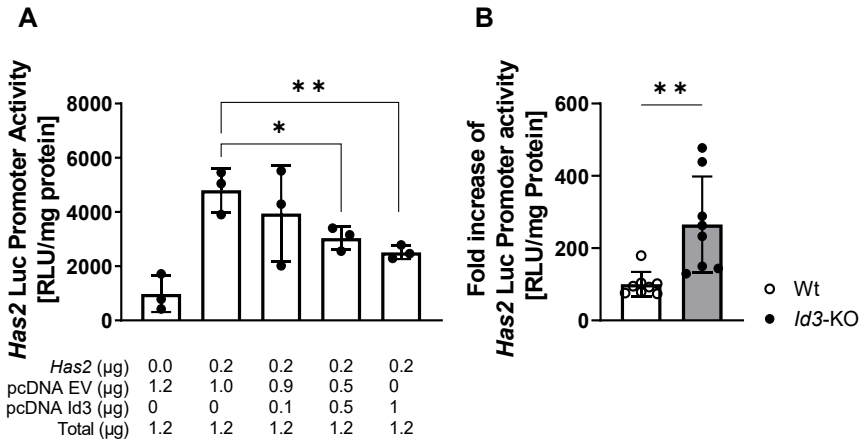

Figure 6: *Id3* suppresses *Has2* promoter activity, while loss of *Id3* stimulates *Has2* promoter activity. A. *Id3*$^{-/-}$ aortic VSMCs were transfected with 0.2 µg of the 1 Kb murine *Has2* promoter-luciferase reporter together with specified concentrations of Id3 and/or pcDNA3.1 empty vector. Presence of Id3 suppressed the promoter activity of *Has2*. Luciferase activity is normalized to protein levels. Data are the result of 3 separate experiments of duplicate samples. **B.** Mouse aortic VSMCs isolated from Wt and *Id3*$^{-/-}$ mice were transfected with 0.2 µg of the 1Kb *Has2* promoter-luciferase reporter together with 0.8 µg of empty vector. *Id3*$^{-/-}$ VSMCs showed increased *Has2* promoter activity. Luciferase activity is normalized to protein levels. Data are the result of 2 separate experiments of triplicate samples. Data represent mean ± SD; *p<0.05; **p<0.01. Experiments and data were provided by Jack Hensien and the McNamara Lab

1.5 Aim of the study

It is clear from a number of studies that Id3 is a key regulator of visceral adiposity and that it is implicated in the transcriptional control of obesity-related genes, such as adiponectin. In the same way, HA is involved in metabolic impairment and AT inflammation upon obesity. Initial work showed that the gene of one isoenzyme responsible for HA synthesis, namely *Has2*, contains multiple E-box elements in its promoter region. Our preliminary *in vitro* data using VSMCs showed that when *Id3* is absent, *Has2* promoter activity is stimulated. Taking this finding into consideration, we sought to investigate whether Id3 can regulate HA synthesis *in vivo* and more specifically in the context of AT inflammation in the setting of obesity.

The aims of the present study were to examine (a) whether HA synthases could be regulated by the transcription factor Id3 *in vivo* using a mouse model, (b) whether an *Id3*-dependent modulation of the HA-rich matrix might also be implicated in the inflammation observed in the AT upon obesity in $Id3^{-/-}$ mice and (c), in case the above aims were verified, whether pharmacological reduction of HA accumulation could ameliorate the inflammatory phenotype of $Id3^{-/-}$ mice.

Last, we aimed to expand our murine findings and translate them into human patients, investigating the effect of loss of function of the human *ID3* gene on the HA content using plasma and AT samples from two different cohorts of patients.

2. Materials and Methods

2.1 Animal experiments

All animal protocols were approved by the Animal Care and Use Committee at the University of Virginia (Approved animal use protocol: 3008).

2.1.1 Breeding schema

C57BL/6J mice were purchased from Jackson Laboratory (stock No. 000664). *Id3*$^{-/-}$ mice were a generous gift of Dr Yuan Zhang (Duke University). *Id3*-deficient mice were bred with C57BL/6J mice to generate *Id3*$^{+/-}$ mice that were used for breeding *Id3*$^{-/-}$ mice and *Id3*$^{+/+}$ littermate controls. The Id3 genotype was confirmed by PCR. Only male mice were used in this study. Female mice were excluded due to major sex-dependent differences in the development of obesity, since it has been shown that male mice develop visceral AT inflammation, glucose tolerance and insulin resistance, effects that are not seen in HFD-fed female mice, despite the similar body weight gain upon HFD[140].

2.1.2 Diets

Male *Id3*$^{+/+}$ (Wt) and *Id3*$^{-/-}$ littermates were given standard laboratory diet (Teklad LM-485, 7012, Envigo, Indianapolis IN) and water *ad libitum*. At 6-8 weeks of age and after their genotype was confirmed, mice were placed on a 60% HFD (Research Diets, D12492, New Brunswick, NJ). High-fat feeding was applied for 4 weeks.

2.1.3 4-MU treatment

Male *Id3*$^{+/+}$ (Wt) and *Id3*$^{-/-}$ littermates were divided into 4 groups: Wt and *Id3*$^{-/-}$ mice on 60% HFD and Wt and *Id3*$^{-/-}$ mice on 60% HFD supplemented with 4-MU. 4-MU has a poor taste; mice tend not to eat it, so it ultimately has an anorectic effect[141]. The HFD used in these experiments was enriched with chocolate flavour and also

contained 50g/kg 4-MU (Western Diet, S8200-E010, Ssniff Spezialdiäten GmbH, Soest, Germany), so that it would be palatable to the mice. The food intake was monitored daily throughout the whole study, in order to exclude the possibility that the changes observed were due to reduced caloric intake and not induced by 4-MU.

Before the treatment started, the mice were subjected to a pair feeding regimen for 2 weeks. Pair feeding is a technique in which the amount of food provided to a control group of mice is matched to that consumed by the experimental group (4-MU group, in this case), so as to determine the extent to which the effect of a treatment on body weight or body composition occurred independently of changes in energy intake[142]. The experimental setup is pictured in **Figure 7.** After 4 weeks of treatment, organs were harvested, and experiments were performed as it will be described in the next chapters.

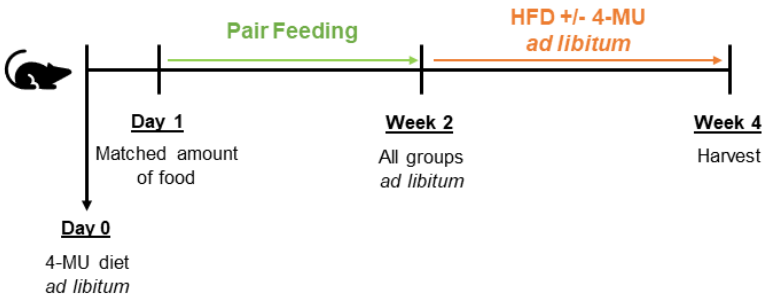

Figure 7: Schematic depiction of the 4-MU treatment setup. 8-week-old *Id3*$^{-/-}$ and Wt littermates were placed on a pair feeding regimen for 2 weeks, which was followed by 2 weeks of HFD with or without 4-MU. At the end of the treatment after 4 weeks in total, the mice were sacrificed, and tissues were harvested.

2.2 Histology and Immunohistochemistry

2.2.1 Tissue preparation

Epididymal, subcutaneous and interscapular brown AT were removed from mice and fixed for 24 hours (h) at 4°C in Roti®-Histofix 4% (Carl Roth GmbH & Co KG, Karlsruhe, Germany). Subsequently, they were dehydrated and embedded in paraffin. Using the rotary

microtome RM 2255 (Leica Microsystems, Wetzlar, Germany), embedded tissue was sliced into sections of a thickness of 5 µm and two consecutive sections were placed on one microscope slide. All lymph nodes were removed prior to analysis.

After drying for 1 day at room temperature (RT) and before staining, all tissue sections were fixed on the slide for 1 h at 60°C. Afterwards, the slides were deparaffinized as follows: three successive incubation steps with Roticlear® (Carl Roth GmbH & Co. KG, Karlsruhe, Germany) for 15 minutes each, followed by a 2-minute incubation in 100%, 95% and 75% ethanol separately in that order. Finally, the tissue sections were washed three times for 5 minutes each time in PBS.

2.2.2 HA immunostaining

To determine the HA content of the AT, deparaffinized tissue sections were treated with an avidin-biotin blocking system (Thermo Fisher Scientific, Waltham, USA) according to the manufacturer's instructions in order to block endogenous biotin structures. After that, the sections were incubated for 1 h at RT with blocking solution to prevent unspecific binding of the antibodies.

HA was visualized using biotinylated HA-binding protein (HABP) (Calbiochem, San Diego, CA, USA) as first antibody and the slides were incubated overnight at 4°C. The next day, all sections were washed with PBS and treated with 3% H_2O_2 solution to inactivate endogenous peroxidases. HABP was detected using a horseradish peroxidase (HRP)-streptavidin conjugate (Sigma-Aldrich, St. Louis, MO, USA) as a secondary antibody and 3, 3'-diaminobenzidine tetrahydrochloride (DAB) (Thermo Fisher Scientific). The secondary antibody was incubated for 1 h at RT. Cell nuclei were counterstained with hemalum solution (Merck KGaA, Darmstadt, Germany) and covered with Roti-Mount mounting medium (Roth, Karlsruhe, Germany). Immunostaining was quantified by the ImageJ Software (National Institutes of health, USA) and %area fraction in ROI was normalized to 100 cells.

2.2.3 Biglycan and decorin immunostainings

Before the tissue was stained for biglycan, a chondroitinase digestion step was included: tissue sections were incubated with chondroitinase (2U/100ul; Sigma Aldrich) diluted in ABC buffer for 1 h in a water bath at 37°C. The sections were then blocked with blocking solution as described before. Bigylcan was visualized by affinity histochemistry using biotinylated biglycan (Calbiochem, San Diego, CA, USA) as first antibody and the slides were incubated overnight at 4°C. The next day, biglycan was detected with goat anti-rabbit IgG-HRP (Santa Cruz Biotechnology Inc., Heidelberg, Germany) as a secondary antibody and DAB (Thermo Fisher Scientific). The secondary antibody was incubated for 1 h at RT. Cell nuclei were counterstained with hemalum and covered with Roti-Mount mounting medium (Roth, Karlsruhe, Germany). Immunostaining was quantified by the ImageJ Software (National Institutes of health, USA) and %area fraction in ROI was normalized to 100 cells.

For decorin visualization, the same procedure as with biglycan was followed, with biotinylated decorin being used as a first antibody.

2.2.4 Aggrecan and versican immunostainings

Aggrecan and versican were visualised using fluorescent immunohistochemistry. In the beginning of these experiments, a heat-induced antigen retrieval step was included in order to restore antigenicity and therefore the tissue sections were incubated in citrate buffer (Zytomed Systems, Berlin, Germany) for 20 minutes at 98°C. After that, the sections were subjected to chondroitinase digestion and blocked with blocking solution, as described before. For aggrecan staining, the sections were stained with rabbit anti-aggrecan antibody (Merck KGaA) and the slides were incubated overnight at 4°C in a dark chamber. The next day, the sections were stained with the secondary antibody goat anti-rabbit AF647 for 1 h at RT in a dark chamber. The slides were finally mounted with Roti-Mount FluorCare DAPI (Carl Roth) for nuclei staining.

For versican visualisation, an anti-versican antibody was used (Merck KGaA) and the same protocol was followed. Immunostaining was quantified by the ImageJ Software (National Institutes of health, USA) and %area fraction in ROI was normalized to 100 cells.

All buffers used for immunohistochemistry experiments are listed in **Table 1**.

Table 1: Buffers and solutions for immunohistochemistry.

Buffer	Composition	Company
PBS (pH 7.4)	137 mM NaCl 2.7 mM KCl 1.5 mM KH_2PO_4 8.3 mM Na_2HPO_4	
Blocking solution	20 mM Tris-HCl 137 mM NaCl 10% (V/V) FCS 1% (M/V) BSA	
3% H_2O_2	3% (V/V) H_2O_2 in PBS	
ABC buffer	0.60 g Tris 1.33 g NaOAc 0.30 g NaCl (pH 8.0 with HCl) 1 mg/ml BSA	Sigma-Aldrich Merck KGaA
1x Citrate buffer (pH 6.0)	10% (V/V) Citrate buffer (10X) in H_2O	Zytomed Systems

2.3 Flow cytometry

2.3.1 Isolation of stromal vascular fraction (SVF)

Epididymal stromal vascular fraction was isolated as previously described and is depicted in **Figure 8**[132,143]**.** AT was minced with scissors and digested with Collagenase type I (Worthington Biochemical Company, Lakewood, NJ, USA) (1 mg/ml) in KRH buffer containing 2.5% BSA for 45 minutes in a shaking incubator at 37°C.

Cell suspension was then centrifuged at 400 x *g* for 5 minutes. The pellet containing the SVF was treated with AKC lysis buffer to lyse remaining red blood cells and then filtered through a 70 µm. Lysis was stopped using FACS buffer and cells were centrifuged at 400 x *g* for 5 minutes.

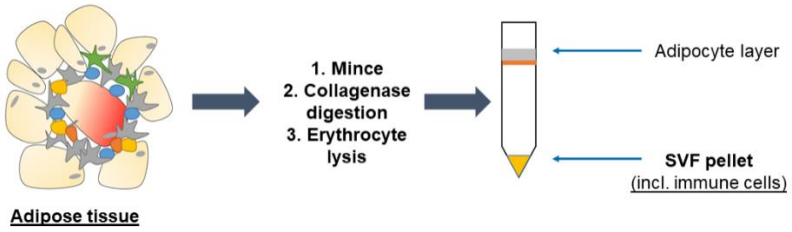

Figure 8: AT digestion and isolation of SVF. AT is minced with scissors and digested with Collagenase type I for 45 minutes in a shaking incubator at 37°C. Cell suspension is centrifuged at 400 x *g* for 5 minutes, treated with AKC lysis buffer and filtered through a 70 µm nylon mesh cell strainer. Lysis is stopped using FACS buffer and cells are centrifuged again. The remaining pellet is the SVF, which is used for flow cytometry staining. Modified from Vu *et al*[144].

2.3.2 Flow cytometry staining protocol

After centrifugation, the cells in the pellet were incubated with Fc-block (FCR-4G8, Invitrogen) diluted in FACS buffer for 10 minutes on ice prior to staining. All cells were stained with LIVE/DEAD fixable yellow cell staining (Invitrogen) in PBS for 30 minutes at 4°C to determine viability and then washed with FACS buffer. Cells were stained on ice and protected from light for 20 minutes. Antibodies were diluted in FACS buffer. All buffers used in flow cytometry experiments are listed in **Table 2.** Murine flow cytometry antibodies were used as depicted in **Table 3.** Cells were run on a CyAN ADP Analyzer (Beckman Coulter Inc., CA, USA). Data were analysed with FlowJo Software (BD, Ashland, OR, USA) using fluorescence minus one (FMO) controls for gate determination when appropriate. Counting beads (CountBright™ Absolute Counting Beads, Molecular Probes) were used for quantitation. Each immune cell was identified by a pattern of surface epitopes alone or in combination with intracellular proteins, as shown in **Table 4.**

Table 2: Buffers used for flow cytometry experiments.

Buffer	Composition	Company
KRH buffer (pH 7.4)	130 mM NaCl, 4.7 mM KCl 1.24 mM $MgSO_4$ 2.5 mM $CaCl_2$ 1 mM HEPES 2.5 mM KH_2PO_4 5 mM D-glucose 200 nM adenosine,	
Digestion buffer	1 mg/mL collagenase type I in FACS buffer or DMEM	Worthington Biochemical Company
AKC lysis buffer	0.15 M NH_4Cl 0.01 M $KHCO_3$ 0.1 mM EDTA in ddH_2O	
FACS buffer	0.1% NaN_3 1% BSA in PBS	

Table 3: Antibodies for flow cytometric staining.

Target Antigen	Fluorochrome	Company	Clone	Working concentration
B220	APC eF780	InVitrogen	RA3-6B2	2 µg/ml
CD45	PerCP	BD Biosciences	30-F11	1 µg/ml
CD19	PeCy7	Biolegend	1D3	2 µg/ml
CD5	eF450	InVitrogen	53-7.3	1 µg/ml
IgM	APC	Biolegend	RMM-1	1 µg/ml
CD3e	eF450	InVitrogen	145-2C11	1 µg/ml
F4/80	APC	InVitrogen	BM8	1 µg/ml
CD206	PE	Biolegend	C068C2	0.5 µg/ml
CD11c	eF780	eBioscience	N418	2 µg/ml
LIVE/DEAD	Yellow	InVitrogen	-	1:300

Table 4: Marker combinations for the identification of immune cells.

Immune cell	Marker combination for identification
Lymphocytes	$CD45^+$
B Lymphocytes	$CD3^-CD19^+$
B1 Lymphocytes	$CD19^+B220^-$
B2 Lymphocytes	$CD19^+B220^+$ (IgM^+)
B1a Lymphocytes	$CD5^+IgM^+$
B1b Lymphocytes	$CD5^-IgM^+$
T Lymphocytes	$CD3^+CD19^-$
Macrophages	$F4/80^+CD11b^+$
M1 macrophages	$CD206^-CD11c^+$
M2 macrophages	$CD206^+CD11c^-$

2.4 HA quantification in the plasma

After 4 weeks of HFD, mice were sacrificed by CO_2 inhalation. Blood was collected via heart puncture of the right ventricle prior to perfusion with PBS and was anticoagulated with 100 mM ethylenediaminetetraacetic acid (EDTA) in isotonic sodium chloride solution. EDTA-anticoagulated blood samples were used for the generation of plasma: whole blood was centrifuged at 6,500 x *g* for 5 minutes at 4°C. The supernatant was carefully collected and placed into a new Eppendorf tube and stored at -80°C.

HA was quantified in the plasma by enzyme-linked immunosorbent assay (ELISA) according to the manufacturer's instructions (Corgenix, Broomfield, CO, USA) and the measured concentration was given in ng/ml.

2.5 Gene expression

For gene expression analysis, AT samples were directly snap-frozen in liquid nitrogen.

2.5.1 RNA extraction

Total RNA was isolated using the RNeasy Plus kit (Qiagen, Valencia, CA, USA). First, the tissue was placed in 1 ml Trizol in labelled MP BioMed Lysing Matrix Tubes (MP Biomedicals, Germany) containing 1.4 mm ceramic lysing beads. Tissue was homogenized using the MP BioMed shaker and were shaken three times for 15 seconds at 4°C, with a 1-2 minutes cooling between shakes. Samples were then centrifuged at 12,000 x *g* for 10 minutes at 4°C. For SVF RNA isolation, the supernatant was removed carefully avoiding lipid accumulation and was placed in a new Eppendorf tube. For adipocyte RNA, the pink layer containing adipocytes was isolated using a 1ml/cc syringe with a 25Ga needle and transferred to a new Eppendorf tube. The procedure for RNA extraction was the same for all samples. After addition of chloroform, samples were centrifuged at maximum speed for 15 minutes at 4°C. Next, isopropyl alcohol was added, samples were incubated for 10 minutes and centrifuged again under same conditions. At this point, RNA was visible as a pellet. The pellet was washed with 1 ml 70% EtOH and centrifuged. The pellets were let to air dry for 5 minutes and then the RNA was re-suspended in 20-30 µl of RNA secure and incubated for 10 minutes in water bath at 55°C. The RNA concentration as well as the quality of the RNA was determined using a NanoDrop™ 1000 Spectrophotometer (Thermo Fisher Scientific) by measuring the absorption at 230 nm, 260 nm and 280 nm.

2.5.2 cDNA synthesis

1 µg of total RNA was converted to cDNA using the iScript cDNA synthesis kit (BioRad, Hercules, CA, USA). Total cDNA was diluted 1:10 in water and 3 µl were used for each real-time PCR reaction

using a BioRad CFX-96 iCycler and SensiFast SYBR Supermix (Bioline, Taunton, MA, USA).

2.5.3 Quantitative Realtime-PCR (qPCR)

To quantify gene expression, cDNA was diluted in water as needed and combined with 0.5 mM of forward and reverse primers, suitable for each experiment, and SYBR Green (SensiFast, BioLine). Semiquantitative real-time PCR was performed on a CFX96 Real-Time System (BioRad). For comparison of relative mRNA expression levels, results were normalized to 18S ribosomal RNA (*18S rRNA*) using the $2^{-\Delta\Delta Cq}$ method. Primer sequences are listed in **Table 5.**

Table 5: Primers used for qPCR.

Gene	*Symbol*	Primer sequence
18s ribosomal RNA	*Rn18s*	5'- GCAATTATTCCCCATGAACG -3' 5'- GGCCTCACTAAACCATCCAA -3'
hyaluronan synthase 1	*Has1*	5'- TATGCTACCAAGTATACCTCG -3' 5'- TCTCGGAAGTAAGATTTGGAC -3'
hyaluronan synthase 2	*Has2*	5'- CAAAAATGGGGTGGAAAGAG -3' 5'- ACAGATGAGGCAGGGTCAAG -3'
hyaluronan synthase 3	*Has3*	5'- CTCAGTGGACTACATCCAGG -3' 5'- GACATCTCCTCCAACACCTC -3'

2.6 HA Binding Assay

2.6.1 Cryosections

Epididymal AT was isolated from Wt and *Id3*$^{-/-}$ mice and was immediately placed in plastic Cryomolds (Tissue-Tek, Sakura, The Netherlands), where it was covered with O.C.T. compound (Tissue-Tek, Sakura). Samples were kept at -80°C and then sliced into cryosections of a thickness of 14 µm using a CM3050 S cryostat (Leica).

2.6.2 B2 cell isolation

Wt animals were sacrificed by CO_2 and spleens were removed and placed in 10ml cold DMEM containing DNase. The spleens were homogenized with the rubber tip of an 1ml syringe plunger and passed through a 100µm cell strainer. The cell suspension containing splenocytes was centrifuged at 300 x *g* for 5 minutes at 4°C and cells were re-suspended in AKC lysis buffer. After one more centrifugation, the pellet was re-suspended in PEB (500 ml PBS, 2.5 g BSA, 2 ml 0.5 EDTA) and 50ul of CD43 (Ly-48) MicroBeads (Miltenyi Biotec, Germany) were added, as per the manufacturer's instructions. CD43 is an antigen expressed in almost all leukocytes, which were magnetically labelled, except from resting B2 cells, which stayed untouched and were collected in the column effluent. For the separation, a magnetic station and LS columns (Miltenyi Biotec) were used. The isolated B2 cells were then labelled with Calcein-AM (1 nM; Calbiochem) in RPMI (Thermo Fisher Scientific) without FBS and washed three times with RPMI containing 10% FBS for 30 minutes at RT.

2.6.3 HA binding assay

Epididymal AT cryosections were treated with or without hyaluronidase from Streptomyces hyalurolyticus (2 U/ml; Sigma-Aldrich) for 45-60 minutes in water bath at 37°C. Calcein-labelled B2

cells were added on the cryosections at a density of $5x10^5$ cells/ml for 30 minutes at RT, while being shaken at 70 rpm in a Thermoshake Incubator Shaker (C. Gerhardt GmbH & Co, Germany). The slides were finally mounted with Roti-Mount FluorCare DAPI (Carl Roth) for nuclei staining. Counting of cells adherent on the tissue (B2 cells double positive for Calcein and DAPI) was performed manually using ZEN 3.0 (Carl Zeiss Microscopy GmbH, Germany). Results were expressed as percentage of the adherent cells on non-digested Wt epididymal AT.

2.7 B2 lymphocyte binding to vascular smooth muscle cells (VSMCs)

B2 lymphocyte binding assays were performed using a modified published protocol and as described before[1,145]. Briefly, aortic VSMCs isolated from Wt and *Id3*$^{-/-}$ mice were seeded in 96-well plates at a density of 10,000 cells/well in DMEM/F12 (Thermo Fisher Scientific) supplemented with 10% FBS and 1% penicillin/streptomycin for 24 h. Cells were treated with or without hyaluronidase from Streptomyces hyalurolyticus (2 U/m; Sigma-Aldrich) for 1 h at 37°C. B2 cells from spleens of Wt mice were isolated using CD43 (Ly-48) MicroBeads (Miltenyi BioTec), labelled for 30 minutes at room temperature with Calcein-AM (1 nM; Calbiochem) and added to VSMC monolayers at a density of $1\text{-}3x10^5$ cells/well. After 90 minutes of incubation at 4°C, cells were washed with ice-cold PBS and fluorescence intensity was measured on a microplate reader (Synergy HT, BioTek; extinction 485 nm, emission 535 nm). Cells were photographed using a Nikon Diaphot 300 fluorescent microscope and Excelis HD camera.

2.8 Human studies

All samples included in the human studies were collected prior to the beginning of the present study at the University of Virginia. Design of the following studies and collection of the samples was performed solely by members of the McNamara Lab.

2.8.1 14180 Study Design

Subjects were recruited through the Bariatric Surgery Clinic at the University of Virginia. All patients were ≥18 years of age and obese, with a BMI around 50 kg/m^2 and provided informed written consent. Omental AT was collected from the patients during surgery. One part of the tissue was snap-frozen in liquid nitrogen and used later to extract DNA in order to perform gene expression analysis by qPCR, as described for the murine studies. The primer sequences are shown in **Table 6**. The rest of the tissue was processed and embedded in paraffin in order to be used for immunohistochemistry. Experiments were performed as discussed in Section 2.2.

The study was approved by the human IRB Committee at the University of Virginia with IRB #14180. All procedures were in accord with the declaration of Helsinki.

Table 6: Primers used for qPCR in human samples.

Gene	*Symbol*	Primer sequence
RNA, 18S ribosomal N5	*RNA18SN5*	5'- GCAATTATTCCCCATGAACG -3' 5'- GGCCTCACTAAACCATCCAA -3'
hyaluronan synthase 1	*HAS1*	5'- TCGGAGATTCGGTGGACTA -3' 5'- AGGAGTCCAGAGGGTTAAGGA -3'
hyaluronan synthase 2	*HAS2*	5'- GTGGATTATGTACAGGTTTGTGA -3' 5'- TCCAACCATGGGATCTTCTT -3'
hyaluronan synthase 3 (version 1)	*HAS3v1*	5'- CCTTCCCCTACCCAGAGC -3' 5'- GAACTGGTAGCCCGTCACAT -3'
hyaluronan synthase 3 (version 2)	*HAS3v2*	5'- TGAGCTCCGGAGCGCGGC -3' 5'- GAACTGGTAGCCCGTCACAT -3'

2.8.2 15328 Study Design

Subjects were recruited from the Cardiac Catheterization Laboratory at the University of Virginia. All patients were ≥18 years of age and provided informed written consent. Blood was collected from the patients and plasma was isolated in order to quantify HA in the plasma, as described for our murine samples. The samples were a mixture of patients that underwent a medically necessary intravascular ultrasound (IVUS) or quantitative coronary arteriography (QCA), in accordance with the standards of the American College of Cardiology. Analysis was performed with adjustment for age, gender, ethnicity, diabetes, smoking, and hypertension.

The study was approved by the human IRB Committee at the University of Virginia with IRB #15328. All methodology was compliant with the principles set forth in the Declaration of Helsinki.

2.8.3 Genotyping

Genotyping of the samples was performed by members of the McNamara lab at UVa. Participants recruited in Cohorts 14180 and 15328 were genotyped as described previously[124,127]. Briefly, genotyping was performed using the Affymetrix Human SNP array 6.0 (~1 million SNPs). Regarding genotype quality control, data were filtered on SNP level call rate < 95%, individual level call rate < 95%, heterozygosity > 53%, and all monomorphic SNPs were removed[127].

2.9 Statistics

Statistical evaluation was performed using the GraphPad Prism Software Version 8.0 (GraphPad Software, La Jolla, CA, USA). All data are presented as mean ± SD. Statistical analysis was performed by unpaired *t* test or Ordinary one-way ANOVA followed by Tukey's multiple comparisons test. If the f-test, which compares variances between two groups, was significant, the nonparametric, unpaired, two-tailed Mann-Whitney test was performed. Shapiro-Wilk test was

used to check normality. $p<0.05$ was considered statistically significant.

3. Results

3.1 Effect of the HFD on *Id3*-KO mice body and adipose tissue weight

Male *Id3*$^{-/-}$ mice and Wt littermate controls were fed either a HFD containing 60% kcal from fat or standard laboratory diet, starting at 8 weeks of age. The body weight of both groups was increased after HFD compared to standard-diet-fed mice. However, no differences in the body weight were observed due to deficiency of *Id3* between the littermates (**Figure 9**). These results are consistent with previous studies showing a limited increase of the body weight of *Id3*$^{-/-}$ mice only after 16 weeks of HFD[132,146].

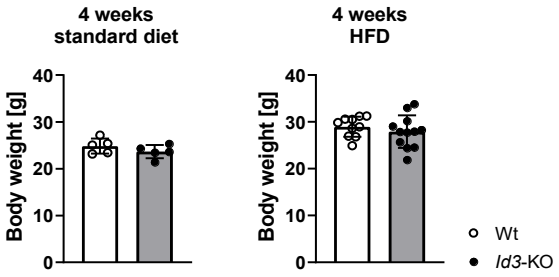

Figure 9: **The body weight was similar between HFD-fed *Id3*$^{-/-}$ and Wt littermates.** Absence of *Id3* did not affect the body weight of the mice either after 4 weeks of standard laboratory diet or after 4 weeks of HFD. HFD induced an increase in the body weight of both genotypes; n=5,10. Data represent mean ± SD.
With permission from Wolters Kluwer Health, Inc.: Misiou, A. *et al,* Helix-Loop-Helix Factor Id3 (Inhibitor of Differentiation 3) A Novel Regulator of Hyaluronan-Mediated Adipose Tissue Inflammation, *Arteriosclerosis, Thrombosis, And Vascular Biology*, 41(2), 796-807, doi: 10.1161/atvbaha.120.315588[1].

At the end of the diet, AT depots were harvested, and the weights were compared. Absence of *Id3* did not affect the AT depot weights of the mice after 4 weeks of standard laboratory diet, whereas HFD-fed mice from both genotypes demonstrated increased AT weight. *Id3*$^{-/-}$ mice had significantly smaller epididymal AT depots compared to Wt littermates in response to HFD. This effect was only seen in the epididymal AT weight, as there was no difference in the weight of

subcutaneous fat, which was increased only in response to HFD and not due to *Id3* deficiency, nor of brown AT **(Figure 10)**.

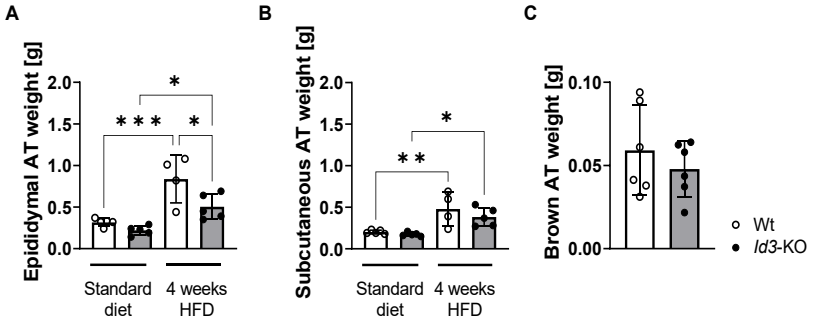

Figure 10: *Id3* deficiency affected the AT weight of the mice. **A-B**. Epididymal and subcutaneous AT weight was not different between *Id3*$^{-/-}$ and Wt littermates after 4 weeks of standard laboratory diet. HFD induced an increase in epididymal and subcutaneous AT depot weights for both groups, but *Id3*$^{-/-}$ mice displayed significantly smaller epididymal AT depots; n=5. **C.** Brown adipose tissue (BAT) weight was not different between *Id3*$^{-/-}$ mice and Wt littermate controls after 4 weeks of feeding HFD; n=6. Data represent mean ± SD; *p<0.05; **p<0.01; ***p<0.001.

With permission from Wolters Kluwer Health, Inc.: Misiou, A. *et al,* Helix-Loop-Helix Factor Id3 (Inhibitor of Differentiation 3) A Novel Regulator of Hyaluronan-Mediated Adipose Tissue Inflammation, *Arteriosclerosis, Thrombosis, And Vascular Biology*, 41(2), 796-807, doi: 10.1161/atvbaha.120.315588[1].

Mice lacking *Id3* also had a lower ratio of epididymal to subcutaneous AT depot weight, indicating again limited expansion of visceral but not subcutaneous depots **(Figure 11)**.

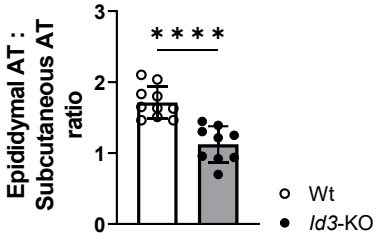

Figure 11: Ratio of epididymal AT to subcutaneous AT depot weight. The ratio of epididymal to subcutaneous AT depot demonstrated reduced expansion of only the visceral AT depot of *Id3*$^{-/-}$ mice; n=9, 10; unpaired *t* test. Data represent mean ± SD; ****p<0.0001.

With permission from Wolters Kluwer Health, Inc.: Misiou, A. *et al,* Helix-Loop-Helix Factor Id3 (Inhibitor of Differentiation 3) A Novel Regulator of Hyaluronan-Mediated Adipose Tissue Inflammation, *Arteriosclerosis, Thrombosis, And Vascular Biology*, 41(2), 796-807, doi: 10.1161/atvbaha.120.315588[1].

Glucose tolerance tests were performed for both genotypes after 4 weeks of HFD, showing no alterations in glucose levels between the two groups **(Figure 12)**.

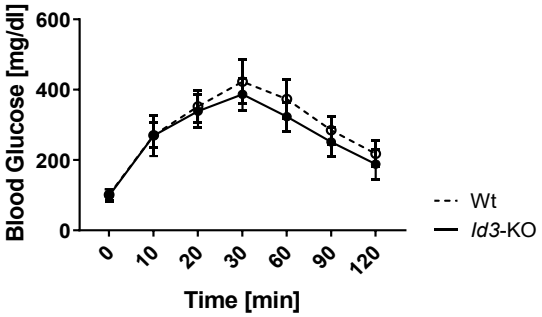

Figure 12: Glucose tolerance was not altered in *Id3*$^{-/-}$ mice. Glucose tolerance test (GTT) was performed after 4 weeks of HFD in *Id3*$^{-/-}$ mice and Wt littermate controls. No differences were seen between the two groups; n=6,7. Data represent mean ± SD.

With permission from Wolters Kluwer Health, Inc.: Misiou, A. *et al,* Helix-Loop-Helix Factor Id3 (Inhibitor of Differentiation 3) A Novel Regulator of Hyaluronan-Mediated Adipose Tissue Inflammation, *Arteriosclerosis, Thrombosis, And Vascular Biology*, 41(2), 796-807, doi: 10.1161/atvbaha.120.315588[1].

3.2 Immune cell composition of *Id3*-KO mice after 4 weeks of HFD

Studies have shown that active immune cell trafficking takes place in the AT during the onset of diet-induced obesity[147]. Therefore, we then analysed the effect of absence of *Id3* on the immune cell populations of the AT after 4 weeks of HFD. Using the SVF isolated from epididymal AT, we performed flow cytometry analysis. We observed an increase in the B cell population in the AT of *Id3*$^{-/-}$ mice compared to littermate controls, whereas the T cell population and the number of total macrophages were not different **(Figure 13A-C).** The composition of the different subsets of B cells in the AT was then examined. B2 cell population was significantly increased in epididymal AT of HFD-fed *Id3*$^{-/-}$ mice while there was no difference in the B1a and B1b B cell populations **(Figure 13D-F)** as well as in the numbers of M1 and M2 macrophages **(Figure 13G and H).**

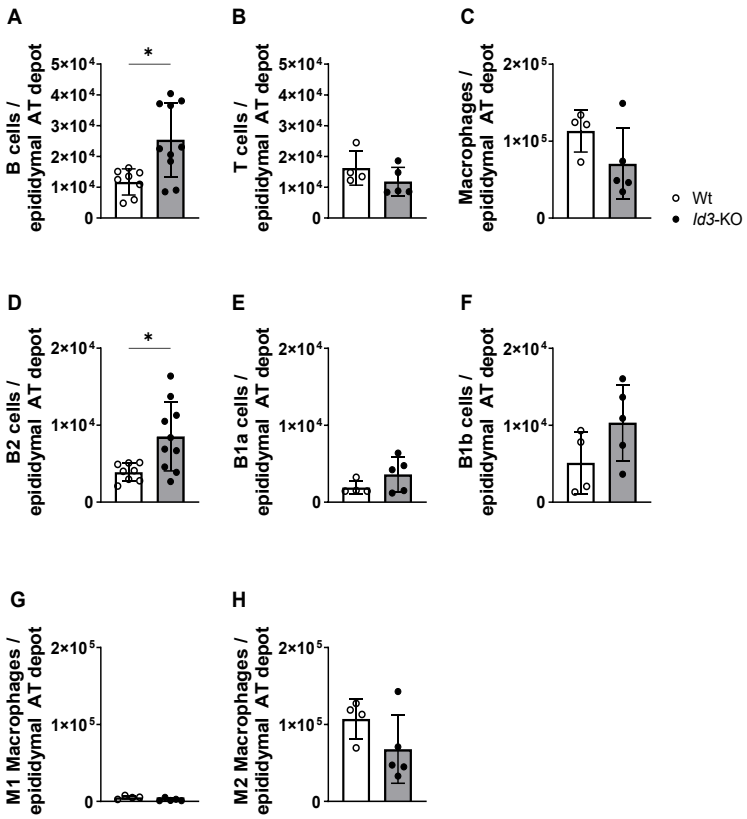

Figure 13: *Id3*-deficient mice had increased B2 cells in AT. A-C. Flow cytometric analysis revealed an increase in B cell population of epididymal AT, but not in T cells or total macrophages; n=4-10; Mann-Whitney test. **D-E.** B2 cell population was elevated in the AT of *Id3*$^{-/-}$ mice compared to Wt littermates; n=4-10; Mann-Whitney test. **G-H.** Numbers of M1 and M2 macrophages in epididymal AT were similar between *Id3*$^{-/-}$ and Wt mice after 4 weeks of HFD; n=4-5. All cell populations are expressed as cell number per epididymal AT depot. Data represent mean ± SD; *p<0.05; ****p<0.0001.

With permission from Wolters Kluwer Health, Inc.: Misiou, A. *et al,* Helix-Loop-Helix Factor Id3 (Inhibitor of Differentiation 3) A Novel Regulator of Hyaluronan-Mediated Adipose Tissue Inflammation, *Arteriosclerosis, Thrombosis, And Vascular Biology*, 41(2), 796-807, doi: 10.1161/atvbaha.120.315588[1].

Total B cell population, including B1 and B2 cells, was also increased in the AT of *Id3*$^{-/-}$ mice under standard laboratory diet, while T cells and total macrophages remained unchanged **(Figure 14A-C)**. More specifically about the different B cell subsets, B1 and not B2 cells were increased in *Id3*$^{-/-}$ mice under standard diet confirming previous findings[137,138] **(Figure 14D and E)**. M1 and M2 macrophages did not show any differences between the two genotypes **(Figure 14F and G)**.

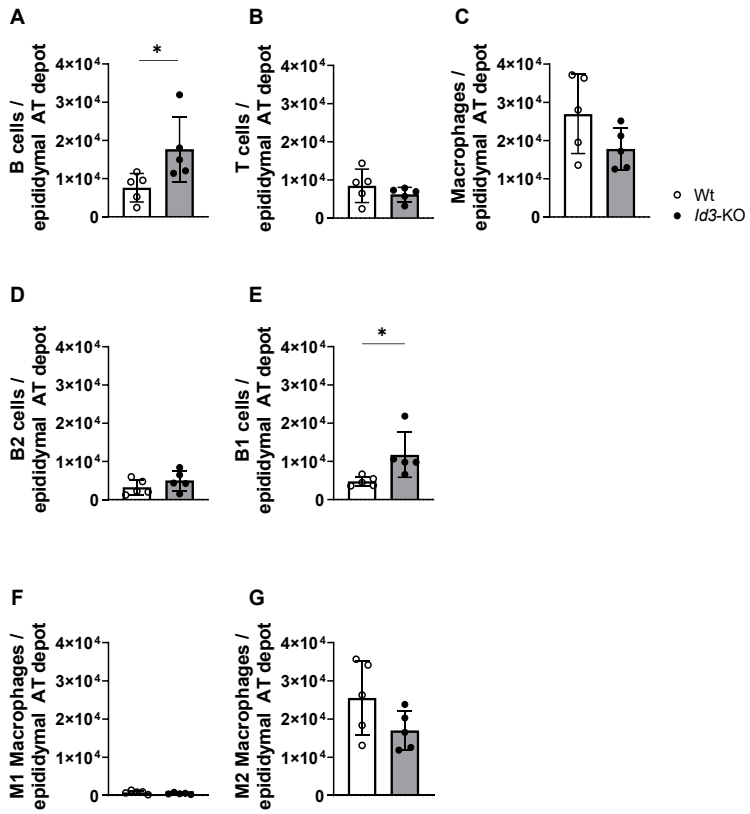

Figure 14: Standard diet-fed *Id3*$^{-/-}$ mice did not demonstrate differences in immune cell populations in the AT. A-C. Flow cytometric analysis showed an increase in the B cell population in epididymal AT of *Id3*$^{-/-}$ mice fed a standard diet, but not in T cells or total macrophages; n=5; unpaired *t* test. **D-E**. There was no increase in B2 cell population, while B1 cells were increased in the AT of standard diet-fed *Id3*$^{-/-}$ mice compared to Wt littermates; n=5; Mann-Whitney test. **F-G**. Numbers of M1 and M2 macrophages in epididymal AT were similar between *Id3*$^{-/-}$ and Wt mice fed a standard diet; n=4-5. All cell populations are expressed as cell number per epididymal AT depot. Data represent mean ± SD; *p<0.05.

With permission from Wolters Kluwer Health, Inc.: Misiou, A. *et al,* Helix-Loop-Helix Factor Id3 (Inhibitor of Differentiation 3) A Novel Regulator of Hyaluronan-Mediated Adipose Tissue Inflammation, *Arteriosclerosis, Thrombosis, And Vascular Biology*, 41(2), 796-807, doi: 10.1161/atvbaha.120.315588[1].

Flow cytometric analysis was performed in order to investigate the immune cell composition of subcutaneous AT after 4 weeks of HFD. Results showed that *Id3*$^{-/-}$ mice had a significant increase in the B cell population in this AT depot, but the number of T cells and macrophages remained the same **(Figure 15A-C)**. After careful analysis of the different B cell subsets, it was demonstrated that in the subcutaneous AT of HFD-fed *Id3*$^{-/-}$ mice there was an increase in the B1 population but not in the B2, meaning there was the opposite effect of the epididymal AT that we observed before **(Figure 15D and E)**. Numbers of M1 and M2 macrophages remained the same **(Figure 15F and G)**.

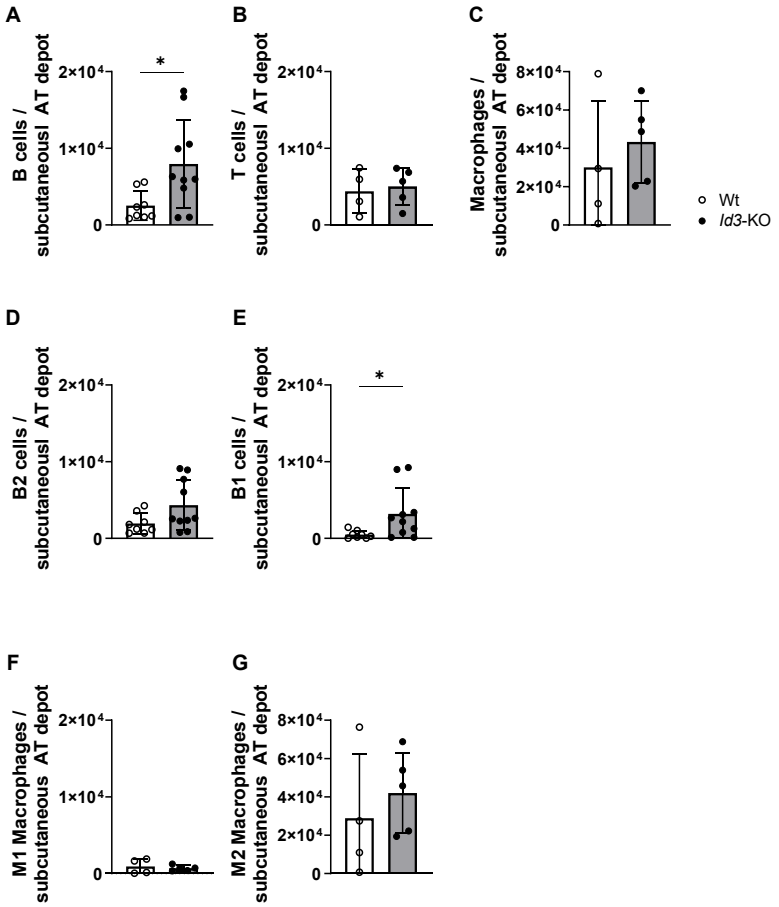

Figure 15: *Id3*-deficient mice had increased B1 cell population in subcutaneous AT. A-C. Flow cytometry analysis showed that in in the subcutaneous AT of HFD-fed *Id3*$^{-/-}$ mice there was an increase in the B cells population, but not in the number of the T cells or macrophages. **D-E**. B1 and not B2 cells were increased in the subcutaneous AT of *Id3*$^{-/-}$ mice compared to Wt littermates; n=4-10; Mann-Whitney test. **F-G**. There was no difference in the population of M1 and M2 macrophages. All cell populations are expressed as cell number per subcutaneous AT depot. Data represent mean ± SD; *p<0.05.

Gating schemes for the analysis of the immune cells in the AT depots are displayed in the **Appendix.**

3.3 Effect of *Id3* and HFD on inflammatory cytokine production

To further specify the inflammatory status of the HFD-fed *Id3*-deficient mice, which was evident by the increase of the B2 cell population, the expression of the pro-inflammatory cytokines *Ifng*, *Il6* and *Tnfa* was examined. SVF from AT was used for RNA isolation and qPCR analysis was performed. Our data showed that *Ifng* mRNA

expression was increased in *Id3*$^{-/-}$ mice under HFD, while there were no changes in the mRNA expression of *Tnfa* and *Il6* **(Figure 16)**.

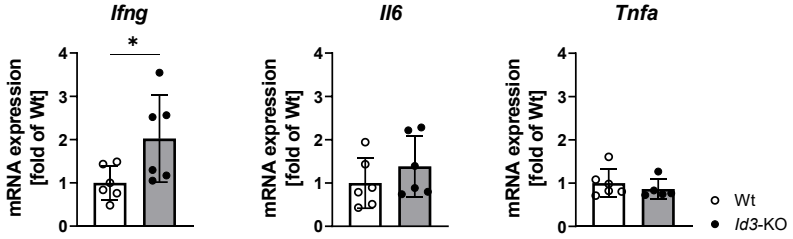

Figure 16: *Id3*-deficient mice expressed higher amounts of *Ifng*. mRNA analysis of epididymal AT from *Id3*$^{-/-}$ mice after 4 weeks on HFD revealed an upregulation in the expression of the pro-inflammatory cytokine *Ifng*, whereas the expression of *Il6* and *Tnfa* were not affected; n=6; unpaired *t* test. Data represent mean ± SD; *p<0.05.

3.4 Effect of *Id3* deficiency on HA in response to HFD

3.4.1 *Id3*-deficient mice have elevated HA levels in epididymal AT and in circulation

To determine whether *Id3* can affect the AT HA content, we performed immunohistochemistry using epididymal and subcutaneous AT paraffin sections. The results of this experiment revealed higher amounts of HA in epididymal AT of HFD-fed *Id3*$^{-/-}$ mice compared to Wt littermates. This effect was not seen in the subcutaneous AT **(Figure 17)**.

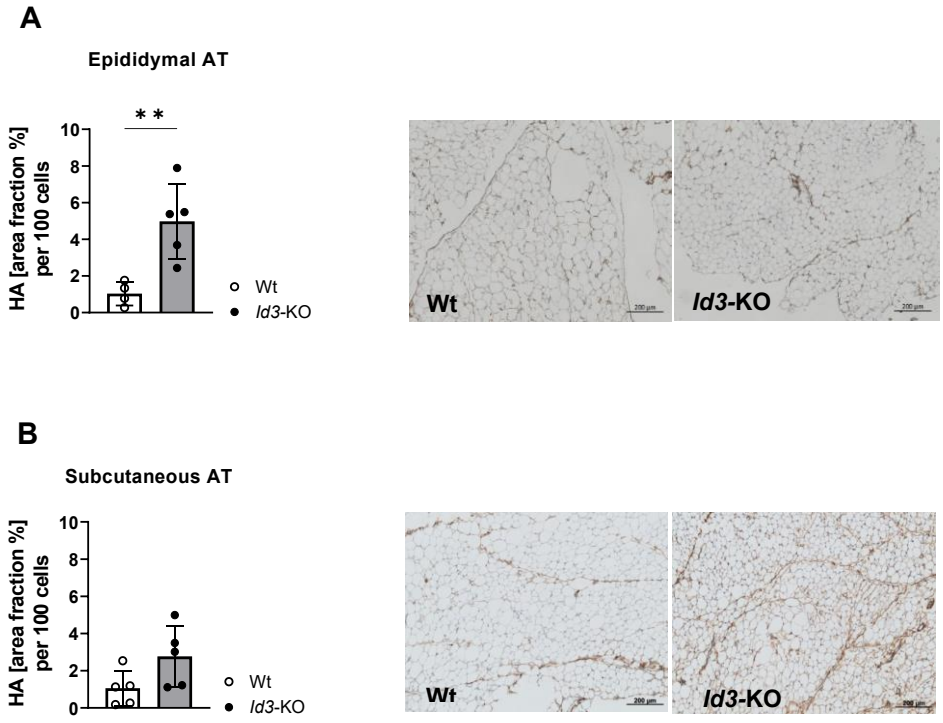

Figure 17: *Id3*-deficient mice had elevated HA levels in epididymal AT. A-B. Quantification of the area fraction of HA per 100 adipocytes showed increased HA content in the epididymal AT of HFD- *Id3*$^{-/-}$ mice, but not in the subcutaneous AT, compared with Wt littermate controls; n=4, 5; unpaired *t* test. Representative images of Wt and *Id3*$^{-/-}$ epididymal and subcutaneous AT stained with hyaluronan binding protein after 4 weeks of HFD are displayed. Scale bar: 200µm. Data represent mean ± SD; **p<0.01.

With permission from Wolters Kluwer Health, Inc.: Misiou, A. *et al,* Helix-Loop-Helix Factor Id3 (Inhibitor of Differentiation 3) A Novel Regulator of Hyaluronan-Mediated Adipose Tissue Inflammation, *Arteriosclerosis, Thrombosis, And Vascular Biology*, 41(2), 796-807, doi: 10.1161/atvbaha.120.315588[1].

Serum levels of HA are also important when evaluating metabolic function, as discussed before. Therefore, plasma was isolated from *Id3*$^{-/-}$ and Wt mice and HA was measured by ELISA. Analysis showed that plasma levels of HA were significantly increased in *Id3*$^{-/-}$ mice **(Figure 18)**.

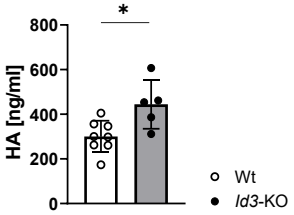

Figure 18: *Id3*-deficient mice had increased serum HA levels. Circulating HA was determined in plasma samples of *Id3*$^{-/-}$ and Wt mice and revealed elevated HA levels in *Id3*$^{-/-}$ mice; n = 5, 8. Data represent mean ± SD; *p<0.05.

With permission from Wolters Kluwer Health, Inc.: Misiou, A. *et al,* Helix-Loop-Helix Factor Id3 (Inhibitor of Differentiation 3) A Novel Regulator of Hyaluronan-Mediated Adipose Tissue Inflammation, *Arteriosclerosis, Thrombosis, And Vascular Biology*, 41(2), 796-807, doi: 10.1161/atvbaha.120.315588[1].

3.4.2 Impact of *Id3* deficiency on *Has* mRNA expression

Next, mRNA expression of the *Has* isoenzymes was evaluated. *Has2* mRNA expression was significantly elevated in whole epididymal AT of *Id3*$^{-/-}$ mice. *Has3* mRNA expression was also increased in the AT of *Id3*$^{-/-}$ mice, although not as greatly as *Has2*. *Has1* mRNA expression was not detectable in epididymal AT **(Figure 19)**.

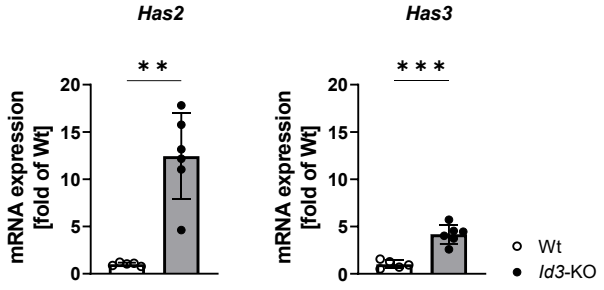

Figure 19: *Id3*-deficient mice showed increased mRNA expression of *Has2* isoenzyme in epididymal AT. mRNA expression of the three *Has* isoenzymes *(Has-1, -2, -3)* was measured in epididymal AT of *Id3*$^{-/-}$ and Wt mice after 4 weeks on HFD. *Has2* and *Has3* mRNA levels were increased and *Has1* expression was not detected. Results are normalized to *18s*; n=5-6; Mann-Whitney test; unpaired *t* test. Data represent mean ± SD; **p<0.01; ***p<0.001.

With permission from Wolters Kluwer Health, Inc.: Misiou, A. *et al,* Helix-Loop-Helix Factor Id3 (Inhibitor of Differentiation 3) A Novel Regulator of Hyaluronan-Mediated Adipose Tissue Inflammation, *Arteriosclerosis, Thrombosis, And Vascular Biology*, 41(2), 796-807, doi: 10.1161/atvbaha.120.315588[1].

As mentioned before, AT contains various cells, such as preadipocytes, fibroblasts, endothelial cells, SMCs and several immune cells[15]. mRNA expression of the *Has* isoenzymes was evaluated in order to examine whether these genes are expressed differentially in the cells present in AT. No difference in the mRNA levels of the *Has* enzymes between isolated SVF from *Id3*$^{-/-}$ and Wt mice was observed **(Figure 20)**.

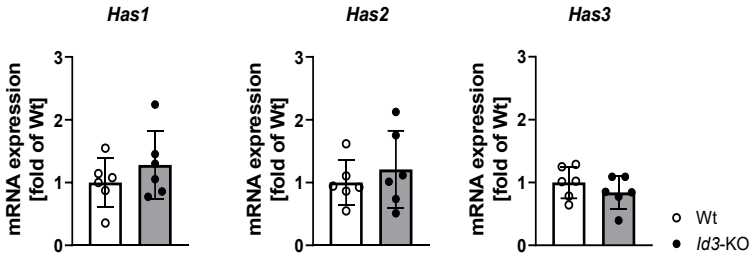

Figure 20: *Id3*-deficient mice did not demonstrate different *Has* mRNA expression in the SVF. mRNA expression of the three HA synthase isoenzymes (*Has1, -2, -3*) was measured in SVF isolated from the epididymal AT of *Id3*$^{-/-}$ and Wt mice fed a HFD for 4 weeks. Expression levels were not different between the experimental groups. Results are normalized to *18s*; n=6. Data represent mean ± SD.

With permission from Wolters Kluwer Health, Inc.: Misiou, A. *et al,* Helix-Loop-Helix Factor Id3 (Inhibitor of Differentiation 3) A Novel Regulator of Hyaluronan-Mediated Adipose Tissue Inflammation, *Arteriosclerosis, Thrombosis, And Vascular Biology*, 41(2), 796-807, doi: 10.1161/atvbaha.120.315588[1].

Next, *Has* mRNA expression was assessed in isolated adipocytes. *Has2* mRNA levels were similar between the two groups, whereas *Has3* was upregulated in adipocytes of *Id3*$^{-/-}$ mice after 4 weeks of feeding a HFD. *Has1* expression was not detected (**Figure 21)**.

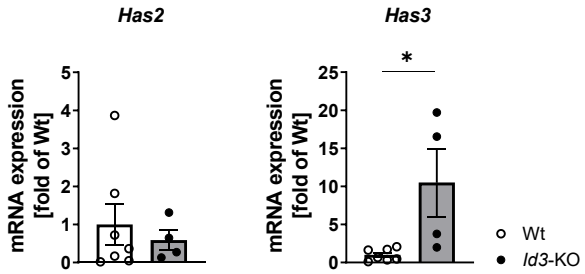

Figure 21: *Id3*-deficient mice had increased *Has3* expression in adipocytes. mRNA expression of HAS isoenzymes (*Has-1, -2, -3*) was measured in isolated adipocytes from the epididymal AT of *Id3*$^{-/-}$ and Wt mice after 4 weeks of HFD. *Has1* expression was not detected and no significant difference in the mRNA levels of *Has2* was observed. *Has3* mRNA expression was increased in the *Id3*$^{-/-}$ mice.

Results are normalized to *18s*; n=4-7; Mann-Whitney test. Data represent mean ± SD; *p<0.05.

With permission from Wolters Kluwer Health, Inc.: Misiou, A. *et al,* Helix-Loop-Helix Factor Id3 (Inhibitor of Differentiation 3) A Novel Regulator of Hyaluronan-Mediated Adipose Tissue Inflammation, *Arteriosclerosis, Thrombosis, And Vascular Biology*, 41(2), 796-807, doi: 10.1161/atvbaha.120.315588[1].

Purified cultured VSCMs from aortas of HFD-fed Wt and *Id3*$^{-/-}$ littermates were used to examine *Has* expression in this cell type. Expression of *Has2* was significantly increased in *Id3*$^{-/-}$ VSCMs compared to Wt cells. *Has1* was also upregulated, although not as highly. Surprisingly, *Has3* mRNA levels were decreased in *Id3*$^{-/-}$ VSMCs **(Figure 22)**.

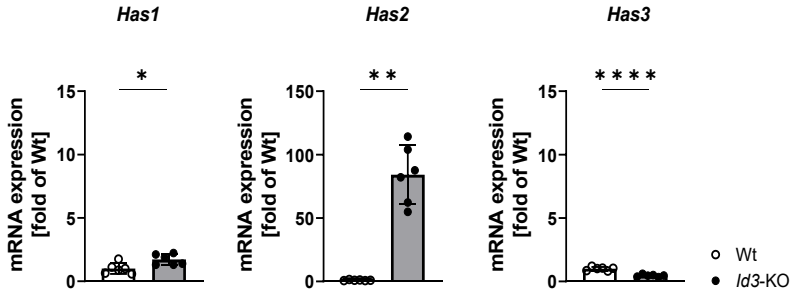

Figure 22. Increased expression of HAS isoenzymes in VSMCs isolated from *Id3*-deficient mice. mRNA expression of HAS isoenzymes (*Has-1, -2, -3*) was measured in cultured aortic VSMCs from *Id3*$^{-/-}$ and Wt mice after 4 weeks of HFD. *Has1* and *Has2* mRNA levels were increased in VSMCs from *Id3*$^{-/-}$ mice, while Has3 expression was decreased. Results are normalized to 18s; n=6; Mann-Whitney test. Data represent mean ± SD; *p<0.05; **p<0.01; ****p<0.0001.

With permission from Wolters Kluwer Health, Inc.: Misiou, A. *et al,* Helix-Loop-Helix Factor Id3 (Inhibitor of Differentiation 3) A Novel Regulator of Hyaluronan-Mediated Adipose Tissue Inflammation, *Arteriosclerosis, Thrombosis, And Vascular Biology*, 41(2), 796-807, doi: 10.1161/atvbaha.120.315588[1].

3.5 Functional effect of increased HA in HFD-fed *Id3*$^{-/-}$ mice

The HA binding assay was used in order to characterize a functional effect of the elevated HA content in the epididymal AT of HFD-fed *Id3*$^{-/-}$ mice. Accumulation of HA in the AT of HFD-fed *Id3*$^{-/-}$ mice led to a bigger number of adherent B2 cells on the AT of these mice, while fewer cells attached in the AT of Wt littermates. After treatment of the tissue with hyaluronidase and thus digestion of the endogenous HA, significantly fewer B2 cells adhered to the AT of *Id3*$^{-/-}$ mice was decreased to baseline levels **(Figure 23)**.

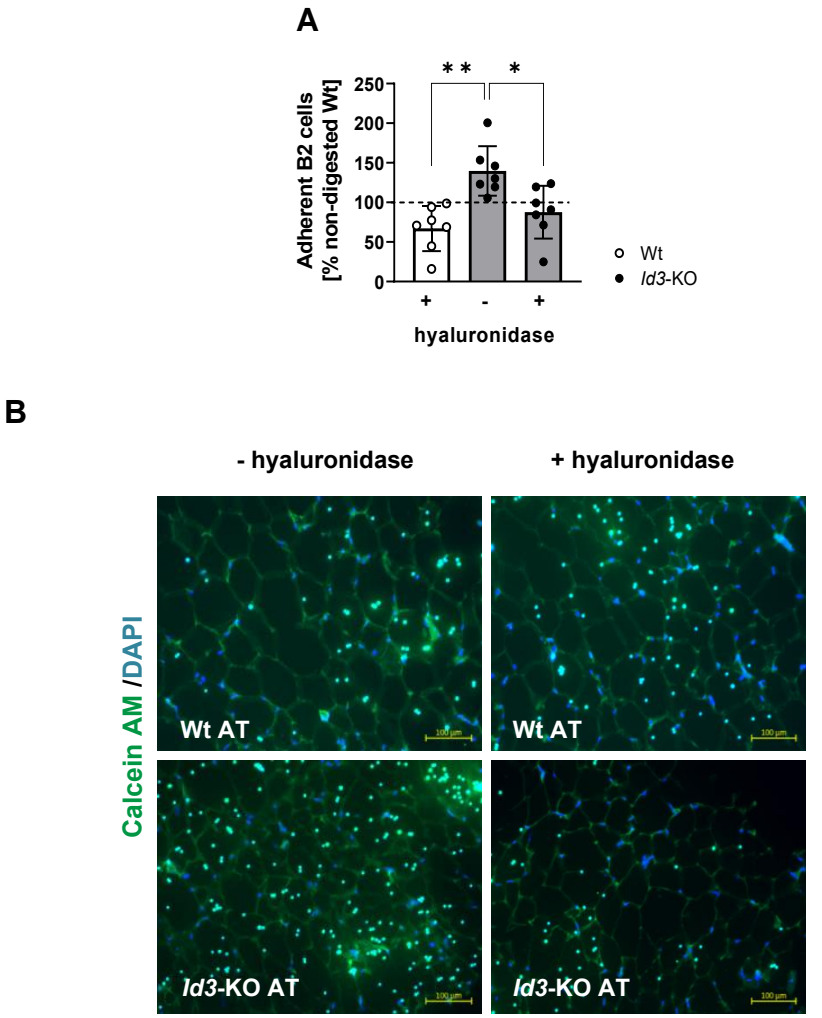

Figure 23: HA promotes B2 cell adhesion in AT of *Id3*$^{-/-}$ mice. **A-B.** accumulation of HA in the epididymal AT of *Id3*$^{-/-}$ mice led to increased adhesion of isolated Calcein-labelled Wt splenic B2 cells in the AT, compared with AT that had been treated with hyaluronidase (plus) prior to the addition of the cells; n=7. Data represent mean ± SD; *p<0.05; **p<0.01.

With permission from Wolters Kluwer Health, Inc.: Misiou, A. *et al,* Helix-Loop-Helix Factor Id3 (Inhibitor of Differentiation 3) A Novel Regulator of Hyaluronan-Mediated Adipose Tissue Inflammation, *Arteriosclerosis, Thrombosis, And Vascular Biology*, 41(2), 796-807, doi: 10.1161/atvbaha.120.315588[1].

3.6 HA promotes B2 cell adhesion in cultured VSMCs of *Id3*$^{-/-}$ mice

Next, VSMCs were isolated from the aortas of Wt and *Id3*$^{-/-}$ mice and were co-incubated with Calcein-stained B2 cells. This experiment aimed to examine whether HA promotes B2 cell binding to a specific cell type found in the AT. Markedly more immune cells attached to *Id3*$^{-/-}$ SMCs, compared to Wt SMC cultures. The observed effect was

completely blunted when the cells were treated with hyaluronidase before the co- incubation with the B2 cells **(Figure 24)**.

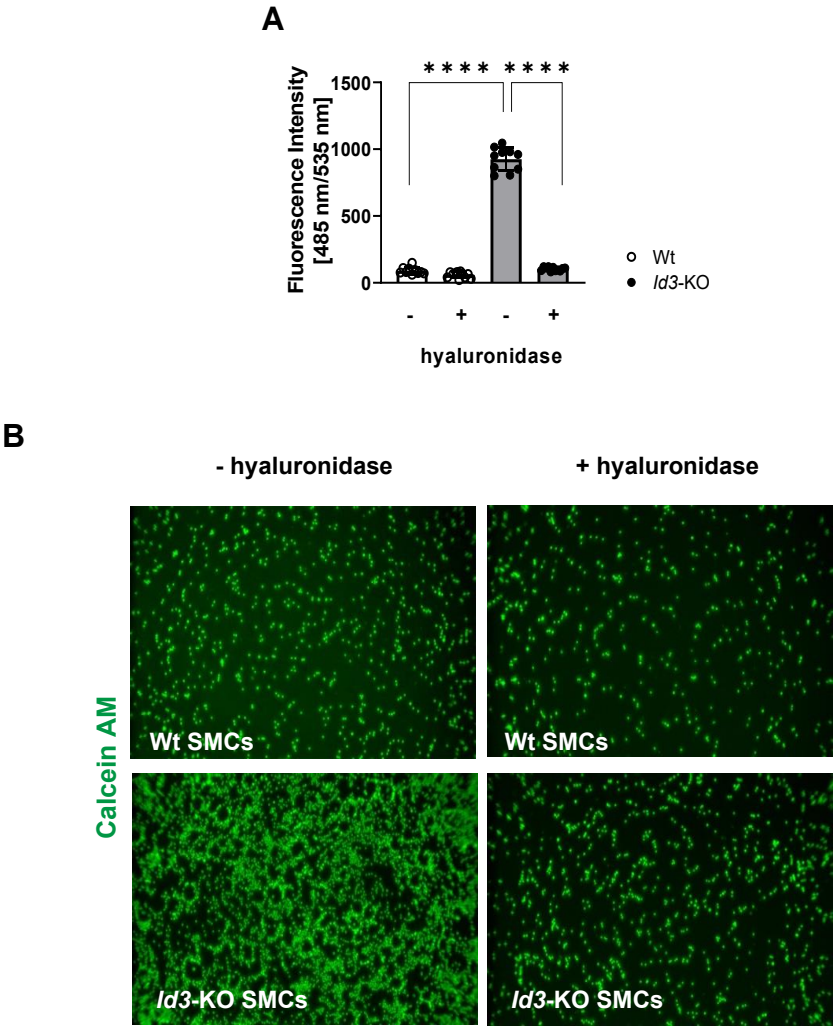

Figure 24: HA promotes B2 cell adhesion in cultured VSMCs of *Id3*$^{-/-}$ mice. **A-B**. Increased adhesion of Calcein-labelled Wt splenic B2 cells to *Id3*$^{-/-}$ aortic VSMCs was blunted after incubation with hyaluronidase (plus). Data are the result of 3 independent experiments. Data represent mean ± SD; ****p<0.0001.

With permission from Wolters Kluwer Health, Inc.: Misiou, A. *et al,* Helix-Loop-Helix Factor Id3 (Inhibitor of Differentiation 3) A Novel Regulator of Hyaluronan-Mediated Adipose Tissue Inflammation, *Arteriosclerosis, Thrombosis, And Vascular Biology*, 41(2), 796-807, doi: 10.1161/atvbaha.120.315588[1].

3.7 Effect of *Id3*-deficiency on other ECM components

In the next series of experiments, we sought to determine whether *Id3* deficiency had an effect on other components of the ECM other than HA. For this purpose, we first examined the presence of E-box elements in the promoter regions of the murine genes of biglycan, decorin, versican and aggrecan since it is well known so far that bHLH factors bind specifically to them, regulating transcription. The sequence information for the first 2000 bases of the promoter regions of the genes of interest were retrieved using the BioMart tool from the Ensebl project[139]. Afterwards, immunohistochemistry was performed using epididymal and subcutaneous AT paraffin sections, as described before.

3.7.1 Effect on Biglycan

The promoter of the *Bgn* gene contains 11 E-box elements (CANNTG) in the first 2000bp of the promoter, which are depicted in **Figure 25**.

CTGGGGCAGTGGGTATATATTTTGTGAGTTTTCATCCTTAAAATAAAAGCCTTGGCTAGGTATGGTGC
TTTGTGCTTCTAATTCCAGCACCCAGGAGGTGGAGGCAAAAGAATCAAGAGTTTAAGGTCATTCTGGA
CTATACAGCAAATCTGAGGTCTGCATGGGGTACAAGAAACCCTATCTCAAAAATCAAAGCAAAAGGAA
AGAGTTATTGAAATATACTTGTTGAGTATAGTAAAGGCTCACTCTTTTGTAATCTCAGCATAGACAGA
TGAAAATTCTCACCATGAATTCAAGGATATCTAGTGGAACTTTATCTCAAAAATAGAAAGAAAAAAAA
AGAGAAGAGATGAAAGATATATAAAATACAAGGCATACAGTTTAAATGAACTATTCAGCAGTTTTCAC
TTAGTATGTTCAGAGCAGTTTCATTGTTTCAAACTGAAGACTCAGAACTGATGAGATGCTGTTTCTTT
CTGTTTCATTCTGGAAATCTCACATGAACAGGCCAGACATAATGTGGCCTTTTGCCACTGGCTGCACT
CACCAAGCAGAATATTCCATATGTGCCTTGGACCTGCTGTAATTCCAGCACTCAGGGGGCAGAGACAT
GAGGATCTGGAGTTCAAGAGCAACTTCACTTACATAGTGAGTTGAAGGCCAGATGGGGCTACATAAGA
TCCTATAAATACATACATACATACATACACACACACACACACACACACACACACACACACACACACACC
ACATGAGCAGACAAAAACCAGCAGCCTGAGAAGCCTGAGTGCTCCCTAGTCTCCTGGTCTGGACCATG
GAATCCAAAGGCATCCACCGGCTCCCAACCCATATCCTGCTTCTCCCAATTTTCTCCTCTCTGCAGCC
AGAAGAGACTGCTCTTGAAGGAAAGTTCGACACTGATTCTGGCTCCAAGCAAAATTCTACTGGAGATT
CTGTCCTCAACTGAGAACATGCAGTGAACTTCACCTTGCCCTCTATCCAGTGGGCCTCTGCCTCAGCC
CCTCACCTGAACTTTCTTTGTTTGCCCTTCCTTACACTTGGTCCCTGGTTTCATCTTTAGATTTCAGT
GTGGCTCCCCAATTTAGTCTCTCCCACCATCTAAGGGCTCACCTTTACATCTTGGAAGCTGCCCTGGA
AAAGGAGAGGTAGGACATCACTGGACAGGTAAATGCTACACTAGGGACCATGTCTCATTTGGACCCTC
AAGAAGCAGTTGAGGTTTGGCAGCCTAGCCCTGTTAGGTCCTGAAATTGAAGGAAGGAAATGCTCATA
AGAGAGACCATGGTTACTGCATCCTGGCCGGCCAGTAGGGGTTGAGCAAGAAGATAAGGAGCTTGTTT
CTCTCCTCCAAATCAGCTTTGCCAACTTCTCAAAGGCTTCAGGGATGTGAGCCAAGAAGGCCTGCAGA
AACTTGGGGTGGGGGTGGGGGGCAAATGCCTCGTTTTAAAGGAGGAAAGGAAGGAGAAGAGGAAAGGC
TAACAGAGCCAGTGGGATCCTGGATCAAGCCCTTCCAGAAGCCTACCATCCTCTACATCTATAATCCC
CAAAGTGCCCCTGGCTTCAGACTTAAGTTCTGGGTAGCCATCAGGTTACCTTTCCTCATCTTCCTCTC
ACTTTCTTCTGCCTAGCCCCACAACAGCAAGCACCTCAGTGTCCCCTTTTGGATAGTGGAAAGTTTGA
CTCTGTGAGACTGTCTGCCCAAAGACACCAAGGGTCTGTCCCTAAGTAAGTGAATGTGTGTTCTTTCA
AACTATGCTTGAGGCAGGGGCCAGGGTGGGGGGCGTGAGGGGGAGGGGTGCCACATAGACCAGCCGTC
TACAAGAAAATTGCTTCCTTTGAAGCTGCCAGGGGGGGCAGGAAGCCTGCCCCCTCCCTCCCAGCTGC
CCTTCCTCCCCCCTTTTCTCCCTCTCTGCTCCACTAGCCCCCTCCCTTCTTGTCTCCCTCTCCGCCCC
GTCCCCTCCCTGTCGGCCCGCCCGCCCA

Figure 25: Illustration of the E-box elements in the promoter of *Bgn*. The first 2000 bases of the 5´flanking sequence of the *Bgn* gene contain 11 E-box elements (shown highlighted). The data were retrieved using the Biomart tool[139].

Quantification of immunostaining showed that higher amounts of biglycan were accumulated in subcutaneous AT of HFD-fed *Id3*$^{-/-}$ mice compared to control littermates. This effect was not seen in the epididymal AT **(Figure 26)**.

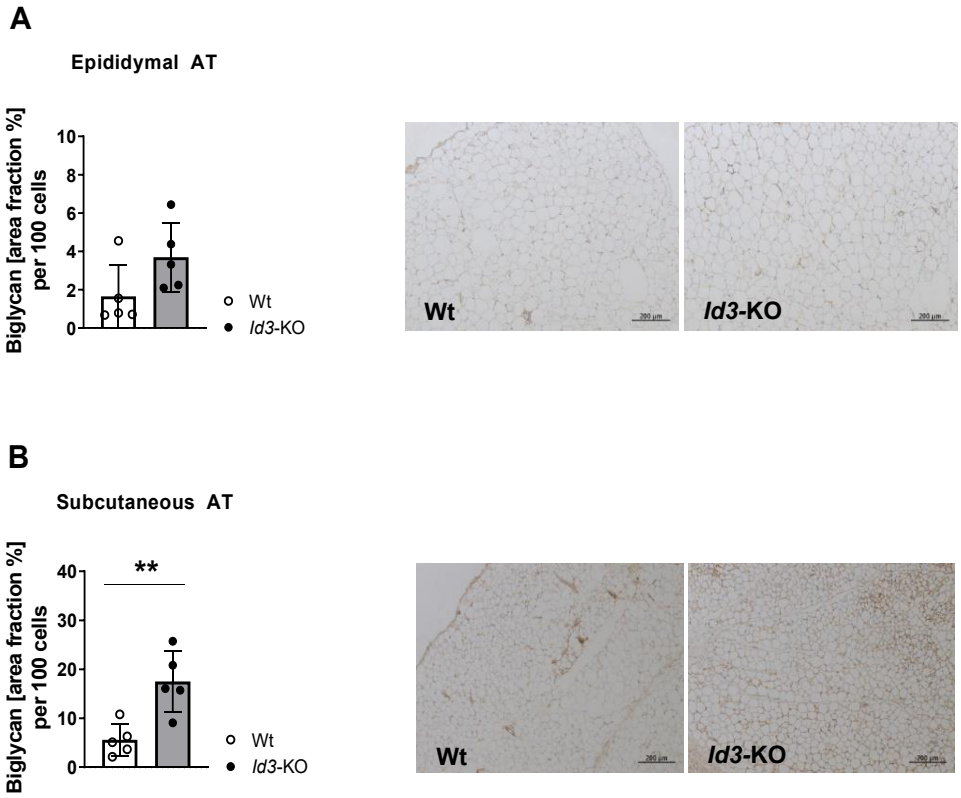

Figure 26: *Id3*-deficient mice have elevated biglycan content in the subcutaneous AT. A-B. Quantification of the area fraction of biglycan per 100 adipocytes showed increased biglycan content in *Id3*$^{-/-}$ subcutaneous AT and no difference in epididymal AT compared with Wt littermate controls; n=4, 5; unpaired *t* test. Representative images of Wt and *Id3*$^{-/-}$ epididymal and subcutaneous AT stating for biglycan after 4 weeks of HFD are displayed. Scale bar: 200µm. Data represent mean ± SD; **p<0.01.

3.7.2 Effect on Decorin

The promoter of the *Dcn* gene contains 8 E-box elements (CANNTG) in the first 2000bp of the promoter which are depicted in **Figure 27**.

AACAGTAACTCTTCCTGTGTGTGTGCTCATTCTCCTTATGATGAAGCACAGCTATGTAACCTGGATTC
AGAATTAGAATCTCTGGGAGCTGCCTTGTGCTTTGGGTCTTACTTAGCTTCATGGGCAGGGAGAGGTC
ACTGGTTCTCAATTTTTATATTTTCAAAACAGGAGGAGCAACTCTTCTTGGCTAGTT**CAATTG**TAAAC
TATATAACACACCAGAAAATAATGGAAAGTAATATTTATGGCGCACTTATACTGAAAGTAAGTTGAAA
TAAATTTGTTCTATACATTGTCTGCTTTCAAGCTCCATCTAAGACTAACCACTGAGTTACGTTTTCTA
TGTATTCCA**CAGGTG**CAGAGACTGAAGCTTGGGGAGGTTAGGGGAGTTGCTTTAATTCCTAAACCTGT
CATCAAAGGGAAGAACCCAGATATGAACTTTAAACCTAACAGCCCCACCAGTAAAAATTCAAACTAAT
TTATATGCATCTTTTGTTTCCTCTTGCCAACTTTATTCTACTTTTCTTTCCTATTTCTTTGCTTTCAT
CTCCTGTCTTATTCTACATTAGGCAATGACTGCTGCCACAATTTGTCCTGACTCACTAGAGTGAAGTT
CAGTGTTGCTAAGAAACAAATCATCGATTAAGAAAGACAATGACTATAGTAACTGTGTTAGAGGGACT
ATGTGTGTTTTCTGGGAGTGAGGCAATGAGCAAGGAGTTATCGCATGTCAGAAGAAACTTATAAATAC
AAGCAACATTCAGAGGAGAAAGTCAATTAGTGCCAGAAGAAAGGGCATGTTCCTTACACCAATGTCAG
CGAA**CACTTG**GACTCAACAGAATCACTCAGCATGCTTCGACTCTGCAAGAATGGAGTGTGTGGAGGGA
GAGGTTAAAAGACAGGCAGTTAGACTTGGGAAAGAAGTCAAAATAAGTCTAGCTACATCCTCCCCCTC
CCTCAGATTCCCTCTCAAGAATTTAATTCCTTCCAGCTCCATAAAAATAAAAAAATATTTCCTGTCAA
AGCATGCACTTAGGTGGGTAAAGGAAGGATAGGGGGAATCTCCTCCTTTTTCATAGATGGTGGCTTCA
AGTCCC**CACCTG**ATCAGAGCCTGGAGGCCTGAGCAGAAAAATGCGAGTCAGAACCTGGGAAGGCAAAC
AGAGCAACCCACAGCATCCAGAGATGGAATTATAAAATCTCCAAAAACTTTCTTCACTGCCTGAATAA
ACATGTTACTCAATTTGCACTTTCTTCTCCTCCCCCTGCCTATTTACTGAAATTTAAAAAGAGCCACA
GAAAGTCCTAATTACATAAGGGACCCATCTATAAAAATTATTATTTTTTTCTTTACTTACAAACTAAA
TCTTATTGTAATCAGTGTCTAGTTTCTATGTGTTTTATTCAACAACAGCAGCAAAGAATAGACAGTAA
GGAAGTTTTTGAAGCCGTAGGTAATGAAAATAATAAACAACATATTTTCCAGATTAAATTCTGGCTTT
GTCCCAGAACACCATAGAAATGCATTCAAAATGCACAGAGAACTCCAGAG**CACTTG**AACTTCAGAGCC
CAGGAGTAATTCTATGGAAGTCTAATTAGTCTTCTCTGCAGACCACATTTAAAAAAGCTTTAGGATTA
ATGCCATTCCATTTTCCAGACCCACACATCTCCAAAGCAAGGGGGAAAAAAGTCATTTCAGAAGGATA
ATAAATACTACTTACAAACAAGACTGGAAAGGGTGGAGACTGGAATGGGGTTGGGGGTGGGGAGACAA
ATTCTTCAGTTACAATCTTTTAGAAAAAAAAAAAAAAGACAAATTTCAAATCAAGTTGCTCCACTAGA
CTACAAAAGCAGTTTGGAATGCTGGGCGGATGCAAAGGGATAAAG**CAAATG**TGGAGGGGGAGGGAGAA
GGGGGCCGATAAAGTTTCTGGCTACAATACAAGAGACGTATCATTAC**CATATG**ATCTAATGTGGGTGT
CAGCTGGATGCGCTCACGCAGTGAAACC

Figure 27: Illustration of the E-box elements in the promoter of *Dcn*. The first 2000 bases of the 5´flanking sequence of the *Dcn* gene contain 8 E-box elements (shown highlighted). The data were retrieved using the Biomart tool[139].

Quantification of immunohistochemistry showed that higher amounts of decorin were accumulated in subcutaneous AT of HFD-fed *Id3*$^{-/-}$ mice compared to control littermates. This effect was not seen in the epididymal AT **(Figure 28)**.

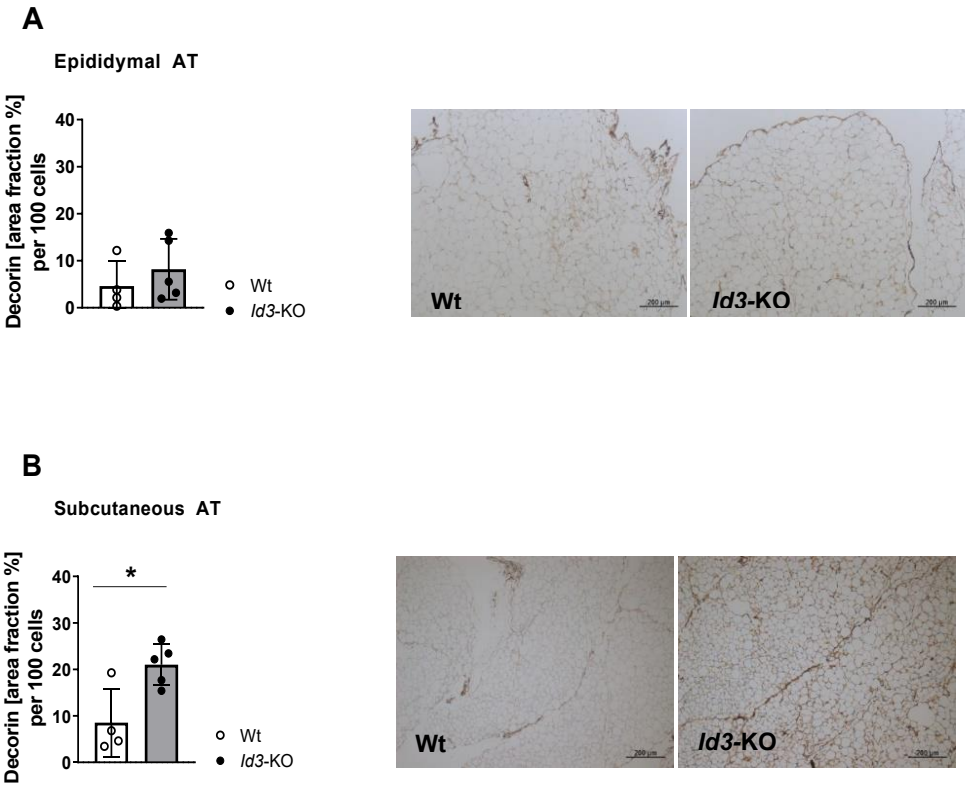

Figure 28: *Id3*-deficient mice have elevated decorin levels in the subcutaneous AT. A-B. Quantification of the area fraction of decorin per 100 adipocytes showed increased decorin content in *Id3*$^{-/-}$ subcutaneous AT and no difference in epididymal AT; n=4, 5; unpaired *t* test**.** Representative images of Wt and *Id3*$^{-/-}$ epididymal and subcutaneous AT stating for decorin after 4 weeks of HFD are displayed. Scale bar: 200µm. Data represent mean ± SD; **p<0.01.

3.7.3 Effect on Aggrecan

The promoter of the *Acan* gene contains 7 E-box elements (CANNTG) which are depicted in **Figure 29**.

TGGGGTCACGAGGCATCAGGCATATACAAAATGGCTGCTGTCTGTTCGTTAAAACTACTCGATGATCA
GTAAC**CATCTG**TTTCCTTATTTACAAAGATGAATTACCTATTGAATATTTGTCTTTGACTTGAATTGC
TCTTCATCAATCCAAGGCCCTCCGGGATATACGTCAAATATGATGCCACTTTGCAGACAAGGACAGTC
CGTGGTCACCCAGAGCGTGACTTGAGAAATGCTTTAGACTTTAAGAGACTAGTGTTTCCTAAGAAAAT
GTTTTTTAGTTTAATTTTTTAACAAAGAGATTGATGTTTCTAGAAAATAACTCATAAGATTCCACTCT
ATTCTTCTAAAAAGCAAACACACTAGCCTCTGAGCAGCGCTGACTACCATTGAAATGTGCTGACTGTG
ACCCAGAGCAGCCAATATA**CAGGTG**GGAAAGAAGGCAGGCCACCCAACAGAA**CACCTG**AGCCACAGCC
CACCCTGGGCTTCACCCCCTGTACAAGAAAGAAACAGTCAAAGAATGCTCTGGGCCAGGGCCAGTCCC
AAAGACCACTAGCCAGTGAGGTATGCACACAATTCCAGCATAGTCAACCTGGGGAAACTGAGGCACAT
CACTTCTGACCTCTCATCAAGAAAAAACTTGGTCGGTTCTCTCTGTAGTCTGCAAAGAACCCACTTCT
TGCCCAGTGAGAGATTCGGGAGATTTCCACTGCACTGCCTGAGGCCACTGTGCTTTAATGAGAAGAAC
ACCCGCTTCCTCTCAAGGCCAGCAGCGGTCTGAATCCCCAGCCCCCAAACACACTGCAGCTTGCCCAG
CTAGCTGCTCCTGTGAGGGGTGACCTTGACTTGAAGTTAGCCCCAACTTGCTGGACAACTCCACCACT
TTCTGAGCCCCATGGTATATGTGAGCATTGTTGGGAGGTGAGAGGTAGTGTTGTAATATTTAACTTAT
TGGACTCGTTAGAGAAATTAAAATCACTGTATGCTGCAACTAGCTTATAGAAGGGATCCAAAGACTCT
TAGATTTTTCTTTTTCCGGGAAACAAATTTATTAAAGAGTGTTGTAGAGGCCAGGCCGTAGCGAATTC
CTGCTTGAGATGTCCTTGGTCTATGTTGCGTTTTGAAGACACCCCTCCCCGCGCCCTCAGCCTTGTGC
CTTGTGCCTCTGTAGCTGCCTCATCTCCTCTCTCCGCCCTTGCGTCTCGGGGTACCCCACCCCCAAAA
CTTTCCAACAGTGTTCTATGAAGATTCTTTCAAATCGCATTCCCAGAGTAGGGGGTCGTCCTGTGCGA
TGGCATCTTTCTGGGTAT**CAGCTG**CAAATCGCATCCCGATACCAGGGAAACACCCCGACCCCAACCCC
AGCACCGGACTGCTACCCTGACAGCAGGAGCCGGGTGCCTTCGGCACTCTGCGGGCGCAGCCCTCCGG
GGCCGCCTGGACTGCGGAGCTGCCGACCGCAATGCAGACGCGGGCCCTCCAGTGCTGCCCGCACAGCT
TTCCTCCGCGGCCCCAGGAGCTGCGGGGTCCGCGCTCCTCTCGTGCCCTGCGCGCCCGGAGCCTTCCC
CAGCTGAGCGCGGTCCCCAGCCCGGGTCCTGCGCGCTCCGGACGTTTCTGCCTTCCCCTCCCCCCGCA
GATTGGCCCCGGGGGTGGGGTTTCCCTGTGCGCTCGCCCCCACCCCTCGTGTGTGCCCTCCCCTCCCC
CGCCCGCCCCTATGTATGTGTCACCGCGCACCATTCCCGCCCACCTACCTCCCCGCGGTGCCAGAGGG
GCTCACAGAGCTGAGGACGCGTGCGGAACGGCTCAAGGTCCCTCACTCTCTCTCCGCATCCTCGCCGG
CTAG**CATCTG**ACG**CAGGTG**CCGAGGGAGTTCGGGCACCTTTCTGTGTCCCTTCCCTTCATCGACCCTG
CTCCGAAACCTAGTCAGCCAGCCACCACTGCGGCCACCGCCCGAGGGGACTTGCGGAGAAGACGCCGG
CGGGAGAAGGGGTTCGCAGGGCCCCCCC

Figure 29: Illustration of the E-box elements in the promoter of *Acan*. The first 2000 bases of the 5´flanking sequence of the *Acan* gene contain 7 E-box elements (shown highlighted). The data were retrieved using the Biomart tool[139].

Quantification of immunohistochemistry showed no differences in the amounts of aggrecan between HFD-fed Wt and *Id3*$^{-/-}$ mice in the epididymal nor subcutaneous AT **(Figure 30)**.

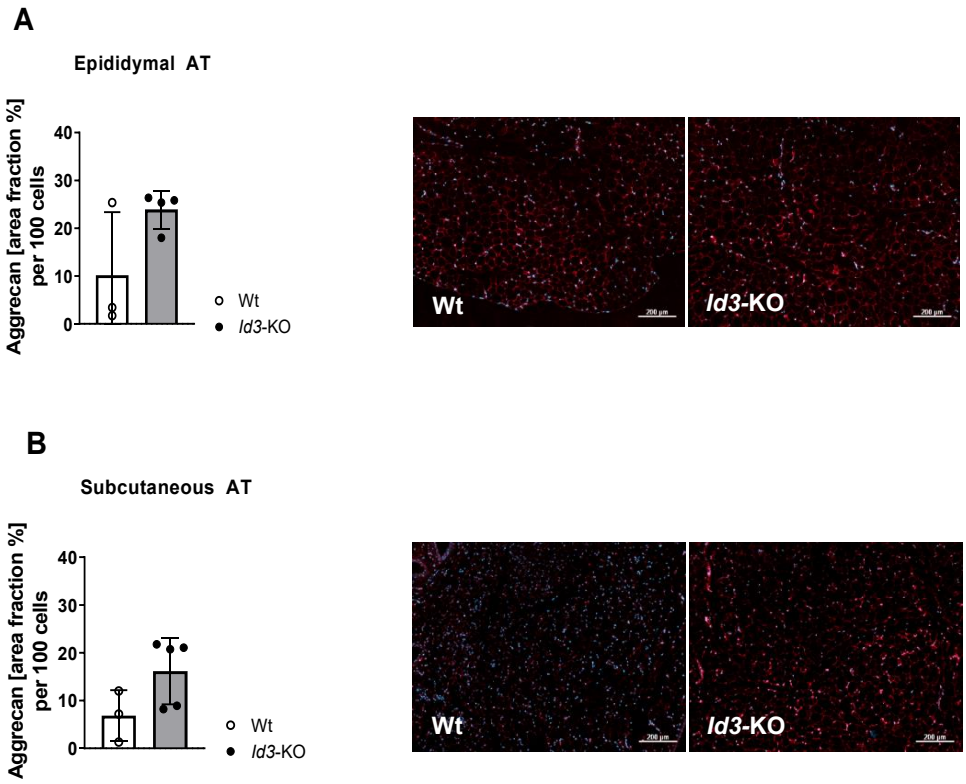

Figure 30: No differences were observed in the levels of aggrecan in the AT. A-B. Quantification of the area fraction of aggrecan per 100 adipocytes showed no differences in the aggrecan content of the Wt and *Id3*$^{-/-}$ epididymal and subcutaneous AT; n=4, 5. Representative images of Wt and *Id3*$^{-/-}$ epididymal and subcutaneous AT stating with anti-aggrecan after 4 weeks of HFD are displayed. Scale bar: 200µm. Data represent mean ± SD.

3.7.4 sEffect on Versican

The promoter of the *Vcan* gene contains 6 E-box elements (CANNTG) which are depicted in **Figure 31**.

Figure 31: Illustration of the E-box elements in the promoter of *Vcan*. The first 2000 bases of the 5´flanking sequence of the *Vcan* gene contain 6 E-box elements (shown highlighted). The data were retrieved using the Biomart tool[139].

Quantification of immunohistochemistry showed no differences in the amounts of versican between the epididymal or subcutaneous AT of both genotypes **(Figure 32)**.

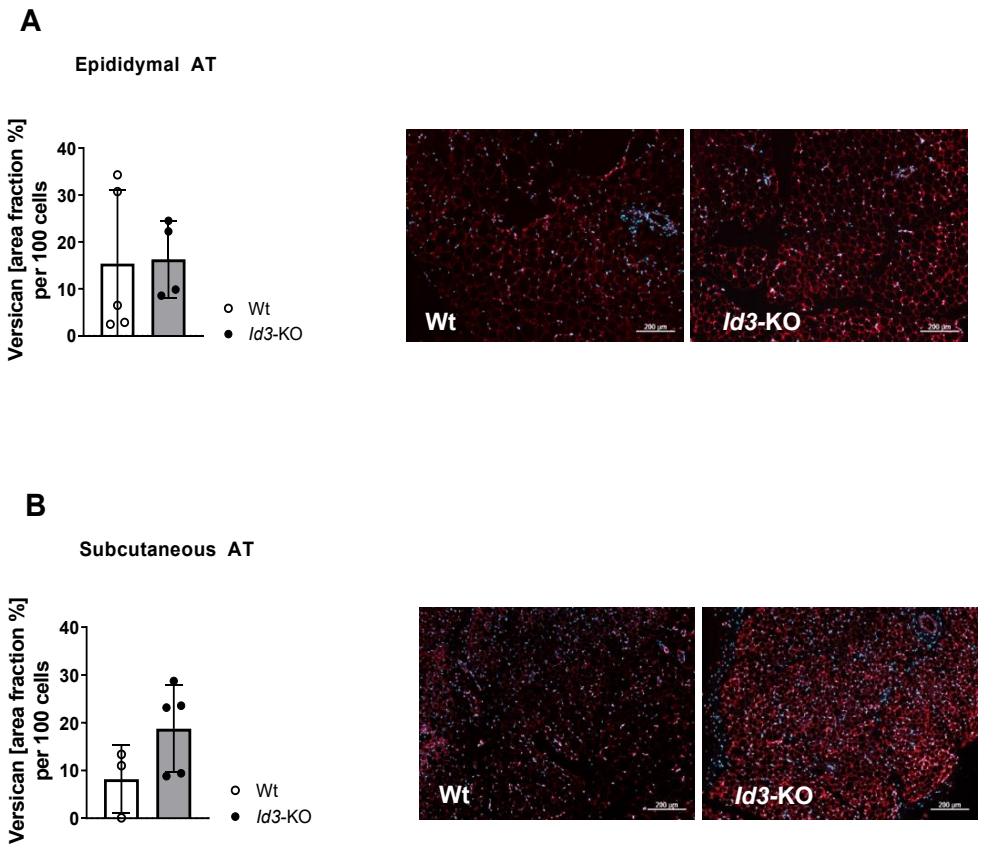

Figure 32: Versican levels were not different in the AT of Wt and *Id3*-deficient mice. A-B. Quantification of the area fraction of versican per 100 adipocytes showed no differences in the versican content of the Wt and *Id3*$^{-/-}$ AT; n=4, 5. Representative images of Wt and *Id3*$^{-/-}$ epididymal and subcutaneous AT stating with anti-versican after 4 weeks of HFD are displayed. Scale bar: 200µm. Data represent mean ± SD.

3.8 Effects of 4-MU treatment

Male *Id3*$^{-/-}$ mice Wt littermate controls were fed a HFD or a HFD supplemented with 4-MU for 4 weeks, starting at 8 weeks of age and including 2 weeks of pair feeding regimen.

3.8.1 Effect of 4-MU on body weight and adipose tissue weight

To begin with, food intake was monitored daily for every mouse of this study, in case the 4-MU addition affected the feeding behaviour of the mice and in order to confirm that any effects observed would not be due to differences in food intake. Results showed that mice from all 4 groups consumed similar amounts of food during the treatment, although some "shredding" behaviour was observed **(Figure 33)**. The body weight of Wt mice was similar after 4 weeks of treatment. However, addition of 4-MU in the diet significantly decreased the body weight of *Id3*$^{-/-}$ mice **(Figure 33)**.

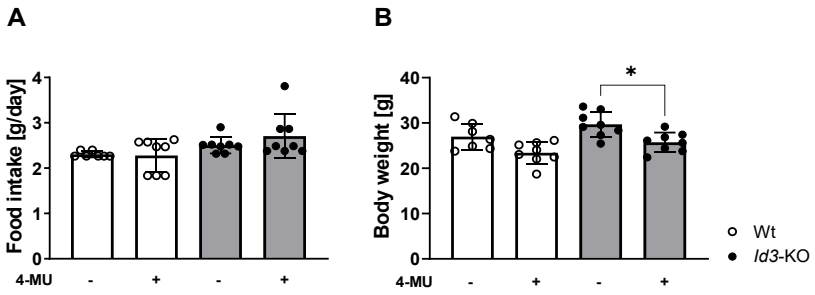

Figure 33: 4-MU led to decreased body weight in *Id3*$^{-/-}$ mice. A. Food intake was calculated as the mean of food consumption per mouse per day for 4 weeks of treatment. **B.** *Id3*$^{-/-}$ mice showed decreased body weight in response to 4-MU treatment; n=7,8. Data represent mean ± SD; *p<0.05.

After 4 weeks of treatment, epididymal AT depots were harvested and their weights were compared. For this series of experiments, we only examined the epididymal fat depot, since this was the only fat pad which presented differences in our previous results. Mice from both genotypes demonstrated significantly reduced AT depot weights after consuming 4-MU, although the effect of *Id3* deficiency on AT weight that we observed before was blunted in this case **(Figure 34)**.

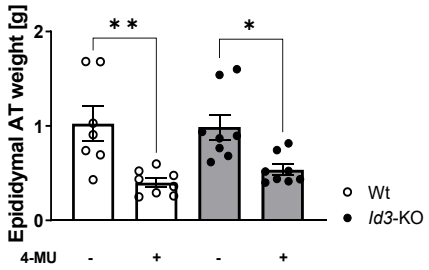

Figure 34: 4-MU led to decreased AT weight in both *Id3*$^{-/-}$ mice and Wt controls. Epididymal AT weight was not different between *Id3*$^{-/-}$ mice and Wt littermate controls after 4 weeks of HFD. Treatment with 4-MU led to reduced AT depot weight in both genotypes; n=7,8. Data represent mean ± SD; *p<0.05.

Glucose tolerance test was performed for *Id3*$^{-/-}$ and Wt mice after 4 weeks of HFD or HFD supplemented with 4-MU. Glucose levels were equivalent among the groups **(Figure 35)**.

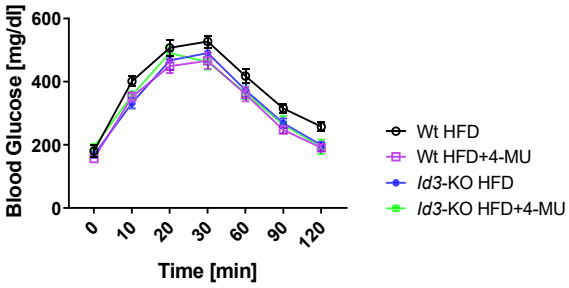

Figure 35: Glucose tolerance was not improved after treatment with 4-MU. GTT was performed after 4 weeks of HFD +/- 4-MU in *Id3*$^{-/-}$ mice and Wt littermate controls. No differences were observed among the 4 groups; n=7,8. Data represent mean ± SD.

3.8.2 Immune cell composition of mice after 4 weeks of HFD with or without 4-MU

Next, we performed flow cytometric analysis of the SVF isolated from epididymal AT. As depicted in **Figure 36,** 4-MU treatment did not lead to any alterations in the cell populations of B cells, T cells and macrophages of *Id3*$^{-/-}$ and Wt littermates, neither in the B cell subsets, B1 and B2. Surprisingly, no effect was observed due to *Id3* deficiency alone, either, which was seen in our previous results.

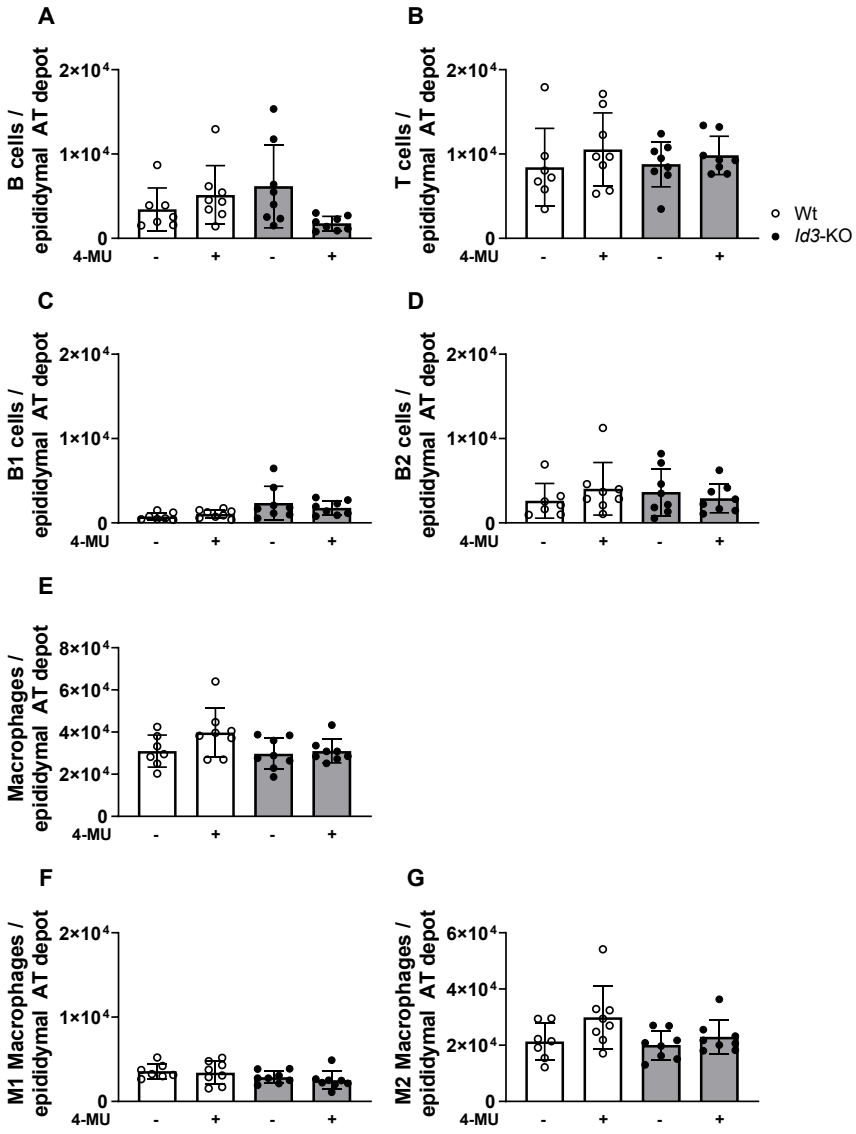

Figure 36: Mice treated with 4-MU did not demonstrate differences in immune cell populations. A-B. Flow cytometric analysis showed no alterations in the B cell population in epididymal AT of *Id3*$^{-/-}$ mice, as well as in T cells; n=7,8. **C-D.** B1 and B2 cell subset populations were not altered in the AT of both *Id3*$^{-/-}$ and Wt mice after 4 weeks of treatment; n=7, 8. **E-G.** Numbers of total macrophages and M1 and M2 macrophages in epididymal AT were similar between *Id3*$^{-/-}$ and Wt mice after 4 weeks of HFD supplemented with 4-MU; n=7,8. All cell populations are expressed as cell number per epididymal AT depot. Data represent mean ± SD.

3.8.3 Effect of 4-MU treatment on HA content

To determine whether the HA inhibitor 4-MU can reduce the elevated HA content that was observed in the AT due to *Id3* deficiency, immunohistochemistry was performed using epididymal AT paraffin sections. Quantification of the staining showed that 4-MU did not inhibit HA accumulation in the AT of neither Wt nor *Id3*$^{-/-}$ mice

(Figure 37). Of note, HA was not increased in the AT of *Id3*$^{-/-}$ mice, in contrast to what was seen in previous experiments.

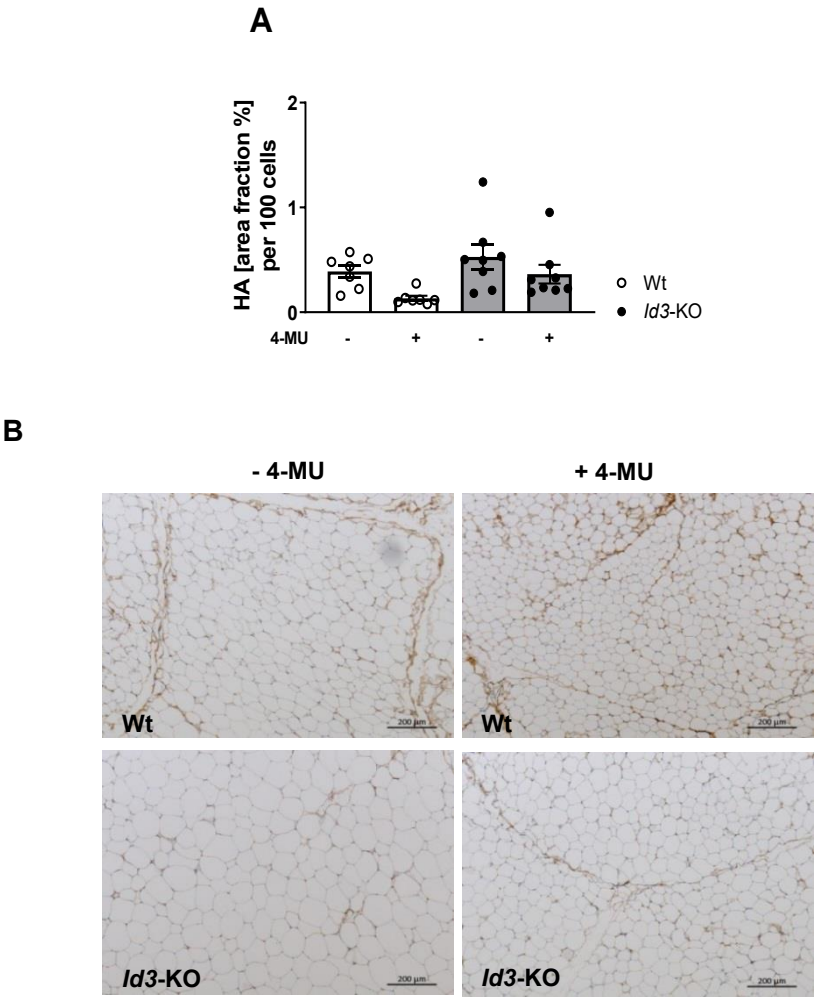

Figure 37: 4-MU treatment did not alter HA content in epididymal AT of *Id3*$^{-/-}$ mice. A. Quantification of the area fraction of HA per 100 adipocytes showed no differences in HA content among the different groups; n=7,8. **B.** Representative images of Wt and *Id3*$^{-/-}$ epididymal AT stained with hyaluronan binding protein after 4 weeks of HFD with or without 4-MU are displayed. Scale bar: 200µm. Data represent mean ± SD.

Moreover, circulating levels of HA were determined by ELISA; no significant differences among the different experimental groups were observed **(Figure 38).**

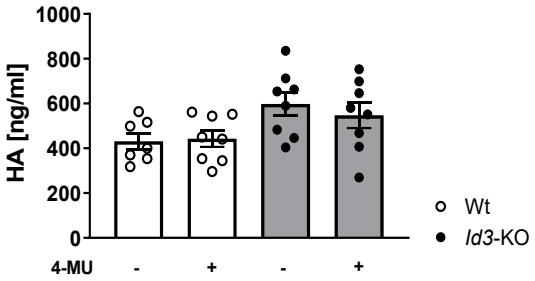

Figure 38: **Levels of serum HA did not present any differences after treating *Id3*$^{-/-}$ mice with 4-MU.** Circulating HA was determined in plasma samples of *Id3*$^{-/-}$ and Wt mice after 4 weeks of HFD with or without 4-MU and revealed no alterations on HA levels; n = 7, 8. Data represent mean ± SD.

3.9 Evaluation of the effects of *ID3* polymorphism on the HA system in patients

3.9.1 Characteristics of the study samples

Baseline characteristics and obesity-related comorbidities of the participants of the studies 14180 and 15328 are summarized in **Table 7.** The cohorts included patients that were homozygote for the common allele (CC) and patients that carried the risk allele, meaning that they were either heterozygote (CT) or homozygote for this less frequent allele (TT). The 2 cohorts were not comparable in terms of age, since the participants in study 15328 were much older. Furthermore, 15328 participants were relatively healthier with lower BMI (median 31.46 for *ID3* risk allele carriers) compared to 14180 subjects, which is reasonable since these patients underwent bariatric surgery. Other important factors considered were the prevalence of diabetes and hypertension, which were lower in the 14180 cohort.

Table 7: Patient baseline characteristics.

	COHORT			
	14180		15328	
	Ancestral Allele	Risk allele	Ancestral Allele	Risk allele
Patients characteristics				
N	13	26	19	20
Age (years)	46.69 ± 11.79	43.35 ± 9.83	64.32 ± 9.14	64 ± 8.96
Men %	23.08	19.23	63.16	60
Women %	76.92	80.77	36.8-9	40
BMI (kg/m^2)	48.92 ± 9.67	49.48 ± 8.17	30.6 ± 6.65	31.46 ± 6.87
Diabetic (%)	15.38	38.46	47.37	45
Current smoker (%)	9.09	21.05	10.53	5
Hypertension (%)	69.23	61.54	78.95	75

Values are the average ± standard deviation.

3.9.2 Effect of *ID3* polymorphism on *HAS* mRNA expression

To determine if loss of function of the human *ID3* gene can affect the regulation of the HAS isoenzymes in human fat, we performed qPCR using RNA from the omental AT of obese subjects from the Study 14180. *HAS* mRNA expression levels are shown in **Figure 39**. Interestingly, our results demonstrated no differences in the expression of the *HAS2* isoenzyme, which was shown to be upregulated in HFD-fed *Id3*$^{-/-}$ mice. The same observation was made for *HAS3,* whereas *HAS1* was not detected in patients homozygote for the risk allele.

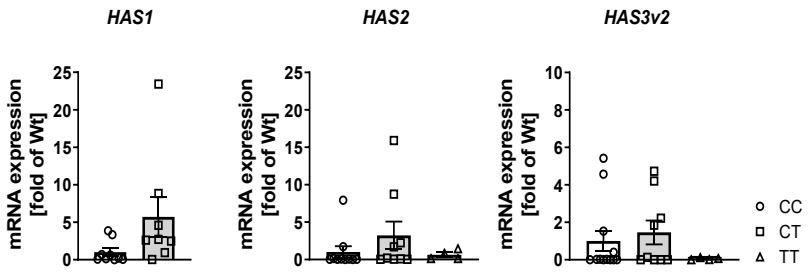

Figure 39: No differences in HAS expression of human subjects with the risk allele of *ID3*. mRNA expression of the three HA synthase isoenzymes (*HAS-1, -2, -3*) was measured in human omental fat isolated from patients that did not carry the risk allele (CC) and patients that were either heterozygote (CT) or homozygote (TT) for the *ID3* polymorphism. Expression levels were not different between the experimental groups. Results are normalized to *RNA18SN5*; n=4-12. Data represent mean ± SD.

3.9.3 Effect of *ID3* polymorphism on HA content in the AT

To further investigate a possible effect of the *ID3* polymorphism on the HA content in the omental fat of obese humans, which could have been undetectable on the mRNA level, we performed immunohistochemistry. HA was stained on the omental fat from the same cohort of patients and our results revealed no increase in the HA in the human obese samples **(Figure 40)**.

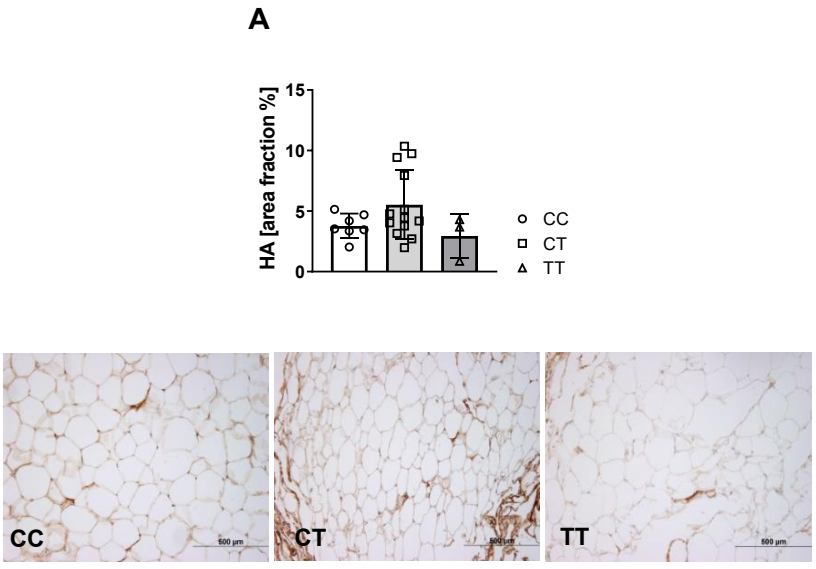

Figure 40: **Human omental fat from subjects with or without the *ID3* risk allele did not present altered HA content. A**. Quantification of the HA staining revealed no differences in the HA content among patients that did not carry the risk allele and patients that were either hetero- or homozygote for it. **B**. Representative

images of the human omental fat stained with hyaluronan binding protein; n=4-12. Scale bar: 200µm. Data represent mean ± SD.

3.9.4 Effect of *ID3* polymorphism on circulating HA level

In an attempt to characterize a possible effect of the human *ID3* SNP on circulating HA, we measured plasma HA in a different cohort of patients (Study 15328). Although there seemed to be a trend towards increased HA levels in the plasma of patients homozygote for the risk allele, our results showed no significant differences **(Figure 41)**.

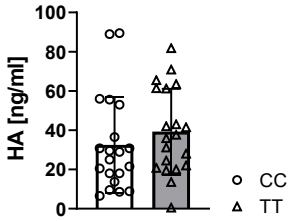

Figure 41: No differences observed in the serum HA of subjects with or without the *ID3* risk allele. Circulating HA was determined in plasma samples from patients that did not carry the risk allele and patients that were homozygote for it. No differences were observed. n = 20. Data represent mean ± SD.

4. Discussion

4.1 Effect of *Id3* deficiency on visceral adiposity

In the present work it was shown that the transcription factor Id3 plays an important role in regulation of HA in the AT in response to obesity. We demonstrated that *Id3* deficiency led to increased *Has2* mRNA expression in male C57BL/6J mice upon HFD feeding and as a result HA accumulated in the AT. This effect was followed by increased inflammatory immune cells in the area, thereby contributing to AT inflammation.

Our study adds further knowledge to previous results showing that Id3 is associated with HFD-induced epididymal AT expansion[132]. An interesting study showed that *Id3* expression was induced in the visceral AT of HFD-fed C57BL/6J mice and that when *Id3* was absent, this fat depot was characterized by decreased expansion. In more detail, *Id3* deficiency led to attenuated visceral AT weight by inhibiting HFD-induced VEGFA, providing evidence that Id3 is implicated in adipose angiogenesis and obesity. Thus, Id3 was identified as a promising target against the visceral obesity. In line with this study, we also confirmed that there was no difference in the weight of brown AT depot in *Id3*$^{-/-}$ mice.

In the present study, we chose to treat the mice with HFD for a shorter period of time, namely 4 weeks. From previous studies we know that the consequences of *Id3* deficiency on visceral adiposity are detectable already early. So, our aim was to examine the events leading to dysmetabolism in *Id3*$^{-/-}$ mice early in the setting of obesity. Indeed, it was demonstrated that *Id3* deficiency affected the early development of HFD-induced obesity, with *Id3*$^{-/-}$ mice displaying significantly smaller visceral AT depots compared to Wt controls even after only 4 weeks of HFD (with similar body weight to Wt mice)[132]. Similarly, mice lacking *Id3* did not present differences in the AT depot weights after 4 weeks of standard laboratory diet, but HFD induced a significant increase in the AT in both *Id3*$^{-/-}$ and Wt mice up to that time point. However, loss of *Id3* led to a significant attenuation

of epididymal AT expansion, but not of subcutaneous, highlighting once more the very specific role of *Id3* in HFD-induced visceral adiposity.

Interestingly, despite smaller epididymal AT depots, glucose tolerance was not improved in mice lacking *Id3*. It is known from the literature that AT expansion during obesity is correlated with worsened metabolic rates, such as insulin resistance, while the distinct AT depots also contribute differently in dysmetabolism[17,148,149]. Human studies where individuals were matched for total body fat (or for subcutaneous fat) but with high versus low levels of visceral AT have demonstrated that patients with visceral obesity display a worsened metabolic profile[150,151]. In line, weight loss can have a beneficial effect on obesity-induced AT inflammation. In humans, it was shown that caloric restriction or bariatric surgery leading to weight loss had a remarkable effect against AT dysmetabolism and restored insulin sensitivity[152–154]. Based on these studies, an improvement in the metabolic profile of mice lacking *Id3* was expected, since their visceral fat depots were significantly smaller. Yet, their glucose levels were equivalent to those of Wt mice, and no metabolic amelioration was detected. This is an effect also observed in a previous study, where both groups presented similar glucose and circulating lipid levels, although this finding was not further investigated[132]. However, we sought to examine this phenomenon, and this led to the new hypothesis, that *Id3* may regulate other processes in the AT that promote dysmetabolism and inflammation.

4.2 Effect of *Id3* deficiency on HA-mediated AT inflammation

Preliminary work of the McNamara lab showed that *Id3* deficiency increased the promoter activity of the *Has2* gene *in vitro*, using aortic SMCs. Therefore, we next hypothesized that Id3 may also regulate the transcription of the *Has* isoenzymes *in vivo* in the HFD-fed *Id3*$^{-/-}$ mouse model.

It is generally known from the literature that the mRNA expression of *Has* isoenzymes is largely cell-type-dependent, with HAS2 being recognised by many studies as the most abundant isoform. For example, HAS2 was revealed to be the main HA-synthesizing enzyme in mesothelial cells, in SMC-rich tissues, as well as in proliferating VSMCs[155]. Specifically, after treatment of VSMCs with PDGF, mRNA levels of *Has2* were increased rapidly and by almost twofold compared with *Has1* and *Has3*, which were only slightly upregulated[156]. Moreover, HAS2 was markedly increased in human SMCs under certain stimuli[157]. Of note, 3T3-L1 adipocytes also produce more HA while differentiating and it was shown that *Has2* mRNA was more abundant than *Has1* and *Has3* and, as result, responsible for HA production[80]. Furthermore, *Has2* mRNA expression was the only isoform that was increased *in vitro* in hypertrophic adipocytes, with hypertrophy being a major characteristic of obesity, while *Has2* mRNA was upregulated in the AT of two different DIO mouse models: in HFD-fed *Ldlr-/-* mice and in *ob/ob* mice. In the visceral AT of both of these obesity models, *Has2* was highly upregulated, whereas *Has1* and *Has3* expression were not detectable[71].

Our data showed increased *Has2* mRNA expression in *Id3*$^{-/-}$ epididymal AT, while the expression of the other isoenzymes did not changed and so we hypothesized that HAS2 is the isoenzyme that is mainly affected in the AT when *Id3* is absent. Id3 is a broadly expressed transcription factor, and hence it is likely that it is expressed in many of the different cell types present in the AT. However, the focus of this study was how *Id3* could regulate HA production, and thus, cell types in AT known for producing HA were examined, and particularly SMCs and adipocytes. Our data demonstrated that *Has2* expression was not different in isolated adipocytes from mice Wt or null for *Id3,* but *Has3* expression was increased in *Id3*$^{-/-}$ mice. Next, we turned our attention to SMCs, another source of HA, especially during their proliferative state[157]. Our qPCR experiments clearly point to an increased mRNA expression of *Has2* in cultured *Id3*$^{-/-}$ VSMCs, leading us to the

conclusion that SMCs are potentially the source of HA in *Id3*$^{-/-}$ AT. *Has1* was also upregulated, although to a lesser degree, highlighting again the possibility that HAS2 is the main isoenzyme affected by *Id3* deficiency in VSMCs. Nevertheless, in order to determine if SMCs are the sole or predominant HA-producing cell type in adipose tissue, a VSMC-specific deletion of *Id3* would be needed. However, this mouse model is a very challenging model to generate, as the available mouse has Myh11Cre on the Y chromosome leading to a very low percentage of littermates that can be used and thus will be investigated in future research.

Consequently, it is reasonably hypothesized that when *Has2* mRNA expression is increased in the AT, so is HA production. HA was increased in the AT of *Ldlr-/-* mice fed a HFD for 16 weeks and in genetically obese *ob/ob* mice. This effect was accompanied by adipocyte hypertrophy and macrophage accumulation[71]. In a different study, HA was found in the AT of C57BL/6J mice fed an obesity diet for 16 weeks, but its content was reduced after injection with hyaluronidase, along with a transient decrease in body weight and fat mass[79]. Based on these findings, we expanded our studies and attempted to further characterize the effect of *Id3* on HA. Immunohistochemistry was performed on epididymal and subcutaneous AT from Wt and *Id3*$^{-/-}$ mice under normal or high fat diet. In agreement with increased *Has2* mRNA expression, increased HA content in the epididymal AT of *Id3*$^{-/-}$ mice fed a HFD for 4 weeks was observed, compared to Wt littermates, whereas there was no difference in the subcutaneous fat depot.

Interestingly, the effect in the AT was coincided with an increase of circulating HA, showing that *Id3* may have a systemic effect on HA production. Elevated serum HA has been linked with several diseases. In particular, circulating HA was increased in patients with chronic viral hepatitis and cirrhosis and was also associated with disease progress[158]. Other pathological conditions that are characterized by elevated plasma HA are arthritis, pneumonia and several kidney diseases[62]. Importantly, increased circulating HA

levels were paralleled with impaired metabolic function in diabetic patients and fasting plasma glucose was correlated positively with HA levels[76]. Moreover, plasma HA was strongly associated with carotid intima-media thickness and BMI values, as HA levels tended to be higher in obese patients[76,159]. These results could be useful for the development of potential biomarkers, which will detect early metabolic dysfunctions that are associated with obesity and could lead to morbidity. This matter will be investigated further in the future.

In our study, we observed that *Id3*$^{-/-}$ mice did not present improvement in their glucose tolerance, despite being leaner. Therefore, we hypothesized that *Id3* may regulate other processes in the AT that promote metabolic dysfunction and inflammation and the first step towards that was to examine the immune cell composition of the AT.

Initial work at this field has shown that during obesity-induced AT inflammation, there is unexpected trafficking of immune cells in the fat, including macrophages, T cells, but also B cells, a cell type that has been neglected so far in the obesity research[160]. Winer *et al* demonstrated that B cells accumulate in the AT of mice that have been receiving HFD even only for 3 weeks, an effect that is evident before the accumulation of other immune cells[33]. The same study also showed that B cells modulate T cell function in DIO AT in an MHC-dependent manner, possibly through B cell antigen presentation to T cells. When B cells were globally depleted from DIO mice, fewer pro-inflammatory M1 macrophages were recruited in the AT, in combination with reduced HFD-induced insulin resistance, thus ameliorating metabolic disease[33]. Likewise, introduction of B cells from spleen of DIO mice into B cell-deficient mice worsened glucose tolerance[33,35]. Taking into consideration that the majority of the CD19^{+} cells in the spleen are B2 cells, the impairment of metabolic function is likely due to B2 cells[33–35]. Moreover, adoptive transfer of B2 cells in HFD-mice lacking completely mature B cells led to dysmetabolism, providing further evidence that B2 cells promote metabolic dysfunction during DIO and corroborating these

previous findings[138]. Of note, B2 cells have also been linked with diabetes in humans: circulating B2 cells from patients with T2DM were found to exert pro-inflammatory action through increased production of IL-8 and decreased production of IL-10, proving that these immune cells might play a -thus far not so appreciated-role in inflammation related with T2DM[161].

Id3 is known for its different roles in B cell biology, though it is not clear yet in which way Id3 may regulate B2 cells and more specifically with regard to HFD-induced AT inflammation.

In the present study, HFD-fed *Id3*$^{-/-}$ mice presented an increase in the B2 cell population, indicating the induction of an inflammatory response. This way, the lack of glucose tolerance improvement in *Id3*$^{-/-}$ mice may be explained, with the data pointing to a dysmetabolism and a local inflammation induced due to *Id3* deficiency. In connection with this, the expression of the pro-inflammatory cytokines TNF-α, IL-6 and IFN-γ was evaluated. Studies have shown that TNF-α and IL-6 were increased during obesity and were also involved in metabolic dysfunction[35,162,163]. Th1 cells are the main producers of IFN-γ, which is implicated in inflammatory responses. Furthermore, DeFuria *et al* demonstrated that splenocytes from obese compared with lean mice secreted higher amounts of IFN-γ, relating this cytokine with obesity-induced inflammation. More recently, IFN-γ was linked with B cells as well. It was shown that a distinct subpopulation of B can produce high amounts of IFN-γ during the early stage of immune responses[164]. Moreover, IFN-γ was found to be elevated in the obesity studies already discussed, where B cells were also increased in the AT of HFD-fed mice. In the same way, production of IFN-γ was reduced in B cell-deficient mice, improving metabolic function[33]. These results are in line with the data of the present study, showing increased *Ifng* mRNA expression in *Id3*$^{-/-}$ mice upon HFD, and suggest that B2 cells promote inflammation in HFD-fed mice through increased production of the inflammatory cytokine IFN-γ.

Form the literature, it is known that global *Id3* deficiency does not lead to disruption in B cell numbers in the spleen, thymus, bone

marrow or peritoneal cavity at baseline[134]. Studies so far have identified Id3 mostly as a regulator of B1b cells in several compartments including AT, where B1b cells were shown to have an anti-inflammatory effect[137,138]. These findings were confirmed by our results showing increased B1 cells in the subcutaneous AT of HFD-fed mice as well as in fat depots of mice under standard diet, meaning that these mice did not present an inflammatory profile. When *Id3* is knocked out specifically in B cells, B2 cells once more not affected[138].

To the best of our knowledge, this is the first study to report an increase in the B2 cell population in the AT due to loss of *Id3* in the setting of obesity, suggesting that Id3 specifically affects processes that promote B2 cell accumulation in the epididymal AT in response to HFD. These findings highlight the importance of B2 cells in AT inflammation and provide valuable data concerning the early inflammatory events that occur in the AT during the first stages of diet-induced obesity[1].

HA plays a vital role in AT dysmetabolism upon HFD, as shown by studies where it was accumulated in the AT of DIO mice, and inhibition of its synthesis reduced the production of pro-inflammatory cytokines[79]. HA is also known for its ability to retain immune cells in the AT. Han and colleagues demonstrated that HA forms a complex with SAA3, and together they promote the recruitment and chemotaxis of monocytes in the AT of obesity mouse models. Digestion of HA with hyaluronidase and separate silencing of SAA3 production both partially decreased monocyte adhesion[71]. Moreover, HA was shown to retain monocytes in cultured hypertrophic 3T3L1 adipocytes, while pretreatment of the adipocytes with hyaluronidase prevented monocyte adhesion, providing evidence that HA is important for the obesity-induced immune cell recruitment in the AT[71]. Further, a study has linked B cells with HA, in the context of wound healing, during which HA is physiologically produced. The findings of this study revealed that HA stimulated B cells through TLR4 to produce cytokines such as IL-6, IL-10 and growth factors, promoting wound healing[165].

Given the evidence that HA is involved in inflammatory responses in AT upon obesity and based on our previous data showing accumulation of HA and B2 cells in the AT of *Id3*$^{-/-}$ mice, we hypothesized that HA might have a specific function in recruiting B2 cells in the epididymal fat depot of these mice after feeding a HFD for 4 weeks. Our results from the HA binding assay showed that significantly more B2 cells attached to the AT of HFD-fed *Id3*$^{-/-}$ mice, together with an increased HA content. Further, digestion of endogenous HA led to a reduction of the adherent B2 cells in the *Id3*$^{-/-}$ AT, proving HA-dependency of pro-inflammatory immune cell adherence to the AT. This is in good agreement with previous studies, showing that treatment with hyaluronidase in the HA-enriched AT reduced the expression of certain pro-inflammatory markers, improving the metabolic profile of the mice[79].

Our *in vitro* data using SMCs also indicate that HA increases the adherence of B2 cells. HA digestion via hyaluronidase treatment on *Id3*$^{-/-}$ aortic SMCs before co-incubation with the immune cells reduced significantly the B2 cells that attached on the SMCs, thereby supporting our hypothesis regarding the importance of the HA matrix in binding immune cells.

Overall, our study revealed that the AT of *Id3*$^{-/-}$ mice was enriched with HA and this was strongly linked with significantly increased adherence of B2 cells in the AT along with elevated expression of *Ifng*, an effect blunted in Wt mice. HA digestion using hyaluronidase reduced the number of B2 cells attaching on the AT, indicating that, locally targeting the HA content in the AT through *Id3* could be beneficial against obesity-induced AT inflammation, mainly through reducing the number of the pro-inflammatory B2 cells and decreasing IFN-γ.

4.3 Effect of *Id3* deficiency on proteoglycans

Apart from HA, the ECM contains plenty of important molecules, for example proteoglycans. It is known from the literature that during AT inflammation, the ECM undergoes dynamic remodelling, and the expression of its components can change dramatically. Research has shown that biglycan mRNA expression was increased in the AT of mice fed a HFD for 8 weeks, along with increased expression of the pro-inflammatory markers IL-6 and TNF-α[101]. Further, biglycan knockout mice showed reduced inflammation in the AT as well as improvement of glucose tolerance compared to Wt mice[100,101]. Another proteoglycan with a potential role in obesity-induced AT inflammation is decorin, although its exact involvement is not yet well understood. It was revealed that decorin expression was significantly upregulated in the obese AT and particularly in cells of the SVF[105]. This effect was also observed in human subjects. AT samples from patients with insulin sensitivity, insulin resistance and T2DM were analysed and an increased decorin expression in the visceral AT of insulin-resistant and diabetic subjects was revealed[105]. On the contrary, a more recent study demonstrated that decorin deficiency deteriorated the glucose tolerance of HFD-fed mice by impairing AT function[106].

The proteoglycan versican has also been associated with AT function in the context of obesity. mRNA levels of versican were increased in mice fed a HFD for 8 and 16 weeks. Analysis showed that versican was mainly produced by adipocytes in this case, while versican content was also increased in the epididymal AT[102].

Considering all the above, it can be concluded that different components of the ECM may be implicated in AT function and obesity-induced inflammation, although the exact mechanisms are not yet well clarified.

Accordingly, we hypothesized that other ECM components might be regulated in HFD-fed *Id3*$^{-/-}$ mice, since our results so far have clearly shown a strong effect of Id3 on HA in the AT in the setting of HFD. For this purpose, we examined whether *Id3* deficiency can impact the

levels of biglycan, decorin, versican and aggrecan in the AT of *Id3*$^{-/-}$ mice after 4 weeks of HFD. These experiments led us to some interesting findings and their interpretation was quite challenging. First, our results showed that the genes that produce these molecules are good candidate genes, whose transcription could be regulated by Id3, since they contain numerous E-box elements in their promoter regions. Immunohistochemistry revealed that only biglycan and decorin were increased in the AT of HFD-fed *Id3*$^{-/-}$ mice, while the content of aggrecan and versican remained unaltered. Interestingly, in both cases the increase was observed in the subcutaneous and not in the epididymal AT of the mice. These results are contradictory with our previous findings showing increased HA in the epididymal fat, but agree with other studies demonstrating increased expression of biglycan and decorin in WAT, including visceral and subcutaneous both in obese human subjects and DIO mice[100,105].

However, a preferential role for *Id3* in HFD-induced visceral adiposity has been established, since *Id3* mRNA expression was induced by high fat feeding in the visceral and not in the subcutaneous fat[132]. Hence, we reached the conclusion that the increased content of biglycan and decorin in the subcutaneous fat was probably HFD-induced (in agreement with these previous studies) and it was not an *Id3*-dependent phenomenon, as was the case with HA. To a certain degree, however, our results are not entirely surprising. For example, decorin has been found to have conflicting roles in different studies, making it clear that defining a role for the components of the very complicated ECM can be challenging.

As the main focus of the present study was to elucidate whether Id3 regulated components of the ECM, and since biglycan and decorin were elevated only in the subcutaneous AT, where Id3 does not have a functional role, no further experiments were performed regarding these proteoglycans. This otherwise very interesting topic is reserved for future research.

4.4 Effects of 4-MU treatment in *Id3*$^{-/-}$ mice

A series of experiments with mice receiving HFD supplemented with 4-MU was included in this study. Since we have shown that the pro-inflammatory phenotype of the HFD-fed *Id3*$^{-/-}$ mice was HA-dependent, our hypothesis for this proof-of-concept experiment was that the inflammatory status of these mice might be attenuated when HA synthesis was inhibited by 4-MU.

4-MU consumption led to decreased body weight in mice deficient for *Id3* compared with HFD-fed *Id3*$^{-/-}$ mice, an effect attributed solely to 4-MU. Furthermore, both *Id3*$^{-/-}$ and Wt littermates had significantly smaller epididymal AT depots when receiving 4-MU. Interestingly, in these experiments *Id3*$^{-/-}$ and Wt mice had similar AT expansion in response to HFD. This finding is in contradiction with our previous results, and it shows that the protective effect of *Id3* deficiency against visceral adiposity was blunted in this case. Regarding metabolic function, GTT performed after 4 weeks of feeding showed equivalent levels of glucose among the groups.

A number of studies have examined the effect of 4-MU on body weight. In a study from 2010, it was shown that *Apoe*$^{-/-}$ mice fed a Western diet with 4-MU for 21 weeks had a trend towards lower body weight[82]. Moreover, decreased VAT weight was seen in mice receiving HFD supplemented with 4-MU for 12 weeks[88]. In a more recent publication, C57BL/6J mice fed a diabetogenic diet supplemented with 4-MU for 17 weeks had significantly reduced body weight gain and total body fat content[89]. In this study, Grandoch *et al* also observed reduced epididymal and brown AT weights. Moreover, 4-MU improved glucose tolerance and insulin resistance of these mice. The food intake of the mice was also similar between the groups and a pair feeding regimen was applied for only 1 week.

In our case, body weight was reduced in both genotypes after mice consumed 4-MU, in agreement with these previous studies. However, the fact that HFD-fed *Id3*$^{-/-}$ mice did not have significantly smaller epididymal AT depots, as seen before, is a matter of concern. One possible explanation for this outcome is that the pair

feeding interfered with the metabolic function of the mice. During pair feeding, the amount of food provided to the pair-fed mice is perhaps different from the amount they would normally ingest. Hence, the animals often consume all their food soon after it is made available to them; as a result, it is possible that they undergo fasting until food is provided again the next day. Consequently, their metabolic status can be misinterpreted and if pair feeding is applied for a long period of time, these consequences can progress over time[142]. It is also possible that animals learn to expect their food at a certain time, again affecting their metabolic functions. A study performed in rats demonstrated that anticipation of meals affects the levels of ghrelin, a hormone secreted by the stomach and small intestine and involved in the stimulation of hunger[166]. Russel *et al* showed that young *cp/cp* rats (a rat model of metabolic syndrome) that underwent pair feeding for 4 weeks presented lower body weight compared to rats that were fed *ad libitum*, although the food intake rates were not different. Furthermore, the reduction of the body weight in young pair-fed rats was accompanied with an improvement in their metabolic status, such as lower insulin and glucose levels, but also increased fatty acid levels, which can have adverse effects[167]. Longer period of pair feeding (12 weeks) also affected *cp/cp* rats, by ameliorating end-stage disease processes associated with metabolic syndrome.

Regardless, however, of the specific effects, it is clear that pair feeding itself can influence metabolic function and needs to be taken into consideration if used in a project where metabolism is examined. Therefore, we suggest that in the present study it is possible that pair feeding induced such changes in metabolism, although subtle, as it was only applied for 2 weeks. This could probably explain why the phenotype of HFD-fed *Id3*$^{-/-}$ mice was not developed as strongly.

Regarding the immune cell composition of Wt and *Id3*$^{-/-}$ mice after treatment with 4-MU, no differences were observed. The population of the pro-inflammatory B2 cells that was increased in HFD-fed *Id3*$^{-/-}$ mice in our first experiments was not replicated this time. This effect was once again blunted probably due to the 2-week food restriction. It seems that in order for the function of *Id3* in response to HFD to

become evident, 2 weeks of feeding *ad libitum* is not sufficient time. Nevertheless, other studies have reported that 4-MU treatment can have a beneficial anti-inflammatory effect and a protective role in immune cell regulation, as was hypothesized initially in the present study. For example, it was found that inhibition of HA synthesis by 4-MU led to decreased T cell proliferation and production of IL-2[81]. Further, 4-MU reduced LPS-induced inflammation in corneal fibroblasts, while it once again reduced the expression of the pro-inflammatory cytokines IL-1, IL-6, IL- 8, TNF-α[168].

Since 4-MU is an inhibitor of HA synthesis, it was expected that HA would be decreased in *Id3*$^{-/-}$ mice fed a HFD supplemented with 4-MU. However, treatment of the mice with 4-MU did not lead to drastic alterations in the HA content in the epididymal AT. Systemic HA was not decreased either, as measured by ELISA. It is very likely that the lack of HA inhibition was due to the pair feeding treatment which may have affected the action of 4-MU as well, apart from the metabolic function of the mice. This alteration can be seen here as well, since the phenotype of the HFD-fed *Id3*$^{-/-}$ mice was once again not replicated; we did not observe an increased HA content in the *Id3*$^{-/-}$ mice compared with Wt mice.

It can be hypothesized that longer 4-MU treatment would be more suitable for an effect on HA content to be evident. For instance, Nagy *et al* reported a reduction of HA levels in the aorta and in circulation after 21 weeks of treatment with 4-MU in *Apoe*$^{-/-}$ mice on Western diet[82]. Regarding the effect of 4-MU on circulating HA, an interesting study showed that a reduction in HA serum levels was seen only one week after C57BL/6 started consuming chow diet supplemented with 4-MU[141]. This was not observed in the present study. Of course, it needs to be considered that HFD induces an increase in circulating HA levels and therefore a prolonged period of treatment would be required until effects of 4-MU can become fully evident.

In addition, the effect of 4-MU on HA synthesis inhibition specifically in the AT has not been studied so thoroughly. *In vitro,* it was shown that treatment of 3T3-L1 adipocytes with 4-MU led to reduction of HA

production, which was accompanied by inhibition of adipogenesis[169]. Moreover, treatment with 4-MU for 17 weeks reduced HA content in BAT[89].

In summary, treatment of *Id3*$^{-/-}$ mice with HFD supplemented with 4-MU did not improve their inflammatory status. However, this was probably a consequence of the fact that the phenotype of the HFD-fed *Id3*$^{-/-}$ mice initially observed in the present study could not be reproduced in this experimental series. We further assume that the application of a 2-week-long pair feeding regimen could have interfered with the metabolic function of the mice and blunted some of the effects that were seen before. This is acknowledged as a limitation of the present study and is reserved for future research.

4.5 *ID3* polymorphism and its potential role on HA regulation

Studies by McNamara and colleagues have shown that a SNP in the coding region of the human *ID3* gene leads to the production of an Id3 protein with reduced function and is strongly correlated with increased risk for atherosclerosis[124,127]. Doran *et al* assessed the six known SNPs of the *ID3* gene in participants of the Diabetes Heart Study, which is a study of genetic and environmental factors of cardiovascular disease in families with increased risk to develop T2DM[170]. After performing a quantitative trait locus association analysis with the SNPs identified in participants of the study, the mutation of the major allele of the *ID3* gene at rs11574 was found to be significantly associated with carotid IMT, whereas the other SNPs were not so strongly correlated with pathophysiological traits, thus recognising this SNP as a novel biomarker of atherosclerotic burden in humans[124]. A subsequent study utilized a larger cohort of patients[127]. Specifically, these subjects belonged in two different groups; the Multi-Ethnic Study of Atherosclerosis (MESA), which included relatively healthy participants, with no prior clinically defined cardiovascular disease and with low levels of diabetes, as well as the

CAVA Study (Coronary Assessment in Virginia cohort), which included much fewer participants that had to undergo a medically necessary cardiac catheterization and was basically the previous study of Study 14180 of the present work. This research revealed that the *ID3* SNP rs11574 risk allele was associated with coronary artery calcium in the MESA cohort and, also, with greater atheroma burden and stenosis in the CAVA cohort. Conclusively, the *ID3* SNP rs11574 was clearly associated with human coronary artery pathophysiology, as demonstrated by these additional cohorts[127].

Based on these previous results highlighting an important role of the *ID3* gene in human atherosclerosis and cardiovascular disease, we expanded our murine studies by examining a possible implication of the *ID3* SNP rs11574 in metabolic function, which is closely related with the risk of cardiovascular disease.

For this purpose and in line with our findings so far, we investigated a potential role of the *ID3* SNP rs11574 in the AT and specifically, in the HA regulation. Since *Id3* deficiency is strongly correlated with HA-mediated inflammation in the AT of mice in the setting of obesity, our hypothesis was that HA might also be present in the AT of obese humans that have the *ID3* polymorphism. More importantly, circulating HA was also increased in HFD-fed *Id3*$^{-/-}$ mice, and so we further hypothesized that by simply measuring plasma HA in obese humans, which are very likely to carry the *ID3* SNP rs11574 according to the previous studies, we could possibly predict the development of more severe dysmetabolism.

Therefore, we analysed human omental fat and plasma samples of two different, small cohorts of patients. First, the samples were genotyped to determine which subjects carry the risk allele and then experiments were performed. Omental fat was examined for HA content and RNA was extracted for measuring gene expression of HAS isoenzymes. These samples were derived from obese patients (as defined by their BMI) that opted for a bariatric surgery, during which omental fat was collected. The plasma samples that were used for HA ELISA were from another cohort of patients that had to

undergo medically necessary IVUS or QCA, so patients with increased risk of cardiovascular disease.

Surprisingly, our findings were not in agreement with our murine studies, since no effect was observed in the HA content in the omental fat of patients that had the *ID3* SNP rs11574. Contrary to expectations, no differences were revealed in the mRNA levels of the HAS isoenzymes between subjects that carried the ancestral allele and those that carried the risk allele, irrespective of whether they were heterozygote or homozygote. Circulating HA levels were not increased in patients with the risk allele either, although plasma HA usually correlates strongly with the progress of several diseases. For example, a study has shown before that serum HA levels were increased in diabetic patients and, of note, were even correlated with BMI[76]. Unfortunately, these interesting findings were not confirmed in our study, although there are some possible explanations for this outcome.

First, the sample size of our human studies needs to be taken into consideration. Our investigations so far have only been on a small scale, and it is reasonable to assume that, among individual patients, the variability can be really high, thus leading to inconclusive results. Most of the studies that were already discussed showed a significant correlation of the *ID3* SNP with human diseases, but they utilized much larger cohorts of patients.

Further, the fact that results from human studies were not consistent with results from murine studies highlights the importance of the validation of the various mouse models, before they can be translated into clinical research. It is also important to emphasize on the differences regarding the AT in humans and mice. Omental fat was isolated from human subjects, whereas epididymal AT was used for the murine experiments. This is due to the fact that murine epididymal AT has been established as the equivalent of human omental fat by the literature. Moreover, epididymal AT is typically the largest fat pad in mice, offering easier handling, compared with the murine omental fat, which does exist but has a much smaller size[171]. However, omental fat has a considerably different composition from

the other WAT depots, since it contains “milky spots”, which are large aggregates of leukocytes that have been implicated in several types of cancer[20,172]. These differences should be considered when designing a mouse model intended to be translated to human diseases.

One additional limitation of the present study is that only a very small part of human omental fat was obtained after the surgery, which might not be representative for the whole tissue. This fact underlines the difficulty of collecting this kind of human data. Moreover, the lack of significant results in the human studies could be explained by the variability which is part of human nature and can possibly influence our measurements and statistical analysis. Notably, the samples used in this work came from the Bariatric Surgery and the Cardiac Catheterization Labs and so variances during the sampling at the time of the surgery are inevitably expected.

In any case, the potential use of the *ID3* SNP rs11574 as a biomarker of atherosclerosis in humans has been discussed and proven in other studies[124,127]. Whether this *ID3* variation can also impact the HA content in humans and thus lead to an early diagnosis of dysmetabolism remains to be deciphered and will be addressed in future research.

5. Conclusion

Overall, this study provides evidence that loss of the transcription factor Id3 results in increased *Has2* expression with resultant increased HA accumulation in the visceral AT after 4 weeks of HFD. This novel finding provides the missing link between the discovery that loss of *Id3* protects from diet-induced visceral AT expansion but does not result in the expected improvement in dysmetabolism, which was one of the main focuses of the present work. Through careful flow cytometry analysis of AT depots from Wt and *Id3*$^{-/-}$ mice, we determined that there was a significant increase in B2 cells in the AT of *Id3*$^{-/-}$ mice, which have been shown to promote AT inflammation and metabolic dysfunction. Additional data using AT and cultured VSMCs revealed that the B2 cell accumulation in the AT was HA-dependent, since this effect was blunted after HA digestion, closing the loop on mechanism. We conclude that *Id3* deficiency in the setting of obesity leads to AT inflammation, which is characterized by increased B2 cell adhesion, with HA being the important mediator.

Our proposed model is depicted in **Figure 42.**

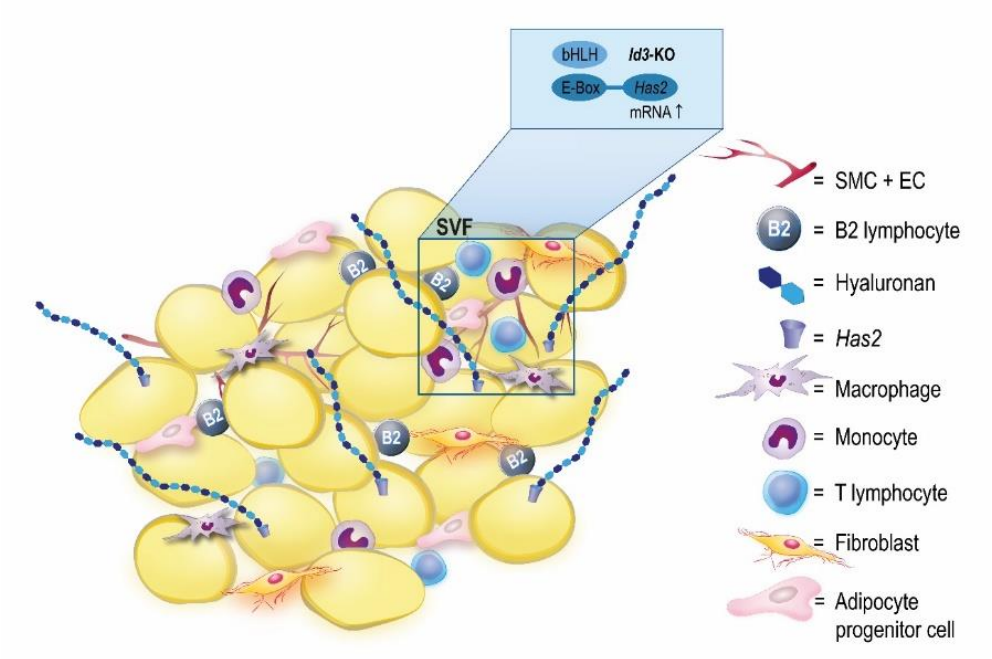

Figure 42: Proposed model of the role of Id3 in HA-dependent AT inflammation. Loss of *Id3* leads to reduced epididymal AT weight and increases *Has2* expression in cells of the SVF in the setting of obesity, resulting in increased HA content. Accumulation of HA induces an increase in the B2 cell population in the AT, thereby promoting HA-dependent binding of B2 cells and contributing to AT inflammation. SVF: stromal vascular fraction; SMC: smooth muscle cell; EC: endothelial cell.

With permission from Wolters Kluwer Health, Inc.: Misiou, A. *et al,* Helix-Loop-Helix Factor Id3 (Inhibitor of Differentiation 3) A Novel Regulator of Hyaluronan-Mediated Adipose Tissue Inflammation, *Arteriosclerosis, Thrombosis, And Vascular Biology*, 41(2), 796-807, doi: 10.1161/atvbaha.120.315588[1].

6. References

1. Misiou A, Garmey JC, Hensien JM, et al. Helix-Loop-Helix Factor Id3 (Inhibitor of Differentiation 3): A Novel Regulator of Hyaluronan-Mediated Adipose Tissue Inflammation. *Arterioscler Thromb Vasc Biol*. 2020;41(2):ATVBAHA120315588. doi:10.1161/ATVBAHA.120.315588
2. Gregory JW. Prevention of Obesity and Metabolic Syndrome in Children. *Front Endocrinol (Lausanne)*. 2019;10:669. doi:10.3389/fendo.2019.00669
3. Arner P. Human fat cell lipolysis: Biochemistry, regulation and clinical role. *Best Pract Res Clin Endocrinol Metab*. 2005;19(4):471-482. doi:10.1016/j.beem.2005.07.004
4. Saklayen MG. The Global Epidemic of the Metabolic Syndrome. *Curr Hypertens Rep*. 2018;20(2). doi:10.1007/s11906-018-0812-z
5. Després JP, Lemieux I. Abdominal obesity and metabolic syndrome. *Nature*. 2006;444(7121):881-887. doi:10.1038/nature05488
6. Huang PL. A comprehensive definition for metabolic syndrome. *DMM Dis Model Mech*. 2009;2(5-6):231-237. doi:10.1242/dmm.001180
7. Zimmet P, Alberti KGMM, Shaw J. Global and societal implications of the diabetes epidemic. *Nature*. 2001;414(6865):782-787. doi:10.1038/414782a
8. Astrup A, Finer N. Redefining type 2 diabetes: “Diabesity” or “obesity dependent diabetes mellitus”? *Obes Rev*. 2000;1(2):57-59. doi:10.1046/j.1467-789x.2000.00013.x
9. Bano G. Glucose homeostasis, obesity and diabetes. *Best Pract Res Clin Obstet Gynaecol*. 2013;27(5):715-726. doi:10.1016/j.bpobgyn.2013.02.007
10. Petersen MC, Shulman GI. Mechanisms of insulin action and insulin resistance. *Physiol Rev*. 2018;98(4):2133-2223. doi:10.1152/physrev.00063.2017
11. DeFronzo RA, Ferrannini E, Groop L, et al. Type 2 diabetes mellitus. *Nat Rev Dis Prim*. 2015;1(July):1-23. doi:10.1038/nrdp.2015.19
12. Xiang L, Mittwede PN, Clemmer JS. Glucose Homeostasis and Cardiovascular Alterations in Diabetes. In: *Comprehensive Physiology*. Vol 5. Hoboken, NJ, USA: John Wiley & Sons, Inc.; 2015:1815-1839. doi:10.1002/cphy.c150001
13. Samuel VT, Shulman GI. The pathogenesis of insulin resistance: Integrating signaling pathways and substrate flux. *J Clin Invest*. 2016;126(1):12-22. doi:10.1172/JCI77812
14. Xu H, Barnes GT, Yang Q, et al. Chronic inflammation in fat plays a crucial role in the development of obesity-related insulin resistance. *J Clin Invest*. 2003;112(12):1821-1830. doi:10.1172/JCI200319451
15. Armani A, Mammi C, Marzolla V, et al. Cellular models for understanding adipogenesis, adipose dysfunction, and obesity. *J Cell*

Biochem. 2010;110(3):564-572. doi:10.1002/jcb.22598

16. Rosen ED, Spiegelman BM. What we talk about when we talk about fat. *Cell*. 2014;156(1-2):20-44. doi:10.1016/j.cell.2013.12.012

17. Luong Q, Huang J, Lee KY. Deciphering white adipose tissue heterogeneity. *Biology (Basel)*. 2019;8(2). doi:10.3390/biology8020023

18. Even PC, Moran TH, Polák J, et al. Relationships between Rodent white Adipose Fat Pads and Human white Adipose Fat Depots. 2016;3. doi:10.3389/fnut.2016.00010

19. Cohen CA, Shea AA, Heffron CL, Schmelz EM, Roberts PC. Intra-Abdominal Fat Depots Represent Distinct Immunomodulatory Microenvironments: A Murine Model. Tang YL, ed. *PLoS One*. 2013;8(6):e66477. doi:10.1371/journal.pone.0066477

20. Meza-Perez S, Randall TD. Immunological Functions of the Omentum. *Trends Immunol*. 2017;38(7):526-536. doi:10.1016/j.it.2017.03.002

21. Chait A, den Hartigh LJ. Adipose Tissue Distribution, Inflammation and Its Metabolic Consequences, Including Diabetes and Cardiovascular Disease. *Front Cardiovasc Med*. 2020;7. doi:10.3389/fcvm.2020.00022

22. Lee M-J, Wu Y, Fried SK. Adipose tissue heterogeneity: Implication of depot differences in adipose tissue for obesity complications. *Mol Aspects Med*. 2013;34(1):1-11. doi:10.1016/j.mam.2012.10.001

23. Wu J, Boström P, Sparks LM, et al. Beige adipocytes are a distinct type of thermogenic fat cell in mouse and human. *Cell*. 2012;150(2):366-376. doi:10.1016/j.cell.2012.05.016

24. Gesta S, Tseng YH, Kahn CR. Developmental Origin of Fat: Tracking Obesity to Its Source. *Cell*. 2007;131(2):242-256. doi:10.1016/j.cell.2007.10.004

25. Rui L. Brown and beige adipose tissues in health and disease. *Compr Physiol*. 2017;7(4):1281-1306. doi:10.1002/cphy.c170001

26. Hotamisligil GS, Shargill NS, Spiegelman BM. Adipose expression of tumor necrosis factor-α: Direct role in obesity-linked insulin resistance. *Science (80-)*. 1993;259(5091):87-91. doi:10.1126/science.7678183

27. Hotamisligil GS, Arner P, Caro JF, Atkinson RL, Spiegelman BM. Increased adipose tissue expression of tumor necrosis factor-α in human obesity and insulin resistance. *J Clin Invest*. 1995;95(5):2409-2415. doi:10.1172/JCI117936

28. Weisberg SP, McCann D, Desai M, Rosenbaum M, Leibel RL, Ferrante AW. Obesity is associated with macrophage accumulation in adipose tissue. *J Clin Invest*. 2003;112(12):1796-1808. doi:10.1172/jci19246

29. Lumeng CN, Bodzin JL, Saltiel AR. Obesity induces a phenotypic switch in adipose tissue macrophage polarization. *J Clin Invest*. 2007;117(1):175-184. doi:10.1172/JCI29881

30. Lumeng CN, DeYoung SM, Bodzin JL, Saltiel AR. Increased

inflammatory properties of adipose tissue macrophages recruited during diet-induced obesity. *Diabetes*. 2007;56(1):16-23. doi:10.2337/db06-1076

31. Nishimura S, Manabe I, Nagasaki M, et al. CD8+ effector T cells contribute to macrophage recruitment and adipose tissue inflammation in obesity. *Nat Med*. 2009;15(8):914-920. doi:10.1038/nm.1964

32. Perry HM, Bender TP, Mcnamara CA, Rothstein TL, Cava A La. B cell subsets in atherosclerosis. 2012. doi:10.3389/fimmu.2012.00373

33. Winer DA, Winer S, Shen L, et al. B cells promote insulin resistance through modulation of T cells and production of pathogenic IgG antibodies. *Nat Med*. 2011;17(5):610-617. doi:10.1038/nm.2353

34. Ying W, Wollam J, Ofrecio JM, et al. Adipose tissue B2 cells promote insulin resistance through leukotriene LTB4/LTB4R1 signaling. *J Clin Invest*. 2017;127(3):1019-1030. doi:10.1172/JCI90350

35. DeFuria J, Belkina AC, Jagannathan-Bogdan M, et al. B cells promote inflammation in obesity and type 2 diabetes through regulation of T-cell function and an inflammatory cytokine profile. *Proc Natl Acad Sci U S A*. 2013;110(13):5133-5138. doi:10.1073/pnas.1215840110

36. Srikakulapu P, McNamara CA. B Lymphocytes and Adipose Tissue Inflammation. *Arterioscler Thromb Vasc Biol*. 2020;40(5):1110-1122. doi:10.1161/ATVBAHA.119.312467

37. Castanon N, Lasselin J, Capuron L. Neuropsychiatric comorbidity in obesity: Role of inflammatory processes. *Front Endocrinol (Lausanne)*. 2014;5(MAY). doi:10.3389/fendo.2014.00074

38. Hynes RO. Extracellular matrix: not just pretty fibrils. doi:10.1126/science.1176009

39. Theocharis AD, Skandalis SS, Gialeli C, Karamanos NK. Extracellular matrix structure. *Adv Drug Deliv Rev*. 2016;97:4-27. doi:10.1016/j.addr.2015.11.001

40. Pozzi A, Yurchenco PD, Iozzo R V. The nature and biology of basement membranes. *Matrix Biol*. 2017;57-58:1-11. doi:10.1016/j.matbio.2016.12.009

41. Hynes RO. Integrins: A family of cell surface receptors. *Cell*. 1987;48(4):549-554. doi:10.1016/0092-8674(87)90233-9

42. Takada Y, Ye X, Simon S. The integrins. *Genome Biol*. 2007;8(5):215. doi:10.1186/gb-2007-8-5-215

43. Hynes RO. Integrins: Bidirectional, allosteric signaling machines. *Cell*. 2002;110(6):673-687. doi:10.1016/S0092-8674(02)00971-6

44. Williams AS, Kang L, Wasserman DH. The extracellular matrix and insulin resistance. *Trends Endocrinol Metab*. 2015;26(7):357-366. doi:10.1016/j.tem.2015.05.006

45. Lotz MK. New developments in osteoarthritis. Posttraumatic osteoarthritis: Pathogenesis and pharmacological treatment options. *Arthritis Res Ther*. 2010;12(3):211. doi:10.1186/ar3046

46. Haak AJ, Tan Q, Tschumperlin DJ. Matrix biomechanics and dynamics in pulmonary fibrosis. *Matrix Biol*. 2018;73:64-76. doi:10.1016/j.matbio.2017.12.004

47. Parker MW, Rossi D, Peterson M, et al. Fibrotic extracellular matrix activates a profibrotic positive feedback loop. *J Clin Invest*. 2014;124(4):1622-1635. doi:10.1172/JCI71386

48. Theocharis AD, Manou D, Karamanos NK. The extracellular matrix as a multitasking player in disease. *FEBS J*. 2019;286(15):2830-2869. doi:10.1111/febs.14818

49. Vigetti D, Viola M, Karousou E, De Luca G, Passi A. Metabolic control of hyaluronan synthases. *Matrix Biol*. 2014;35:8-13. doi:10.1016/j.matbio.2013.10.002

50. Toole BP. Hyaluronan: from extracellular glue to pericellular cue. *Nat Rev Cancer*. 2004. doi:10.1038/nrc1391

51. Bordon KCF, Wiezel GA, Amorim FG, Arantes EC. Arthropod venom Hyaluronidases: Biochemical properties and potential applications in medicine and biotechnology. *J Venom Anim Toxins Incl Trop Dis*. 2015;21(1). doi:10.1186/s40409-015-0042-7

52. Camenisch TD, Spicer AP, Brehm-Gibson T, et al. Disruption of hyaluronan synthase-2 abrogates normal cardiac morphogenesis and hyaluronan-mediated transformation of epithelium to mesenchyme. *J Clin Invest*. 2000;106(3):349-360. doi:10.1172/JCI10272

53. Tien JYL, Spicer AP. Three vertebrate hyaluronan synthases are expressed during mouse development in distinct spatial and temporal patterns. *Dev Dyn*. 2005;233(1):130-141. doi:10.1002/dvdy.20328

54. Viola M, Vigetti D, Genasetti A, et al. Molecular control of the hyaluronan biosynthesis. *Connect Tissue Res*. 2008;49(3-4):111-114. doi:10.1080/03008200802148405

55. Tammi RH, Passi AG, Rilla K, et al. Transcriptional and post-translational regulation of hyaluronan synthesis. *FEBS J*. 2011;278(9):1419-1428. doi:10.1111/j.1742-4658.2011.08070.x

56. Jiang D, Liang J, Noble PW. Hyaluronan as an immune regulator in human diseases. *Physiol Rev*. 2011;91(1):221-264. doi:10.1152/physrev.00052.2009

57. Stern R, Asari AA, Sugahara KN. Hyaluronan fragments: An information-rich system. *Eur J Cell Biol*. 2006;85(8):699-715. doi:10.1016/j.ejcb.2006.05.009

58. Chajara A, Raoudi M, Delpech B, Leroy M, Basuyau JP, Levesque H. Increased hyaluronan and hyaluronidase production and hyaluronan degradation in injured aorta of insulin-resistant rats. *Arterioscler Thromb Vasc Biol*. 2000;20(6):1480-1487. doi:10.1161/01.ATV.20.6.1480

59. Saari H. Oxygen derived free radicals and synovial fluid hyaluronate. *Ann Rheum Dis*. 1991;50(6):389-392. doi:10.1136/ard.50.6.389

60. Stern R, Jedrzejas MJ. The Hyaluronidases: Their Genomics, Structures, and Mechanisms of Action. doi:10.1021/cr050247k

61. Nedvetzki S, Gonen E, Assayag N, et al. *RHAMM, a Receptor for Hyaluronan-Mediated Motility, Compensates for CD44 in Inflamed CD44-Knockout Mice: A Different Interpretation of Redundancy*.; 2004. www.pnas.orgcgidoi10.1073pnas.0407378102. Accessed April 13, 2020.

62. Liang J, Jiang D, Noble PW. Hyaluronan as a therapeutic target in human diseases. *Adv Drug Deliv Rev*. 2016. doi:10.1016/j.addr.2015.10.017

63. Karousou E, Misra S, Ghatak S, et al. Roles and targeting of the HAS/ hyaluronan/CD44 molecular system in cancer. *Matrix Biol*. 2016;59:3-22. doi:10.1016/j.matbio.2016.10.001

64. Misra S, Hascall VC, Markwald RR, Ghatak S. Interactions between hyaluronan and its receptors (CD44, RHAMM) regulate the activities of inflammation and cancer. *Front Immunol*. 2015;6(MAY):201. doi:10.3389/fimmu.2015.00201

65. Lesley J, Hyman R, English N, Catterall JB, Turner GA. CD44 in inflammation and metastasis. *Glycoconj J*. 1997;14(5):611-622. doi:10.1023/A:1018540610858

66. Turley EA, Noble PW, Bourguignon LYW. Signaling properties of hyaluronan receptors. *J Biol Chem*. 2002;277(7):4589-4592. doi:10.1074/jbc.R100038200

67. RAGAN C, MEYER K. The hyaluronic acid of synovial fluid in rheumatoid arthritis. *J Clin Invest*. 1949;28(1):56-59. doi:10.1172/JCI102053

68. Nettelbladt O, Scheynius A, Bergh J, Tengblad A, Hallgren R. Alveolar accumulation of hyaluronan and alveolar cellular response in bleomycin-induced alveolitis. *Eur Respir J*. 1991;4(4).

69. Söderberg M, Bjermer L, Hättgren R, Lundgren R. Increased hyaluronan (Hyaluronic acid) levels in bronchoalveolar lavage fluid after histamine inhalation. *Int Arch Allergy Immunol*. 1989;88(4):373-376. doi:10.1159/000234719

70. McKee CM, Penno MB, Cowman M, et al. Hyaluronan (HA) fragments induce chemokine gene expression in alveolar macrophages: The role of HA size and CD44. *J Clin Invest*. 1996;98(10):2403-2413. doi:10.1172/JCI119054

71. Han CY, Subramanian S, Chan CK, et al. Adipocyte-Derived Serum Amyloid A3 and Hyaluronan Play a Role in Monocyte Recruitment and Adhesion. *Diabetes*. 2007;56(9):2260-2273. doi:10.2337/db07-0218

72. de la Motte CA, Hascall VC, Drazba J, Bandyopadhyay SK, Strong SA. Mononuclear leukocytes bind to specific hyaluronan structures on colon mucosal smooth muscle cells treated with polyinosinic acid:polycytidylic acid: inter-alpha-trypsin inhibitor is crucial to structure and function. *Am J Pathol*. 2003;163(1):121-133. doi:10.1016/s0002-9440(10)63636-x

73. DeGrendele HC, Estess P, Picker LJ, Siegelman MH. CD44 and its ligand hyaluronate mediate rolling under physiologic flow: A novel lymphocyte-endothelial cell primary adhesion pathway. *J Exp Med*. 1996;183(3):1119-1130. doi:10.1084/jem.183.3.1119

74. Khan AI, Kerfoot SM, Heit B, et al. Role of CD44 and

Hyaluronan in Neutrophil Recruitment. *J Immunol*. 2004;173(12):7594-7601. doi:10.4049/jimmunol.173.12.7594

75. Cuff CA, Kothapalli D, Azonobi I, et al. The adhesion receptor CD44 promotes atherosclerosis by mediating inflammatory cell recruitment and vascular cell activation. *J Clin Invest*. 2001;108(7):1031-1040. doi:10.1172/jci12455

76. Mine S, Okada Y, Kawahara C, Tabata T, Tanaka Y. Serum hyaluronan concentration as a marker of angiopathy in patients with diabetes mellitus. *Endocr J*. 2006;53(6):761-766. doi:10.1507/endocrj.K05-119

77. Morita M, Yano S, Ishibashi Y, Nakata N, Kurioka S, Sugimoto T. Close relationship between serum hyaluronan levels and vascular function in patients with type 2 diabetes. *Biomarkers*. 2014;19(6):493-497. doi:10.3109/1354750X.2014.940502

78. Mahadevan P, Larkins RG, Fraser JRE, Fosang AJ, Dunlop ME. Increased hyaluronan production in the glomeruli from diabetic rats: a link between glucose-induced prostaglandin production and reduced sulphated proteoglycan. *Diabetologia*. 1995;38(3):298-305. doi:10.1007/BF00400634

79. Kang L, Lantier L, Kennedy A, et al. Hyaluronan accumulates with high-fat feeding and contributes to insulin resistance. *Diabetes*. 2013. doi:10.2337/db12-1502

80. Allingham PG, Brownlee GR, Harper GS, Pho M, Nilsson SK, Brown TJ. Gene expression, synthesis and degradation of hyaluronan during differentiation of 3T3-L1 adipocytes. *Arch Biochem Biophys*. 2006;452(1):83-91. doi:10.1016/j.abb.2006.05.010

81. Mahaffey CL, Mummert ME. Hyaluronan Synthesis Is Required for IL-2-Mediated T Cell Proliferation. *J Immunol*. 2007;179(12):8191-8199. doi:10.4049/jimmunol.179.12.8191

82. Nagy N, Freudenberger T, Melchior-Becker A, et al. Inhibition of hyaluronan synthesis accelerates murine atherosclerosis: novel insights into the role of hyaluronan synthesis. *Circulation*. 2010;122(22):2313-2322. doi:10.1161/CIRCULATIONAHA.110.972653

83. García-Vilas JA, Quesada AR, Medina MÁ. 4-Methylumbelliferone inhibits angiogenesis in vitro and in vivo. *J Agric Food Chem*. 2013;61(17):4063-4071. doi:10.1021/jf303062h

84. Tammi RH, Passi AG, Rilla K, et al. Transcriptional and post-translational regulation of hyaluronan synthesis. *FEBS J*. 2011;278(9):1419-1428. doi:10.1111/j.1742-4658.2011.08070.x

85. Kultti A, Pasonen-Seppänen S, Jauhiainen M, et al. 4-Methylumbelliferone inhibits hyaluronan synthesis by depletion of cellular UDP-glucuronic acid and downregulation of hyaluronan synthase 2 and 3. *Exp Cell Res*. 2009;315(11):1914-1923. doi:10.1016/J.YEXCR.2009.03.002

86. McKallip RJ, Ban H, Uchakina ON. Treatment with the Hyaluronic Acid Synthesis Inhibitor 4-Methylumbelliferone Suppresses LPS-Induced Lung Inflammation. *Inflammation*. 2015;38(3):1250-1259. doi:10.1007/s10753-014-0092-y

87. Colombaro V, Declèves AE, Jadot I, et al. Inhibition of

hyaluronan is protective against renal ischaemia-reperfusion injury. *Nephrol Dial Transplant*. 2013;28(10):2484-2493. doi:10.1093/ndt/gft314

88. Sim M-O, Ham JR, Lee H-I, Seo K-I, Lee M-K. Long-term supplementation of umbelliferone and 4-methylumbelliferone alleviates high-fat diet induced hypertriglyceridemia and hyperglycemia in mice. *Chem Biol Interact*. 2014;216:9-16. doi:10.1016/j.cbi.2014.03.003

89. Grandoch M, Flögel U, Virtue S, et al. 4-Methylumbelliferone improves the thermogenic capacity of brown adipose tissue. *Nat Metab*. doi:10.1038/s42255-019-0055-6

90. Proteoglycans, key regulators of cell–matrix dynamics. *Matrix Biol*. 2014;35:1-2. doi:10.1016/J.MATBIO.2014.05.001

91. Iozzo R V., Schaefer L. Proteoglycan form and function: A comprehensive nomenclature of proteoglycans. *Matrix Biol*. 2015;42:11-55. doi:10.1016/j.matbio.2015.02.003

92. Korpetinou A, Skandalis SS, Labropoulou VT, et al. Serglycin: At the crossroad of inflammation and malignancy. *Front Oncol*. 2014;4 JAN:327. doi:10.3389/fonc.2013.00327

93. Choi Y, Chung H, Jung H, Couchman JR, Oh ES. Syndecans as cell surface receptors: Unique structure equates with functional diversity. *Matrix Biol*. 2011;30(2):93-99. doi:10.1016/j.matbio.2010.10.006

94. Nastase M V, Janicova A, Roedig H, Hsieh LT-H, Wygrecka M, Schaefer L. Small Leucine-Rich Proteoglycans in Renal Inflammation: Two Sides of the Coin. *J Histochem Cytochem*. 2018;66(4):261-272. doi:10.1369/0022155417738752

95. Moreth K, Iozzo R V, Schaefer L. Small leucine-rich proteoglycans orchestrate receptor crosstalk during inflammation. *Cell Cycle*. 2012;11(11):2084-2091. doi:10.4161/cc.20316

96. Li L, Ly M, Linhardt RJ. Proteoglycan sequence. *Mol Biosyst*. 2012;8(6):1613-1625. doi:10.1039/c2mb25021g

97. Nastase M V, Young MF, Schaefer L. Biglycan: a multivalent proteoglycan providing structure and signals. *J Histochem Cytochem*. 2012;60(12):963-975. doi:10.1369/0022155412456380

98. Fisher LW, Terminel JD, Dejter SW, et al. *Proteoglycans of Developing Bone**. Vol 258.; 1983. http://www.jbc.org/. Accessed January 14, 2021.

99. Tang T, Thompson JC, Wilson PG, et al. Biglycan deficiency: increased aortic aneurysm formation and lack of atheroprotection. *J Mol Cell Cardiol*. 2014;75:174. doi:10.1016/J.YJMCC.2014.07.014

100. Ward MG, Ajuwon KM. Biglycan deletion alters adiponectin expression in murine adipose tissue and 3T3-L1 adipocytes. *PLoS One*. 2012;7(11):e50554. doi:10.1371/journal.pone.0050554

101. Adapala VJ, Ward M, Ajuwon KM. Adipose tissue biglycan as a potential anti-inflammatory target of sodium salicylate in mice fed a high fat diet. *J Inflamm (Lond)*. 2012;9(1):15. doi:10.1186/1476-9255-9-15

102. Han CY, Kang I, Harten IA, et al. Adipocyte-Derived Versican and Macrophage-Derived Biglycan Control Adipose Tissue

Inflammation in Obesity. *Cell Rep*. 2020;31(13):107818. doi:10.1016/j.celrep.2020.107818

103. Fisher LW, Termine JD, Young MF. Deduced protein sequence of bone small proteoglycan I (biglycan) shows homology with proteoglycan II (decorin) and several nonconnective tissue proteins in a variety of species. *J Biol Chem*. 1989;264(8):4571-4576. doi:10.1016/s0021-9258(18)83781-4

104. Iozzo R V. *MATRIX PROTEOGLYCANS: From Molecular Design to Cellular Function*.; 1998. www.annualreviews.org. Accessed January 14, 2021.

105. Bolton K, Segal D, McMillan J, et al. Decorin is a secreted protein associated with obesity and type 2 diabetes. *Int J Obes*. 2008;32(7):1113-1121. doi:10.1038/ijo.2008.41

106. Svärd J, Røst TH, Sommervoll CEN, et al. Absence of the proteoglycan decorin reduces glucose tolerance in overfed male mice. *Sci Rep*. 2019;9(1):4614. doi:10.1038/s41598-018-37501-x

107. Morawski M, Brückner G, Arendt T, Matthews RT. Aggrecan: Beyond cartilage and into the brain. *Int J Biochem Cell Biol*. 2012;44(5):690-693. doi:10.1016/j.biocel.2012.01.010

108. Talusan P, Bedri S, Yang S, et al. Analysis of intimal proteoglycans in atherosclerosis-prone and atherosclerosis-resistant human arteries by mass spectrometry. *Mol Cell Proteomics*. 2005;4(9):1350-1357. doi:10.1074/mcp.M500088-MCP200

109. Voros G, Sandy JD, Collen D, Lijnen HR. Expression of aggrecan(ases) during murine preadipocyte differentiation and adipose tissue development. *Biochim Biophys Acta - Gen Subj*. 2006;1760(12):1837-1844. doi:10.1016/J.BBAGEN.2006.08.016

110. Wingender E, Schoeps T, Rgen Dö Nitz J. TFClass: an expandable hierarchical classification of human transcription factors. doi:10.1093/nar/gks1123

111. Murre C. Helix-loop-helix proteins and lymphocyte development. *Nat Immunol*. 2005;6(11). doi:10.1038/ni1260

112. Forrest S, McNamara C. Id family of transcription factors and vascular lesion formation. *Arterioscler Thromb Vasc Biol*. 2004;24(11):2014-2020. doi:10.1161/01.ATV.0000143932.03151.ad

113. Massari ME, Murre C. MINIREVIEW Helix-Loop-Helix Proteins: Regulators of Transcription in Eucaryotic Organisms. 2000;20(2):429-440.

114. Ruzinova MB, Benezra R. Id proteins in development, cell cycle and cancer. *Trends Cell Biol*. 2003;13(8):410-418. doi:10.1016/S0962-8924(03)00147-8

115. Benezra R, Davis RL, Lockshon D, Turner DL, Weintraub H. The protein Id: A negative regulator of helix-loop-helix DNA binding proteins. *Cell*. 1990;61(1):49-59. doi:10.1016/0092-8674(90)90214-Y

116. Ling F, Kang B, Sun XH. Id proteins: Small molecules, mighty regulators. In: *Current Topics in Developmental Biology*. Vol 110. Academic Press Inc.; 2014:189-216. doi:10.1016/B978-0-12-405943-6.00005-1

117. Lasorella A, Noseda M, Beyna M, Iavarone A. Id2 is a retinoblastoma protein target and mediates signalling by Myc

oncoproteins. *Nature*. 2000;407(6804):592-598. doi:10.1038/35036504

118. Yates PR, Atherton GT, Deed RW, Norton JD, Sharrocks AD. Id helix-loop-helix proteins inhibit nucleoprotein complex formation by the TCF ETS-domain transcription factors. *EMBO J*. 1999;18(4):968-976. doi:10.1093/emboj/18.4.968

119. Roberts EC, Deed RW, Inoue T, Norton JD, Sharrocks AD. Id Helix-Loop-Helix Proteins Antagonize Pax Transcription Factor Activity by Inhibiting DNA Binding. *Mol Cell Biol*. 2001;21(2):524-533. doi:10.1128/mcb.21.2.524-533.2001

120. Roschger C, Cabrele C. The Id-protein family in developmental and cancer-associated pathways Fritz Aberger. *Cell Commun Signal*. 2017;15(1):1-26. doi:10.1186/s12964-016-0161-y

121. Ueda-Hayakawa I, Mahlios J, Zhuang Y. Id3 Restricts the Developmental Potential of γδ Lineage during Thymopoiesis. *J Immunol*. 2009;182(9):5306-5316. doi:10.4049/jimmunol.0804249

122. Matsumura ME, Li F, Berthoux L, et al. Vascular Injury Induces Posttranscriptional Regulation of the Id3 Gene. *Arterioscler Thromb Vasc Biol*. 2001;21(5):752-758. doi:10.1161/01.ATV.21.5.752

123. Taylor AM, Li F, Thimmalapura P, et al. Hyperlipemia and Oxidation of LDL Induce Vascular Smooth Muscle Cell Growth: An Effect Mediated by the HLH Factor Id3. *J Vasc Res*. 2006;43:123-130. doi:10.1159/000090131

124. Doran AC, Lehtinen AB, Meller N, et al. Id3 Is a Novel Atheroprotective Factor Containing a Functionally Significant Single-Nucleotide Polymorphism Associated With Intima–Media Thickness in Humans. *Circ Res*. 2010;106(7):1303-1311. doi:10.1161/CIRCRESAHA.109.210294

125. Doran AC, Lipinski MJ, Oldham SN, et al. B-cell aortic homing and atheroprotection depend on Id3. *Circ Res*. 2012. doi:10.1161/CIRCRESAHA.111.256438

126. Lipinski MJ, Campbell KA, Duong SQ, et al. Loss of Id3 increases VCAM-1 expression, macrophage accumulation, and atherogenesis in Ldlr-/- mice. *Arterioscler Thromb Vasc Biol*. 2012;32(12):2855-2861. doi:10.1161/ATVBAHA.112.300352

127. Manichaikul A, Rich SS, Perry H, et al. A Functionally Significant Polymorphism in ID3 Is Associated with Human Coronary Pathology. Abbate A, ed. *PLoS One*. 2014;9(3):e90222. doi:10.1371/journal.pone.0090222

128. Moldes M, Lasnier FO, Fe`ve B, Fe`ve F, Pairault J, Djian P. *Id3 Prevents Differentiation of Preadipose Cells*. Vol 17.; 1997. http://mcb.asm.org/. Accessed April 10, 2020.

129. Tontonoz P, Kim JB, Graves RA, Spiegelman BM. ADD1: a novel helix-loop-helix transcription factor associated with adipocyte determination and differentiation. *Mol Cell Biol*. 1993;13(8):4753-4759. doi:10.1128/mcb.13.8.4753

130. Moldes M, Boizard M, Le Liepvre X, Fève B, Dugail I, Pairault J. Functional antagonism between inhibitor of DNA binding (Id) and adipocyte determination and differentiation factor 1/sterol

regulatory element-binding protein-1c (ADD1/SREBP-1c) trans-factors for the regulation of fatty acid synthase promoter in adipocyte. *Biochem J*. 1999;344(3):873-880. doi:10.1042/0264-6021:3440873

131. Doran AC, Meller N, Cutchins A, et al. The helix-loop-helix factors Id3 and E47 are novel regulators of adiponectin. *Circ Res*. 2008;103(6):624-634. doi:10.1161/CIRCRESAHA.108.175893

132. Cutchins A, Harmon DB, Kirby JL, et al. Inhibitor of differentiation-3 mediates high fat diet-induced visceral fat expansion. *Arterioscler Thromb Vasc Biol*. 2012;32(2):317-324. doi:10.1161/ATVBAHA.111.234856

133. Rivera RR, Johns CP, Quan J, Johnson RS, Murre C. Thymocyte selection is regulated by the helix-loop-helix inhibitor protein, Id3. *Immunity*. 2000;12(1):17-26. doi:10.1016/S1074-7613(00)80155-7

134. Pan L, Sato S, Frederick JP, Sun X-H, Zhuang Y. Impaired Immune Responses and B-Cell Proliferation in Mice Lacking the Id3 Gene . *Mol Cell Biol*. 1999;19(9):5969-5980. doi:10.1128/mcb.19.9.5969

135. Murre C. Helix-loop-helix proteins and lymphocyte development. *Nat Immunol*. 2005;6(11):1079-1086. doi:10.1038/ni1260

136. Perry HM, Oldham SN, Fahl SP, et al. Helix-Loop-Helix Factor Inhibitor of Differentiation 3 Regulates Interleukin-5 Expression and B-1a B Cell Proliferation. doi:10.1161/ATVBAHA

137. Rosenfeld SM, Perry HM, Gonen A, et al. B-1b Cells Secrete Atheroprotective IgM and Attenuate Atherosclerosis. *Circ Res*. 2015;117(3):e28-e39. doi:10.1161/CIRCRESAHA.117.306044

138. Harmon DB, Srikakulapu P, Kaplan JL, et al. Protective Role for B-1b B Cells and IgM in Obesity-Associated Inflammation, Glucose Intolerance, and Insulin Resistance. *Arterioscler Thromb Vasc Biol*. 2016;36(4):682-691. doi:10.1161/ATVBAHA.116.307166

139. Kinsella RJ, Kähäri A, Haider S, et al. Ensembl BioMarts: A hub for data retrieval across taxonomic space. *Database*. 2011;2011. doi:10.1093/database/bar030

140. Pettersson US, Waldén TB, Carlsson PO, Jansson L, Phillipson M. Female Mice are Protected against High-Fat Diet Induced Metabolic Syndrome and Increase the Regulatory T Cell Population in Adipose Tissue. *PLoS One*. 2012;7(9). doi:10.1371/journal.pone.0046057

141. Kuipers HF, Nagy N, Ruppert SM, et al. The pharmacokinetics and dosing of oral 4-methylumbelliferone for inhibition of hyaluronan synthesis in mice. *Clin Exp Immunol*. 2016;185(3):372-381. doi:10.1111/cei.12815

142. Ellacott KLJ, Morton GJ, Woods SC, Tso P, Schwartz MW. Assessment of Feeding Behavior in Laboratory Mice. *Cell Metab*. 2010;12(1):10-17. doi:10.1016/J.CMET.2010.06.001

143. Perry HM, Oldham SN, Fahl SP, et al. Helix-loop-helix factor inhibitor of differentiation 3 regulates interleukin-5 expression and B-1a B cell proliferation. *Arterioscler Thromb Vasc Biol*. 2013;33(12):2771-2779. doi:10.1161/ATVBAHA.113.302571

144. Vu J, Ying W. Isolation and Analysis of Stromal Vascular Cells from Visceral Adipose Tissue. *BIO-PROTOCOL*. 2017;7(16). doi:10.21769/bioprotoc.2444

145. Grandoch M, Hoffmann J, Röck K, et al. Novel effects of adenosine receptors on pericellular hyaluronan matrix: Implications for human smooth muscle cell phenotype and interactions with monocytes during atherosclerosis. *Basic Res Cardiol*. 2013. doi:10.1007/s00395-013-0340-6

146. Kaplan JL, Marshall MA, McSkimming CC, et al. Adipocyte progenitor cells initiate monocyte chemoattractant protein-1-mediated macrophage accumulation in visceral adipose tissue. *Mol Metab*. 2015. doi:10.1016/j.molmet.2015.07.010

147. Duffaut C, Galitzky J, Lafontan M, Bouloumié A. Unexpected trafficking of immune cells within the adipose tissue during the onset of obesity. *Biochem Biophys Res Commun*. 2009;384(4):482-485. doi:10.1016/J.BBRC.2009.05.002

148. Zhang M, Hu T, Zhang S, Zhou L. Associations of Different Adipose Tissue Depots with Insulin Resistance: A Systematic Review and Meta-analysis of Observational Studies. *Sci Rep*. 2015;5. doi:10.1038/srep18495

149. Després JP, Lemieux I, Bergeron J, et al. Abdominal Obesity and the Metabolic Syndrome: Contribution to global cardiometabolic risk. *Arterioscler Thromb Vasc Biol*. 2008;28(6):1039-1049. doi:10.1161/ATVBAHA.107.159228

150. Després J. Is visceral obesity the cause of the metabolic syndrome? *Ann Med*. 2006;38(1):52-63. doi:10.1080/07853890500383895

151. Pouliot MC, Després JP, Nadeau A, et al. Visceral obesity in men: Associations with glucose tolerance, plasma insulin, and lipoprotein levels. *Diabetes*. 1992;41(7):826-834. doi:10.2337/diab.41.7.826

152. Cancello R, Henegar C, Viguerie N, et al. Reduction of macrophage infiltration and chemoattractant gene expression changes in white adipose tissue of morbidly obese subjects after surgery-induced weight loss. *Diabetes*. 2005;54(8):2277-2286. doi:10.2337/diabetes.54.8.2277

153. Poitou C, Perret C, Mathieu F, et al. Bariatric surgery induces disruption in inflammatory signaling pathways mediated by immune cells in adipose tissue: A RNA-seq study. *PLoS One*. 2015;10(5). doi:10.1371/journal.pone.0125718

154. ClÉment K, Viguerie N, Poitou C, et al. Weight loss regulates inflammation-related genes in white adipose tissue of obese subjects. *FASEB J*. 2004;18(14):1657-1669. doi:10.1096/fj.04-2204com

155. Jacobson A, Brinck J, Briskin MJ, Spicer AP, Heldin P. *Expression of Human Hyaluronan Synthases in Response to External Stimuli*. Vol 348.; 2000.

156. Evanko SP, Johnson PY, Braun KR, Underhill CB, Dudhia J, Wight TN. Platelet-derived growth factor stimulates the formation of versican-hyaluronan aggregates and pericellular matrix expansion in arterial smooth muscle cells. *Arch Biochem Biophys*. 2001;394(1):29-

38. doi:10.1006/abbi.2001.2507

157. Sussmann M, Sarbia M, Meyer-Kirchrath J, Nüsing RM, Schrör K, Fischer JW. Induction of Hyaluronic Acid Synthase 2 (HAS2) in Human Vascular Smooth Muscle Cells by Vasodilatory Prostaglandins. *Circ Res*. 2004;94(5):592-600. doi:10.1161/01.RES.0000119169.87429.A0

158. Guéchot J, Poupon RE, Giral P, Balkau B, Giboudeau J, Poupon R. Relationship between procollagen III aminoterminal propeptide and hyaluronan serum levels and histological fibrosis in primary biliary cirrhosis and chronic viral hepatitis C. *J Hepatol*. 1994;20(3):388-393. doi:10.1016/S0168-8278(94)80013-8

159. Nieuwdorp M, Holleman F, De Groot E, et al. Perturbation of hyaluronan metabolism predisposes patients with type 1 diabetes mellitus to atherosclerosis. *Diabetologia*. 2007;50(6):1288-1293. doi:10.1007/s00125-007-0666-4

160. Duffaut C, Galitzky J, Lafontan M, Bouloumié A. Unexpected trafficking of immune cells within the adipose tissue during the onset of obesity. *Biochem Biophys Res Commun*. 2009;384(4):482-485. doi:10.1016/j.bbrc.2009.05.002

161. Jagannathan M, Mcdonnell M, Liang Y, et al. Toll-like receptors regulate B cell cytokine production in patients with diabetes. 2010;53(7):1461-1471. doi:10.1007/s00125-010-1730-z

162. Uysal KT, Wiesbrock SM, Marino MW, Hotamisligil GS. Protection from obesity-induced insulin resistance in mice lacking TNF- α function. *Nature*. 1997;389(6651):610-614. doi:10.1038/39335

163. Vozarova B, Weyer C, Hanson K, Tataranni PA, Bogardus C, Pratley RE. Circulating Interleukin-6 in Relation to Adiposity, Insulin Action, and Insulin Secretion. *Obes Res*. 2001;9(7):414-417. doi:10.1038/oby.2001.54

164. Bao Y, Liu X, Han C, et al. Identification of IFN--producing innate B cells. *Cell Res*. 2014;24(2):161-176. doi:10.1038/cr.2013.155

165. Iwata Y, Yoshizaki A, Komura K, et al. CD19, a Response Regulator of B Lymphocytes, Regulates Wound Healing through Hyaluronan-Induced TLR4 Signaling. *Am J Pathol*. 2009;175:649-660. doi:10.2353/ajpath.2009.080355

166. Drazen DL, Vahl TP, D'Alessio DA, Seeley RJ, Woods SC. Effects of a Fixed Meal Pattern on Ghrelin Secretion: Evidence for a Learned Response Independent of Nutrient Status. *Endocrinology*. 2006;147(1):23-30. doi:10.1210/en.2005-0973

167. Russell JC, Proctor SD, Kelly SE, Brindley DN. Pair feeding-mediated changes in metabolism: stress response and pathophysiology in insulin-resistant, atherosclerosis-prone JCR:LA-cp rats. *Am J Physiol Metab*. 2008;294(6):E1078-E1087. doi:10.1152/ajpendo.90257.2008

168. Li F, Hao P, Liu G, et al. Effects of 4-methylumbelliferone and high molecular weight hyaluronic acid on the inflammation of corneal stromal cells induced by LPS. *Graefe's Arch Clin Exp Ophthalmol*. 2017;255(3):559-566. doi:10.1007/s00417-016-3561-1

169. Ji E, Jung MY, Park JH, et al. Inhibition of adipogenesis in 3T3-L1 cells and suppression of abdominal fat accumulation in high-fat diet-feeding C57BL/6J mice after downregulation of hyaluronic acid. *Int J Obes*. 2014;38(8):1035-1043. doi:10.1038/ijo.2013.202

170. Bowden DW, Rudock M, Ziegler J, et al. Coincident Linkage of Type 2 Diabetes, Metabolic Syndrome, and Measures of Cardiovascular Disease in a Genome Scan of the Diabetes Heart Study. 1985. doi:10.2337/db06-0003

171. Bjørndal B, Burri L, Staalesen V, Skorve J, Berge RK. Different adipose depots: Their role in the development of metabolic syndrome and mitochondrial response to hypolipidemic agents. *J Obes*. 2011;2011. doi:10.1155/2011/490650

172. Wilkosz S, Grenham A, Nadeem I, et al. A comparative study of the structure of human and murine greater omentum. doi:10.1007/s00429-004-0446-6

7. Appendix

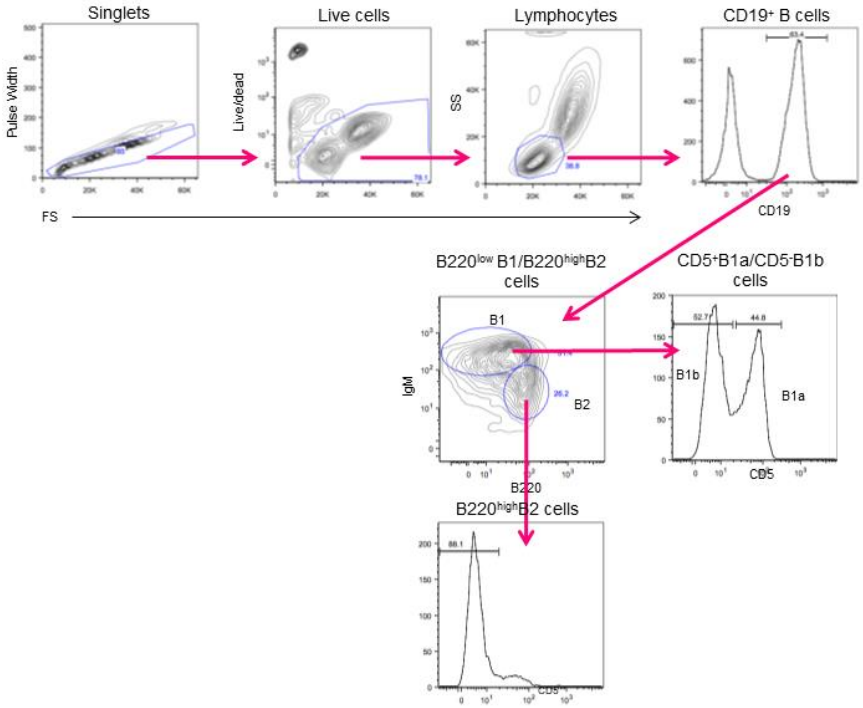

Figure 43: Gating scheme for the flow cytometric analyses of immune cells in the AT after 4 weeks of HFD. Flow cytometric identification of B220^{high} B2 cells and B220^{low} B1 cells that include CD5^{+} B220^{low} B1a and CD5^{-} B220^{low} B1b cells.

With permission from Wolters Kluwer Health, Inc.: Misiou, A. *et al,* Helix-Loop-Helix Factor Id3 (Inhibitor of Differentiation 3) A Novel Regulator of Hyaluronan-Mediated Adipose Tissue Inflammation, *Arteriosclerosis, Thrombosis, And Vascular Biology*, 41(2), 796-807, doi: 10.1161/atvbaha.120.315588[1].

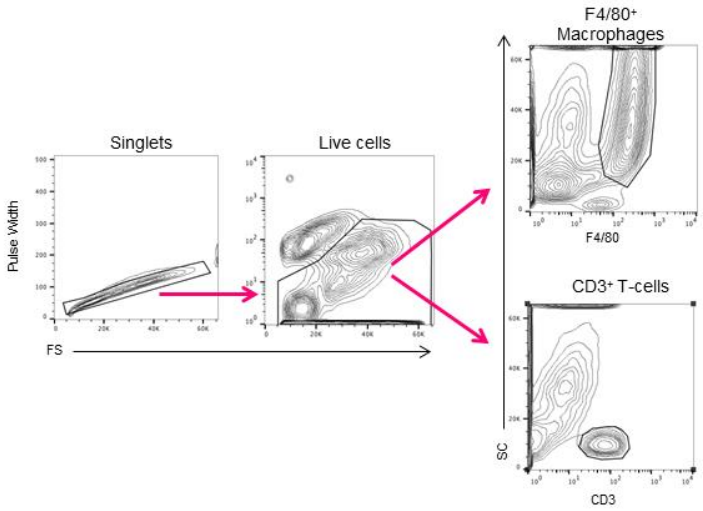

Figure 44: Diagram for the analyses of AT macrophages and T cells after 4 weeks of HFD. Representative flow plots demonstrate flow cytometry gating strategy to identify F4/80⁺ macrophages and CD3⁺ T cells.

With permission from Wolters Kluwer Health, Inc.: Misiou, A. *et al,* Helix-Loop-Helix Factor Id3 (Inhibitor of Differentiation 3) A Novel Regulator of Hyaluronan-Mediated Adipose Tissue Inflammation, *Arteriosclerosis, Thrombosis, And Vascular Biology*, 41(2), 796-807, doi: 10.1161/atvbaha.120.315588[1].

8. List of Figures

9. List of tables

Acknowledgments

Firstly, I would like to thank **Prof. Dr. med. Maria Grandoch:** Thank you for the guidance, the constant support and for always being there for me, not only as a supervisor. I learnt a lot from you, and you were an excellent mentor that helped me become a better scientist and believe more in myself.

I would also like to thank **Prof. Dr. Jens Fisher** for giving me the opportunity to be a part of the Institute of Pharmacology. To all my colleagues in Pharmacology: thank you all for your help, patience and understanding. Of course, a very big special “Thank you” to my office-mates, **Felicia Hartmann** and **Marco Piroth**, for the fun (and sad) times in the office, the struggles that we went through together, Marco teaching me how to calculate and Felicia being “überfordert”. I am extremely happy and grateful to have met you.

A very big part of my PhD was the time I spent in Charlottesville. For this, I would like to thank **Dr. Sandra Berger**, the coordinator of IRTG 1902, for her help and advice. Furthermore, **Dr. Coleen McNamara** was an excellent supervisor and mentor for me in Charlottesville, and her advice and scientific way of thinking will stay with me forever. Her hospitality and warm house deserve extra acknowledgment as I will never forget my first Thanksgiving in 2018. **James Garmey** worked very hard and helped immensely with this project, and for that I truly thank him. To my Charlottesville helpers/friends/saviours: **Dr. Tori Osinski** and **Dr. Aditi Upadhye**: thank you for all the support in the lab and for being great friends outside of the lab, for the laughs, for the beers and for making my time there so special. To the rest of the lab in Charlottesville and especially **Chantel McSkimming** and **Melissa Marshall**: thank you for making me looking forward to doing new experiments with you – I learnt a lot.

Last but not least, I would like to thank my family in Greece. My mum, dad and big sister Ioanna, for making me who I am and for trusting me without even fully understanding what it is exactly that I

do. My younger sister, Konstantina, because she is the person that I text every 5 minutes and she still tolerates me. I love you and I miss you. Natasha, thank you for believing in me from the very beginning. Finally, to my friends in Greece that I always miss and my boyfriend Michalis for the love and support: you are a part of me, and I thank you for everything.